UNIVERSITÁ DI BOLOGNA

Dipartimento di Scienze della Terra

e Geologico-Ambientali

DOTTORATO DI RICERCA IN SCIENZE DELLA TERRA

XXII CICLO

Coordinatore: Prof. Roberto Barbieri

Settori scientifico disciplinari di afferenza: GEO04/GEO03/GEO02

Tesi di Dottorato

TECTONIC GEOMORPHOLOGY AND ACTIVE STRAIN OF THE NORTHERN APENNINES MOUNTAIN FRONT

Presentata da:

Dott. Alessio Ponza

Supervisori:

Dott. Vincenzo Picotti

Prof. Frank J. Pazzaglia

Esame finale anno 2010

TECTONIC GEOMORPHOLOGY AND ACTIVE STRAIN OF THE NORTHERN APENNINES MOUNTAIN FRONT

ABSTRACT

INTRODUCTION

PAPER 1

Topographic expression of active faults in the foothills of the Northern Apennines

Vincenzo Picotti, Alessio Ponza and Frank J. Pazzaglia, (2009). Tectonophysics 474, 285-294.

PAPER 2

Thrust-fold growth history at the mountain front of the Northern Apennines from quantitative landscape analysis

Alessio Ponza, Frank J. Pazzaglia and Vincenzo Picotti. Submitted to Geomorphology 9 November 2009

PAPER 3

The active deep mountain front of the Northern Apennines: seismicity and geomorphology

Alessio Ponza, Vincenzo Picotti, Silvia Pondrelli, Frank J. Pazzaglia, Claudio Berti. Submitted to Tectonics 9 November 2009.

DISCUSSION AND CONCLUSIONS

REFERENCES

Abstract

The Northern Apennines (NA) chain is the expression of the active plate margin between Europe and Adria. Given the low convergence rates and the moderate seismic activity, ambiguities still occur in defining a seismotectonic framework and many different scenarios have been proposed for the mountain front evolution. Differently from older models that indicate the mountain front as an active thrust at the surface, a recently proposed scenario describes the latter as the frontal limb of a long-wavelength fold ($>$ 150 km) formed by a thrust fault tipped around 17 km at depth, and considered as the active subduction boundary. East of Bologna, this frontal limb is remarkably very straight and its surface is riddled with small, but pervasive high-angle normal faults. However, west of Bologna, some recesses are visible along strike of the mountain front: these perturbations seem due to the presence of shorter wavelength (15 to 25 km along strike) structures showing both NE and NW-vergence. The Pleistocene activity of these structures was already suggested, but not quantitative reconstructions are available in literature.

This research investigates the tectonic geomorphology of the NA mountain front with the specific aim to quantify active deformations and infer possible deep causes of both short- and long-wavelength structures.

This study documents the presence of a network of active extensional faults, in the foothills south and east of Bologna. For these structures, the strain rate has been measured to find a constant throw-to-length relationship and the slip rates have been compared with measured rates of erosion.

Fluvial geomorphology and quantitative analysis of the topography document in detail the active tectonics of two growing domal structures (Castelvetro - Vignola foothills and the Ghiardo plateau) embedded in the mountain front west of Bologna. Here, tilting and river incision rates (interpreted as that long-term uplift rates) have been measured respectively at the mountain front and in the Enza and Panaro valleys, using a well defined stratigraphy of Pleistocene to Holocene river terraces and alluvial fan deposits as growth strata, and seismic reflection profiles relationships. The geometry and uplift rates of the anticlines constrain a simple trishear fault propagation folding model that inverts for blind thrust ramp depth, dip, and slip.

Topographic swath profiles and the steepness index of river longitudinal profiles that traverse the anticlines are consistent with stratigraphy, structures, aquifer geometry, and seismic reflection profiles.

Available focal mechanisms of earthquakes with magnitude between Mw 4.1 to 5.4, obtained from a dataset of the instrumental seismicity for the last 30 years, evidence a clear vertical separation at around 15 km between shallow extensional and deeper compressional hypocenters along the mountain front and

adjacent foothills.

In summary, the studied anticlines appear to grow at rates slower than the growing rate of the longer-wavelength structure that defines the mountain front of the NA. The domal structures show evidences of NW-verging deformation and reactivations of older (late Neogene) thrusts.

The reconstructed river incision rates together with rates coming from several other rivers along a 250 km wide stretch of the NA mountain front and recently available in the literature, all indicate a general increase from Middle to Late Pleistocene. This suggests focusing of deformation along a deep structure, as confirmed by the deep compressional seismicity. The maximum rate is however not constant along the mountain front, but varies from 0.2 mm/yr in the west to more than 2.2 mm/yr in the eastern sector, suggesting a similar (eastward-increasing) trend of the apenninic subduction.

Abstract

La catena dell'Appennino settentrionale é l'espressione dell'attivitá del margine di placca tra Europa ed Adria. Dati i moderati tassi di convergenza e la moderata attivitá sismica, permangono delle ambiguitá nel definire un chiaro quadro sismotettonico, nonostante numerosi modelli evolutivi siano stati proposti per il fronte montano. Diversamente da alcuni modelli precedenti, i quali indicano il fronte montano come un thrust attivo in superficie, una recente proposta interpretativa descrive quest'ultimo come il lembo frontale di una piega and ampia lunghezza d'onda ($>$ 150 km), prodotta da un sovrascorrimento che termina circa a 17 km di profonditá e che é considerato come il fronte di subduzione attiva. É importante notare che, ad Est di Bologna, questo lembo frontale ha andamento lineare e che la sua superficie é interessata da faglie ad alto angolo di estensione limitata, ma pervasive. Tuttavia, ad Ovest di Bologna, sono visibili alcune interruzioni lungo strike del fronte montano: questi perturbazioni sembrano dovute alla presenza strutture a lunghezza d'onda piú limitata (da 15 a 25 km lungo strike) che mostrano vergenze orientate sia verso NE che verso NW. L'attiviá di queste di strutture é stata giá evidenziata, ma sue quantificazioni non sono presenti in letteratura.

Questo progetto di ricerca si occupa della geomorfologia tettonica del fronte montano dell'Appennino Settentrionale, con l'obiettivo specifico di quantificare e ipotizzare in profonditá le possibili cause delle strutture sia a breve che ad ampia lunghezza d'onda.

Questo studio documenta la presenza di una rete di faglie estensionali attive, al piede della catena a Sud

e ad Est di Bologna. Di queste strutture é stato misurato il tasso di deformazione per determinare una relazione costante tra rigetto e lunghezza ed inoltre si sono comparati i loro tassi di scorrimento con tassi di erosione precedentemente misurati e presenti in letteratura.

La geomorfologia fluviale e l'analisi quantitativa della topografia documentano in dettaglio l'attivitá tettonica di due strutture a domo (la zona al piede delle catena presso Castelvetro e Vignola e l'altipiano del Ghiardo) incassate nel fronte montano ad Ovest di Bologna. Qui, sono stati misurati i tassi di basculamento e di incisione fluviale (interpretati come rappresentativi dei tassi di sollevamento di lungo termine) rispettivamente al fronte montano e nelle valli dei fiumi Enza e Panaro. Queste misurazioni sono state compiute grazie all'utilizzo di una stratigrafia di dettaglio dei terrazzi fluviali pleistocenici ed olocenici e dei depositi di conoide e grazie al loro confronto con profili sismici a riflessione. La geometria ed i tassi di sollevamento ottenuti per queste anticlinali vengono inserti come vincoli in un semplice modello di propagazione di faglia trishear che restituisce la profonditá, l'immersione ed il rigetto del thrust cieco.

I profili topografici di swath (inviluppo medio della topografia) e gli indici di pendenza dei profili longitudinali dei fiumi che incidono la topografia, in corrispondenza delle anticlinali, risultano coerenti con la stratigrafia, le strutture, la geometria degli acquiferi ed i profili sismici a riflessione.

Sono stati analizzati i meccanismi focali dei terremoti con magnitudo Mw compresa tra 4.1 e 5.1, provenienti da una banca dati della sismicitá strumentale degli ultimi 30 anni. Tali tensori evidenziano, a circa 15 km di profonditá, una netta separazione verticale tra gli ipocentri estensionali localizzati piú in superficie e quelli compressivi piút profondi, distribuiti omogeneamente lungo il fronte montano e la zona adiacente al piede della catena.

In sostanza, le anticlinali studiate sembrano crescere con un tasso piú lento di quello della struttura a piú ampia lunghezza d'onda che definisce il fronte montano dell'Appennino Settentrionale. Le strutture a domo sono caratterizzate da deformazioni con vergenza Nord-Ovest e dalla riattivazione di sovrascorrimenti piú antichi (tardo neogenici).

Il tassi di incisione fluviale che sono stati ottenuti in questo studio, insieme ai tassi provenienti da alcuni altri fiumi recentemente studiati nell' Appennino Settentrionale lungo un fronte di 250 km, indicano in modo coerente un generale incremento dal Medio al Tardo Pleistocene. Tale dato lascia supporre che vi sia una concentrazione della deformazione lungo la struttura profonda, come documentato dalla sismicitá di tipo compressivo. I valori massimi di incisione non sono comunque costanti lungo il fronte montano, ma aumentano regolarmente dai 2 mm/anno nella zona ad Ovest fino a circa 2.2 mm/anno nel settore ori-

entale: questo andamento che aumenta muovendo verso Est risulta simile al trend di subduzione appenninica.

Introduction

1.1 Background

Landscape in tectonically active areas results from a complex integration of vertical and horizontal motions of crustal rocks and erosion by surface processes (Burbank and Anderson, 2001). Many landscapes can be thought of as the result of the competition between processes acting to grow the topography and those that tend to lower it. Tectonic geomorphology focuses on the study of this competition and on the interpretation of the geodynamic and geomorphic implication of such landscapes (Burbank and Anderson, 2001). In tectonic geomorphology, a key model currently adopted for reading landscape evolution was proposed by J. Hack (1960). According to this model, when rates of deformation and rates of erosion are sustained for long intervals, landscapes will evolve into a sort of long-term balance or dynamic equilibrium. Thus, variations through time of tectonic and/or erosion rates tend to shift this balance out of equilibrium. In the real landscape, to discern whether a geomorphic system is in a nearly-steady or unsteady state of equilibrium,it is useful to compare (time scales of deformation and of geomorphic processes) the scaling of the elements that characterize the system, the response time or inertia of those elements with respect to imposed changes, and the rates, magnitude and duration of the tectonic forcing (Burbank and Anderson 2001). For example, because of the different of erosion efficiency, fluvial channel processes equilibrate a fault rupture, generated by tectonic impulse of an earthquake, faster than the hillslope processes. In the hillslopes, the fault scarp will persist as a feature in the topography for a longer time. At short time scales, tectonic forcing is commonly unsteady (such as in the example mentioned above), since it results from discrete events as the earthquakes. Increasing the time scale of the analysis to over 10000 years, can smooth out the unsteadiness of the tectonic forcing and average the rates of deformation (Burbank and Anderson 2001). Features such as moraines, marine or river terraces are important geomorphic markers in the field of tectonic geomorphology, because they are created and persist on the landscape at time scales tipical of a single glacial-interglacial cycle (e.g. Bull, 1991; Meyer et al., 1995; Pazzaglia et al., 1998), providing the ideal interval within which document and average past rates of tectonic forcing. Moreover river terraces have been used to document fault offsets or folds (Rockwell et al., 1984; Molnar et al., 1994), and are still

commonly used to measure the rate of vertical stream incision, typically interpreted as the rate of base level fall, inclusive of rock uplift and associated crustal deformation (Wegmann and Pazzaglia, 2009). Terrace deposits are unconsolidated allostratigraphic units with a basal unconformity called a "strath", typically cut across bedrock, and a constructional bench-like top called a "tread" (see Fig. 1) The formation of the landform called "strath terrace" (Bull, 1991) corresponds to a time of erosion and widening of the valley caused by the thin mobile alluvial cover of a bedrock channel (Pazzaglia and Brandon, 2001).

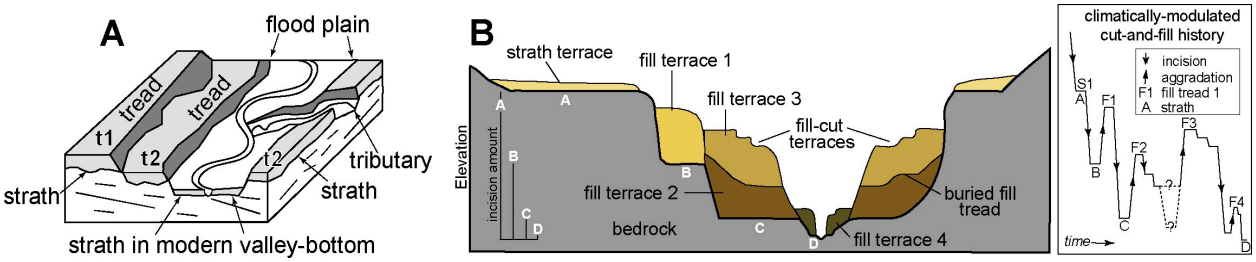

Figure 1: Cartoon and photographic relationships between terraces, terrace deposits and incisionaggradation history as used in this study, modified from Burbank and Anderson, 2001.

The formation of thick alluvial deposits called "fill terraces" (Bull, 1991) corresponds to the time of valley aggradation when the channel is vertically raised above its strath. The passage from aggradation to downcutting, in response to a decrease in sediment supply and/or greater effective discharge (Schumm, 1969; Hancock and Anderson, 2002), leaves the aggradational surface abandoned as a terrace in the valley (Burbank and Anderson, 2001). The initial gradient of the strath is the gradient of the channel that cuts it, approximated in most cases by the modern channel gradient so long as the modern channel has a thin mobile alluvial bed in contact with the bedrock (Wegmann and Pazzaglia, 2009). Where a strath lies in the landscape, when it was carved, and when it was abandoned by incision are predominant considerations leading to a useful terrace genesis model, particularly one that is portable to tectonic problems. The longitudinal profile of correlated strath surfaces and the vertical separation between those surfaces and modern channel bedrock allows to constrain rates of tectonic deformation.

A river that is neither aggrading nor degrading can be considered to be in equilibrium (Bull, 1991). In such a river the formation of terraces is the geomorphic and sedimentologic expression of unsteady vertical channel incision (e.g. Schumm et al., 1987; Bridgland, 2000) that may occur over short-time scales in response to transient changes in sediment and water input to channels, or due to changes in base-level as an effect of changed climatic conditions. The rate of fluvial incision into bedrock is commonly interpreted as the

rate of rock uplift with the built-in assumption that strath formation is a shorter-term transient phenomenon embedded in a long-term quasi-equilibrium channel profile (Mackin, 1948) more or less represented by the gradient of the modern river profile (Knox, 1975; Bull and Knuepfer, 1987; Merritts et al., 1994; Personius, 1995; Burbank et al., 1996; Lave and Avouac, 2000; Pazzaglia and Brandon, 2001; Wegmann and Pazzaglia, 2002). Finally, the use of fluvial terraces to constrain rock deformation is based on the premise that vertical channel incision is primarily a response to rock uplift, and that other contributions to downcutting, such as distal base-level fall and climatically modulated changes in watershed hydrology can be independently determined (e.g., Rockwell et al., 1984; Lavé and Avouac, 2000). Within these settings, kinematic scenarios resulting in different uplift patterns at the surface should be distinguished using the geometry of fluvial terraces (Wilson et al., 2009). In order to use this terraces geometry and calculate tectonic rates, the formation age of the strath must be constrained.

Nevertheless, the absence of well-documented age for these surfaces is the most typical difficulty in extracting tectonic informations (Burbank and Anderson, 2001). Radiocarbon dating is used for the Holocene and Upper Pleistocene deposits, sampling where possible directly above the strath. As support to the difficulty in finding datable material, the creation of soil chronosequences, based on soil characters related to age and climate has been proved useful. Particularly for Holocene to uppermost Pleistocene soils (Eppes et al., 2008), this method serves as a descriptive methodology for correlating alluvial bodies and their topping soils, and for recognizing alluvial bodies on top of which soils develop.

Observations from tectonically active settings demonstrate that straths lie at variable distances above the modern valley bottom, but their ages tend to cluster around periods coincident with known climatic changes, leading geomorphologists to claim for climate change as the main driver of the periodic incision necessary for terrace genesis (Bull, 1991; Merritts et al., 1994; Meyer et al., 1995; Burbank et al., 1996; Pazzaglia et al., 1998; Lav and Avouac, 2001; Pazzaglia and Brandon, 2001).

In absence of numeric ages, particularly for deposits older than the radiocarbon method can detect, the best approximation for terrace strath age is the chronology of the marine oxygen isotope record as a long-term framework for identifying likely times of strath cutting and channel aggradation or incision (e.g. Bridgland and westaway, 2008).

In contrast to efforts aimed at directly measuring tectonic geomorphic processes, the interactions between deformation and surface processes can also be studied theoretically. Complex models for landscape evolution in different tectonic environments have recently been formulated. In particular simple models (for

both detachment and transport-limited systems) predict power-law relations between channel gradient and drainage area in the form of equation (e.g. Whipple and Tucker, 1999; Willgoose et al., 1991).

Given the complexity of the Northern Apennines and the different scenarios proposed for the evolution of the mountain front, we choose to study this area using tectonic geomorphology.

1.2 Geological setting

The Northern Apennines are a fold and thrust belt developed as the pro-wedge of the subducting Adria plate since the Oligocene. They are a known worldwide as an example of a retreating boundary (sensu Royden 1993), for their coeval character of compression at the front and extension at the hinterland (Elter et al., 1975). The main mountain front of the Northern Apennines is commonly interpreted as a continuous thrust structure (also known as Pede-Apenninic Thrust Front PTF, Boccaletti et al., 1985) that offsets Quaternary deposits and locally may be emergent (e.g. Boccaletti et al., 2004; Lavecchia et al., 2003; 2004; Picotti and Pazzaglia, 2008), as an out-of-sequence thrust rooted deep in the wedge. In contrast, the buried front of the Northern Apennines, i.e. the outermost thrust, is sometimes viewed as the true active front of the Northern Apennines (Scrocca, 2006), but this view cannot explain the rapid Quaternary growth of the main geomorphic feature, i.e. the mountain front, since the thrust front creates almost no relief. Near Bologna, the PTF or its attendant splays do not appear to be emergent. Here the PTF is a deep, steep, blind structure associated with the frontal limb of an antiform that defines the mountain front (Picotti and Pazzaglia, 2008). Progressively deformed alluvial fan and river terrace growth strata (Picotti and Pazzaglia, 2008) clearly document this large-wavelength foreland-dipping flexure, in which however, small, but pervasive high-angle normal faults (Picotti et al., 2007) are embedded. However, locally west of Bologna, in the Emilia foothills and adjacent Po Plain, shallow splays of the PTF remain active in the Miocene - Pliocene thrust belt (e.g. Scrocca et al., 2007). The geometry of the Quaternary activity is complex. Since the middle Pleistocene, deformation appears to be concentrated in building the mountain front and defining the southern boundary of the Po basin (Picotti and Pazzaglia, 2008), however, geomorphic and stratigraphic features suggest as well shortening to the northwest, oblique to the pre-Quaternary direction (Gasperi et al., 1999; Picotti et al., 2007), having a clear topographic expression moving west of Bologna, where the shape of the mountain front is more irregular and affected by local dome and swell interference short- wavelength structures (see Fig. 2).

Why are there not short-wavelength structures east of Bologna? Is it possible to identify a geometric and

cinematic continuity of the deep thrust west of Bologna? In which term are the short-wavelength structures connected with the deep structure? How this tectonic data frame matches with the seismicity of the area? To answer these scientific problem, the Northern Apennines mountain front has been analyzed with in three different papers published or submitted to scientific reviews.

1.3 Aim and outline of the thesis

In order to respond to the previous questions, aim of this research is to use the tectonic geomorphology to analyze and quantify the active deformations of the Northern Apennines mountain front, in places where tectonic activity has been suggested (Bernini and Papani, 1987; Gasperi et al., 1999) but no quantitative reconstruction are available in literature. The resulting tectonic dataframe is to be integrated and validated by the comparison with subsurface, seismic, geomorphic and geodetic independent datasets. As already mentioned, three scientific papers form the core of this research.

In paper 1, ***Topographic expression of active faults in the foothills of the Northern Apennines***, the imprint that active faults leave in the earthÕs surface is identified, using a combination of geomorphic and geologic metrics including triangular facets, the shape of mountain front, the drainage network, and incised river valleys with inset terraces. The goal is to provide a representative view of high angle, mostly normal faults in the foothills of the Northern Apennines in the lower Reno valley and east of Bologna, including documentation of their throw, strike lengths, and slip rates. These data are further explored to discuss the role of high angle faulting in shaping the Apennine landscape and the broader, formative underlying tectonic/geodynamic processes.

Paper 2, titled ***Thrust-fold growth history at the mountain front of the Northern Apennines from quantitative landscape analysis***, focus on the analysis of fluvial channels, Quaternary deposits, and swath topographic profiles. Two areas of study are located $\sim$ 40 km and $\sim$ 80 km west of Bologna, respectively in the Castelvetro - Vignola foothills and the Ghiardo plateau near San Polo d'Enza (see Fig. 2 and 3 in Paper 2). In particular, at Castelvetro (Mo), two distinct anticlines show evidence of interaction of two deformation trends: the so-called Apenninic WNW and the anti-Apenninic NE, with a final dome-and-swell geometry. The Ghiardo plateau is an east-west-elongated hill that sits several kilometers north of the mountain front. This area attracted our interest because here the mountain front is defined by to-

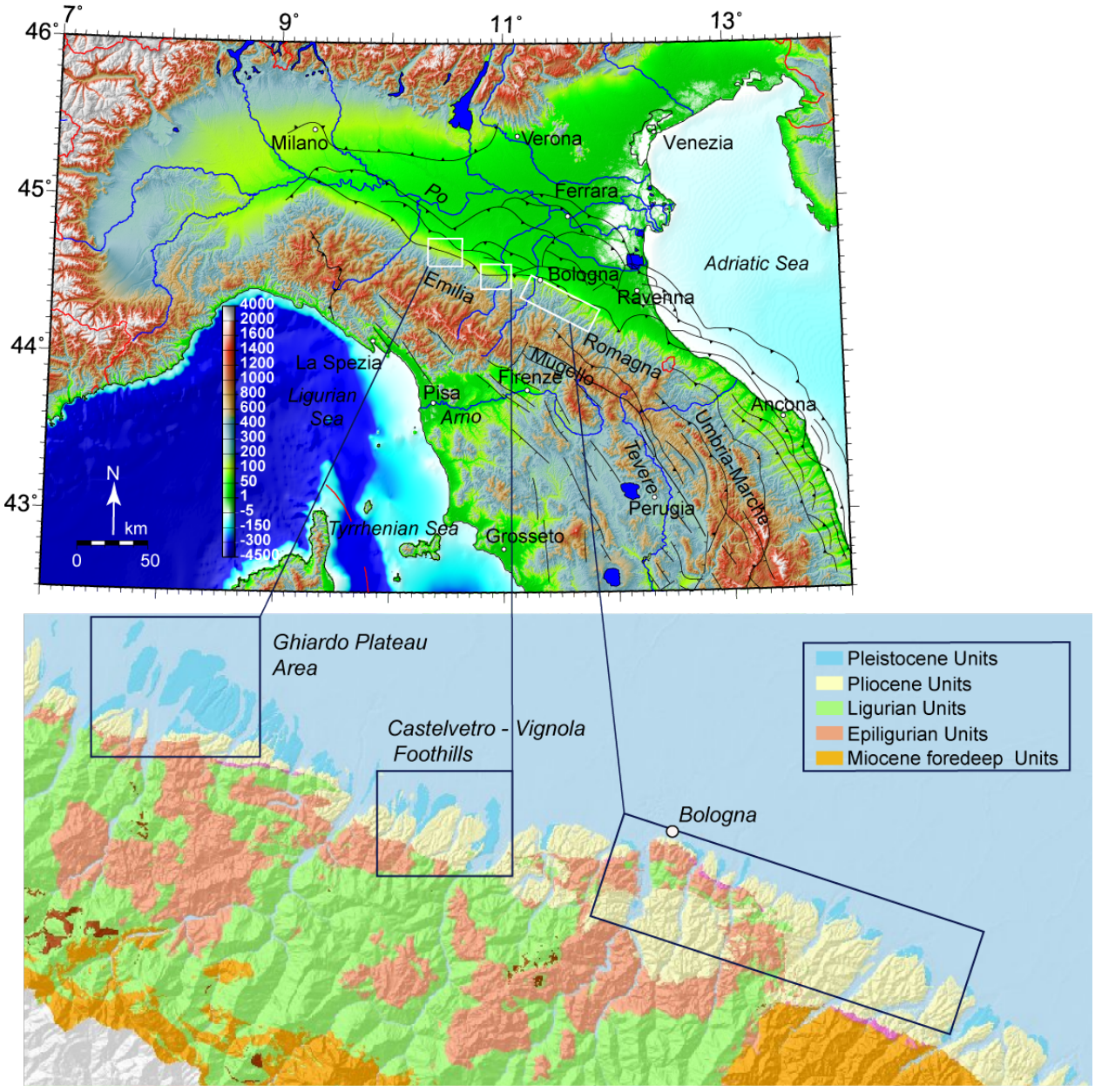

Figure 2: The foothills of the Northern Apennines: the boxes represent the areas investigated in the three papers presented in this thesis.

pographically striking flatirons underlain by middle Pleistocene conglomerates, that led Bernini and Papani (1987) and Boccaletti et al. (2004) to argue for emergence of the PTF. The main goal is to extract the signal of channel response to active tectonics by stream channel steepness analysis and test the sensitivity of the method in an area of low-noise background of climate change and lithologic variation. The behavior of steepness index of river longitudinal profiles has been analyzed for channels that have comparable discharge in the reaches where they traverse across the culmination of the anticlines. Topographic swath profiles and the steepness index have been compared with field stratigraphic, structural mapping, aquifer geometry, and seismic reflection profiles relationships.

Paper 3, ***The active deep mountain front of the Northern Apennines: seismicity and geomorphology***, improves the previous study in the Castelvetro - Vignola foothills and in the Ghiardo Plateau, with the aim to quantify and determine the style of the deformation of the local short-wavelength anticlines. The two domal structures have been studied in detail, using Pleistocene river terraces as growth strata, and reflection seismic profiles. River incision and uplift rates for the Enza and Panaro valleys have been measures, as well as the tilting rate of the mountain front, using a terrace and alluvial fan stratigraphy that produced a unified inter-basin chronostratigraphy across the Northern Apennines (Eppes at al., 2008, Picotti and Pazzaglia 2008, Wegmann and Pazzaglia 2009, Wilson et al., 2009).

The connection of these surficial compressional structures with the deep structure building the mountain front have been investigated, and a simple trishear fault propagation folding model has been constrained with the geometry and uplift rates of the anticlines.

In conclusion, the activity and structural characteristics of the different wave-length structures have been compared, at regional scale, with moment tensors available for the seismicity with magnitude between Mw 4.1 to 5.4 for the last 30 years, the velocity field for Africa-Europe convergence reconstructed from GPS data (D'Agostino et al. 2008), the Late Pleistocene to Holocene Apenninic trend of river incision obtained from rates measured in the Enza and the Panaro valleys by this study, in the Reno valley by Picotti and Pazzaglia (2008), in the the Bidente valley by Wegmann and Pazzaglia (2009) and finally by Wilson et al., (2009) in the Stirone valley. On the basis of this comparison, a seismotectonic interpretation of the evolution of the mountain front has been proposed.

Tectonophysics 474 (2009) 285–294

Contents lists available at ScienceDirect

Tectonophysics

journal homepage: www.elsevier.com/locate/tecto

Topographic expression of active faults in the foothills of the Northern Apennines

Vincenzo Picotti [a], Alessio Ponza [a,*], Frank J. Pazzaglia [b]

[a] Università di Bologna, Dipartimento di Scienze della Terra e Geologico Ambientali, Via Zamboni 67, 40127 Bologna, Italy
[b] Department of Earth and Environmental Science, Lehigh University, 31 Williams, Bethlehem, PA 18015, USA

ARTICLE INFO

Article history:
Received 6 March 2008
Received in revised form 16 September 2008
Accepted 2 January 2009
Available online 19 January 2009

Keywords:
Active faults
Topography
Surface processes
Foothills
Northern Apennines

ABSTRACT

Active faults that rupture the earth's surface leave an imprint on the topography that is recognized using a combination of geomorphic and geologic metrics including triangular facets, the shape of mountain fronts, the drainage network, and incised river valleys with inset terraces. We document the presence of a network of active, high-angle extensional faults, collectively embedded in the actively shortening mountain front of the Northern Apennines, that possess unique geomorphic expressions. We measure the strain rate for these structures and find that they have a constant throw-to-length ratio. We demonstrate the necessary and sufficient conditions for triangular facet development in the footwalls of these faults and argue that rock-type exerts the strongest control. The slip rates of these faults range from 0.1 to 0.3 mm/yr, which is similar to the average rate of river incision and mountain front unroofing determined by corollary studies. The faults are a near-surface manifestation of deeper crustal processes that are actively uplifting rocks and growing topography at a rate commensurate with surface processes that are eroding the mountain front to base level.

1. Introduction

Fault distribution may strongly influence landscape evolution in actively deforming areas and are of particular interest for seismic hazard assessment and especially when characterized by high slip rates (McCalpin and Nelson, 1996; Keller and Pinter, 1996). Along tectonically active mountain fronts, high angle normal faults are commonly easily recognized by their sharp relief caused by uplift of the footwall and enhanced subsidence of the hangingwall basin, causing development of exposed escarpments. In contrast, normal faults distal to the active mountain front may less distinct because of burial by sediments washed into the subsiding hangingwall basin, or concealment by surficial processes, such as large-scale mass movements in the footwall block. Nevertheless, high angle normal faults embedded in the hinterland of mountain ranges have clear geodynamic implications for the processes that uplift and deform rocks to make mountains despite their variable slip rates. How those faults interact with surface processes to make topography remains a topic of vigorous discussion (e.g. Roberts and Michetti, 2004).

In this paper, we investigate the foothills of the Northern Apennines, a mountain range characterized by rapid Pliocene and Pleistocene uplift and exhumation (Balestrieri et al., 2003; Bartolini, 2003). The Apennines mountain front and its adjoining foothills are riddled with geologic and geomorphic evidence of active tectonics such as growing folds and faults that collectively represent the near-surface structural response of ongoing Adria-Europe convergence (Bertotti et al., 1997; Capozzi and Picotti, 2002; Simoni et al., 2003; Picotti and Pazzaglia, 2008). This mountain front is commonly described as an out-of sequence structure that is backstepping with respect to the tip of the northern Apennines deformed wedge, presently buried below the plain of the Po river (Fig. 1; Picotti and Pazzaglia, 2008, with references). The northeast verging accretionary wedge of the Northern Apennines is considered inactive because it is sealed by almost undeformed alluvial deposits of Middle Pleistocene to Holocene (see Fig. 1b). Locally, in the Emilia foothills and adjacent Po Plain, however, some thrusts appear reactivating the thrust belt in various ways (e.g. Scrocca et al., 2007), but with remarkable differences, such as a northwest vergence (Picotti et al., 2007). Furthermore, the mountain front of the Northern Apeninnes is thought to be the emergence of a thrust cutting through the Quaternary (e.g. Boccaletti et al., 2004). In a recent paper, Picotti and Pazzaglia (2008) documented that the structure, also known as Pede-Apenninic Thrust Front, does not exist as continuous feature in the upper crust, whereas the present-day compression is accounted by a steep blind ramp, located at around 15 to 18 km of depth. In this frame of ongoing subduction and active compression in the middle crust, the normal faults we intend to describe are active in the upper crust only (Fig. 1b) and have been related to two different processes (see Picotti and Pazzaglia, 2008). In the south, toward the water divide, the stretching, documented also by geodetic strain measurements (e.g. GPS data in Serpelloni et al., 2005), is thought to be associate to the retreat of the upper (Tyrrhenian) plate, a process prograding from the Tyrrhenian back-arc basin toward the northeast since the Pliocene time (Elter et al., 1975). To the north, at the foothills close to the mountain front, the normal faults appear associated to the growing ramp anticline as upper crustal expression

* Corresponding author. Tel.: +39 051 2094574; fax: +39 051 2094522.
E-mail address: alessio.ponza@unibo.it (A. Ponza).

0040-1951/$ – see front matter © 2009 Elsevier B.V. All rights reserved.
doi:10.1016/j.tecto.2009.01.009

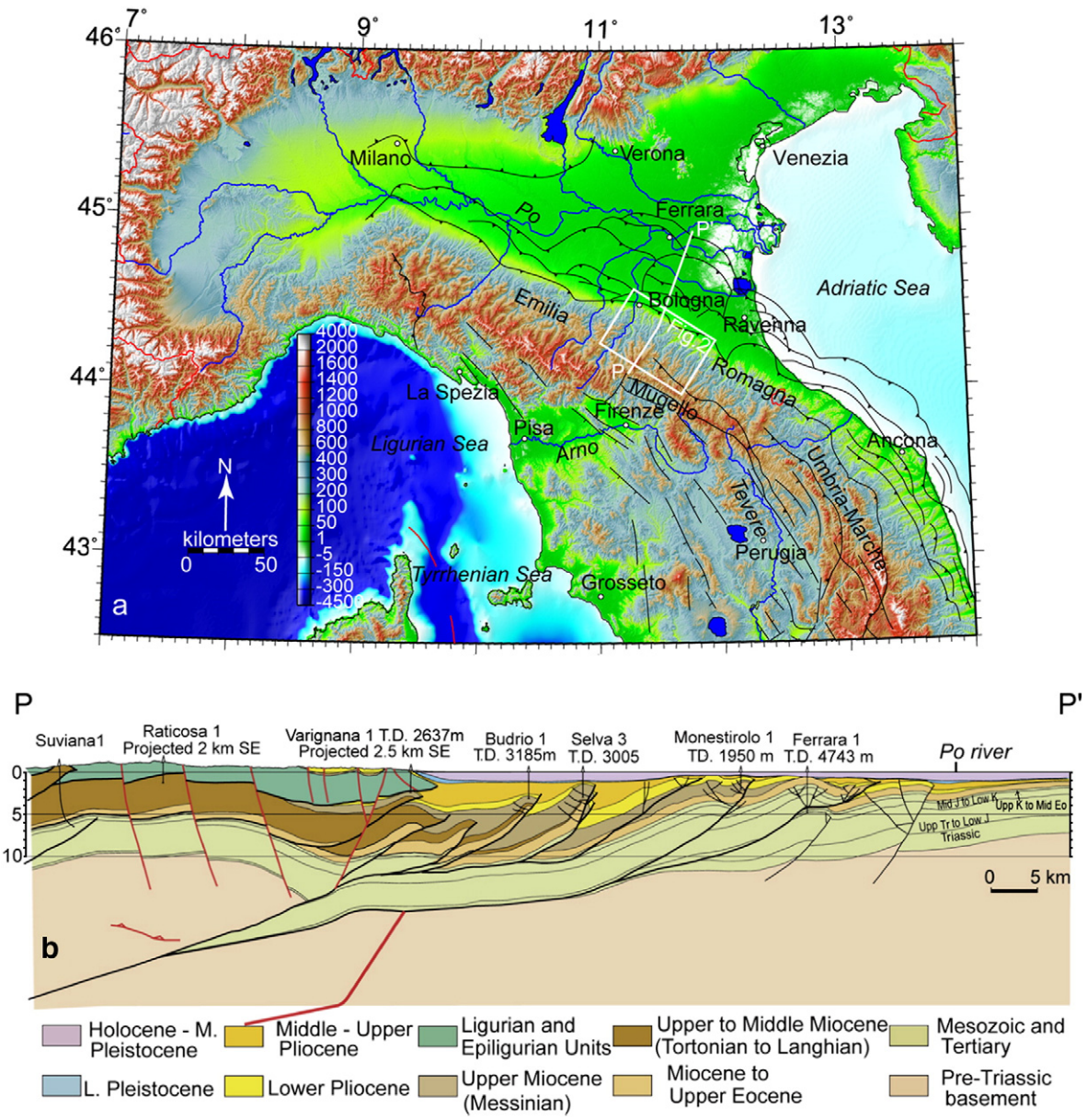

Fig. 1. a) Location of the studied area in the foothills of the Northern Apennines at the boundary between the extensional and the compressional realms. Note the track of the cross section PP′, and the location of Fig. 2 (white box). b) Cross section across the front of the Northern Apennines, showing the structural style of the frontal accretion, already inactive. The red faults represent the active features, normal faults at the surface and compressional structures in the middle crust (modified after Picotti and Pazzaglia, 2008). (For interpretation of the references to colour in this figure legend, the reader is referred to the web version of this article.)

of the middle crustal thrust. The association of normal faulting on the crest of the anticlines is common (e.g. Morley, 2007) and it is due to the inversion of the local stress field in the outer arch of the fold.

Our goal is to provide a representative view of high angle, mostly normal faults in the foothills of the Northern Apennines around Bologna including documentation of their throw, strike lengths, and slip rates. These data are further explored to discuss the role of high angle faulting in shaping the Apennine landscape and the broader, formative underlying tectonic/geodynamic processes.

The most important data applied for our analysis is a geologic map synthesized from our observations and key published maps and reports (see Picotti and Pazzaglia, 2008 and reference therein), supplied with balanced cross sections, regional DEM-based topographic and river course analyses, aerial photography and satellite imagery. Also, offsets of surface of sedimentary recent deposits such as alluvial terraces have been utilized in identifying recent faults. We present a dataset of faults, some of which already known in literature, and discuss the data in terms of their structural development, their interaction with the other landscape-shaping processes such as rock-type resistance to erosion, and some of their implications for seismic hazards. Our data argue for the predominance of high angle normal faults embedded in the carapace of an actively shortening mountain range. Furthermore, we find that footwall blocks tend to have higher rates of watershed-averaged cosmogenically-measured erosion (Cyr and Granger, 2008) than directly adjacent hangingwall blocks.

2. Data

2.1. The S. Luca–Reno fault

The surface trace of the S. Luca–Reno fault develops 7 km with north–south trend. It is a normal fault that dips to the west and defines the eastern flank of the lower reach of the Reno River valley (Figs. 2

and 3). The fault runs along the markedly linear eastern flank of the Reno valley and is characterized by west-facing mountain-front facets, already reported by Boccaletti et al. (2004). Virtually all of the terraces of the river deposits are preserved on the west side of this part of the Reno valley with the Reno channel restricted to the east side of its markedly asymmetric valley. Evidence for west to east shifting of the mouth of the Reno during the Pleistocene is also mirrored by coarse fluvial deposits of Reno provenance interbedded with the littoral Sabbie di Imola toward the Lavino valley which is west of current river location. The S. Luca–Reno fault terminates in the north at the Bologna mountain front escarpment whereas its southern tip steps eastward and is developed as an ENE-striking fault (Fig. 3). The bedrock of the footwall consists of Lower Miocene limestones and marly limestones. At the mountain front, the youngest geological unit cut by this fault is the Middle Pleistocene Sabbie di Imola (about 700 kyr), as any offset of younger Pleistocene terraces or hillslope deposits is ambiguous. Offset of the Sabbie di Imola indicates ~150 m of throw (see Fig. 4a and b), for a mean slip rate of ~0.2 mm/yr (profile AA′ in Fig. 4a). In the middle of the fault, the footwall lithology transitions to mudstones and scaly argillites and the throw increases to 230 m (Fig. 4b) with a slip rate of ~0.3 mm/yr (profile BB′ in Fig. 4b). In spite of this major fault activity, the footwall does not show facets and its topographic crest is shifted to the east. The displacement–length ratio (Dmax/L) for this structure is around 0.03 and falls on the line defining normal faults proposed by Kim and Sanderson (2005).

The triangular facets, generally considered valid indicators of mountain fronts bound by active faults, rarely represent the original, exhumed fault plane but rather its degradational scarp (e.g. Bull and Fadden, 1977). Thus, the facet slope reflects a balance between the rate of fault slip, soil development, and hillslope erosion (Menges, 1990). Rock resistance strongly controls the latter for faults, so that faceted surfaces are not preserved in exposure, where the footwall is dominated by mudstones and argillites, as in the southern reach of the S. Luca–Reno fault. In the northern reach of the fault, the calcareous nature of the bedrock allows development of triangular facets. Here a 15 m long tunnel (excavated during the WW II as bomb shelter) offers a cross section through the footslope, with its surficial deposits and structural features for study (Fig. 5). The exposure is characterized by a colluvial ~1 m thick, consisting of bedrock clasts embedded floating in a brownish soil matrix. This colluvium unconformably overlies a wedge of slope debris, dipping 35° toward west, consisting of a stratified sedimentary breccia, mostly cemented and matrix supported, with local clast-supported layers (see picture in Fig. 5). The breccia unconformably overlies a smooth surface of bedrock, dipping 40°, representing the buried triangular facet (see picture in Fig. 5).

No absolute determination is available for the surficial units, but their texture, stratigraphy, and soil development of the colluviums is very similar to Holocene colluviums described for the Reno valley (Eppes et al., 2008), whereas the breccia is a late Pleistocene periglacial deposit.

Two possible alternatives are provided, both supported by available data (see Fig. 5). Fig. 5a illustrates both slope deposits covering the Qt5 alluvium of Picotti and Pazzaglia (2008) that is well dated to the onset of deglaciation at around 19 ky. Fig. 5b shows the units burying the Qt4 alluvium that is believed to be ~35 ky old (Wegmann and Pazzaglia, in review). Both interpretations support a latest Pleistocene age for the slope breccia (19–11 ky) and a Holocene age for the colluvium (see Fig. 6 of Picotti and Pazzaglia, 2008). Similar colluvial units commonly bury the treads of terraces Qt4, Qt5, and Qt6 in the Reno valley and these colluvial wedges have yielded primarily middle Holocene radiocarbon ages (Amorosi et al., 1996; Eppes et al., 2008).

The bedrock exposures for the first 2 m down-tunnel show a tight (around 10 cm) spacing of anastomising fractures that dip 45–50° to the west, whereas the next 5 m show a frequency decrease (about 40 cm of spacing) of similarly dipping fractures. These fractures do not show evidence of slip, disappear toward the interior of the tunnel, and clearly control the dip of the external slope and are believed to belong to the damage zone (*sensu* Chester and Logan, 1986; Billi et al., 2003; Kim et al., 2004) associated with the master fault. This must have been located a few meters to the west of the slope and now mostly eroded.

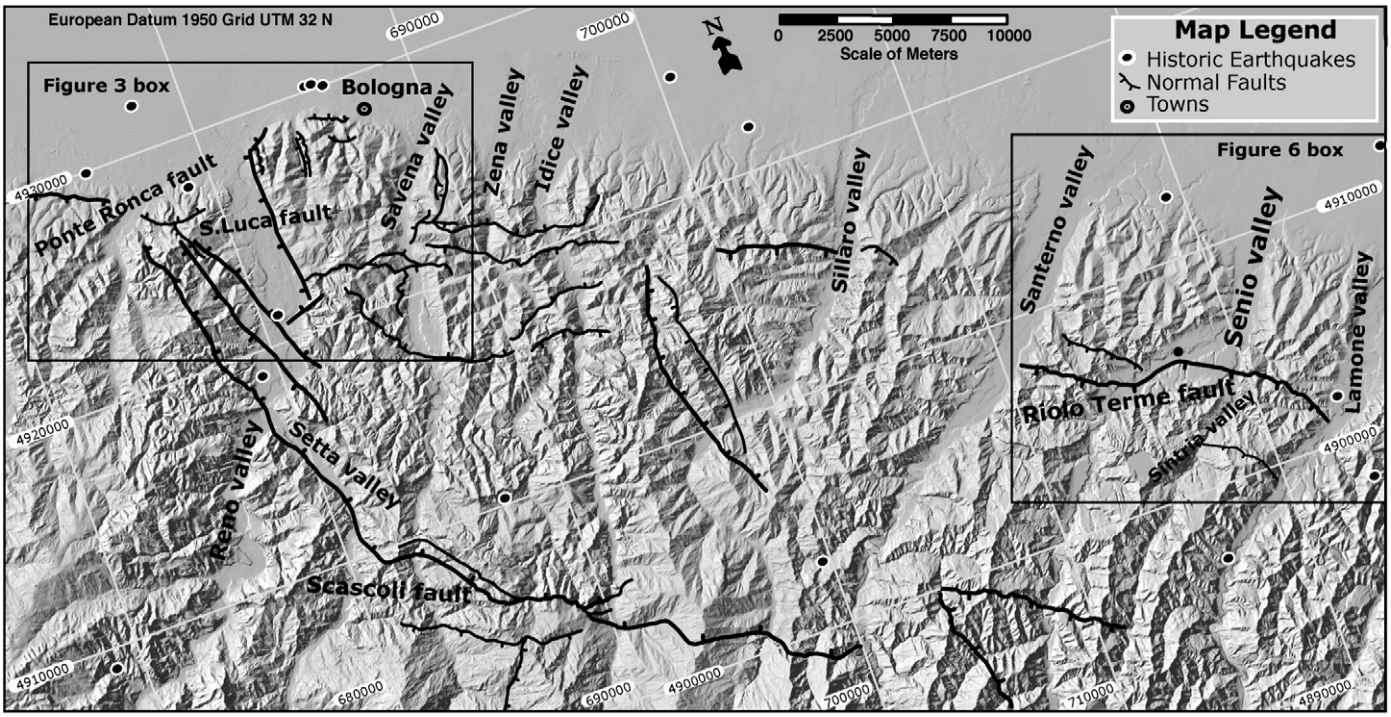

Fig. 2. The foothills of the Northern Apennines around Bologna and the faults described in this paper. The normal faults are represented with barbs on the downthrown limb. The dots represent the location of historical events (last 700 years) after the Italian catalog CPTI (from http://emidius.mi.ingv.it/DOM/).

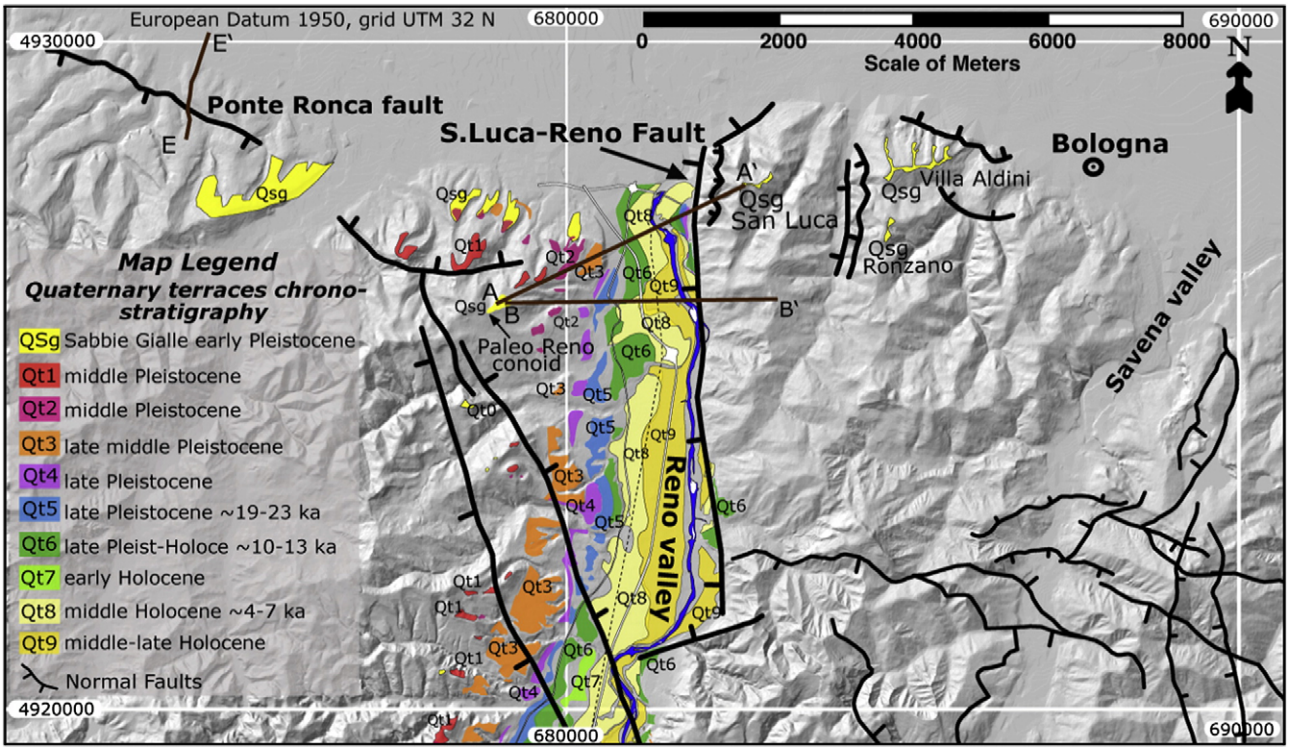

Fig. 3. DEM map of the lower intramontane reach of the Reno valley, showing the position of the active faults and the Pleistocene to Holocene continental deposits (modified after Picotti and Pazzaglia 2008). AA′ and BB′ are the traces of cross sections in this figure, EE′ is the trace of the seismic profile shown in Fig. 6.

Two additional fault planes (Fig. 5), showing millimetric normal movement with top to the west parallel to the master fault, are exposed several meters further into the tunnel interior.

2.2. The Riolo Terme fault

The Riolo Terme fault strikes WNW and its surface trace can be followed for approximately 12 km. Its terminations are poorly defined due to small displacement and lack of stratigraphic correlation points, because it affects homogeneous bedrock. Furthermore, the fault cuts across Pliocene and Pleistocene mudstones (Argille Azzurre Fm), which makes it difficult to identify its exact location, except where distinct biozones are recognized and correlated in the hangingwall and footwall (Fig. 6). We studied this fault through two profiles across the interfluves where biostratigraphic data are available from two unpublished thesis works (Viaggi, 1991; Sami, 1992, Fig. 6). The profiles show a general dip to the northeast, with a decrease of the dip from south to north. The southwest dipping normal fault creates an asymmetric hogback with steeper southern slopes. Given this lithology and the present-day climatic conditions, the gradient of the southern slopes are determined by weathering, whereas the northern slopes are soil-mantled and transport-limited. As an example of the role of rock resistance in weathering-limited southern slopes, the highest hill visible in the profiles of Fig. 6 consists of bedded gypsum of Messinian age, particularly resistant also because of the effective infiltration associated to karst evolution.

The Riolo Terme fault in the Santerno–Senio interfluves (Fig. 6b, profile C–C′) displaces the Upper Pliocene sequence of the Argille Azzurre by about 260 m, whereas another smaller normal fault about 2 km to the north is associated with around 100 m of

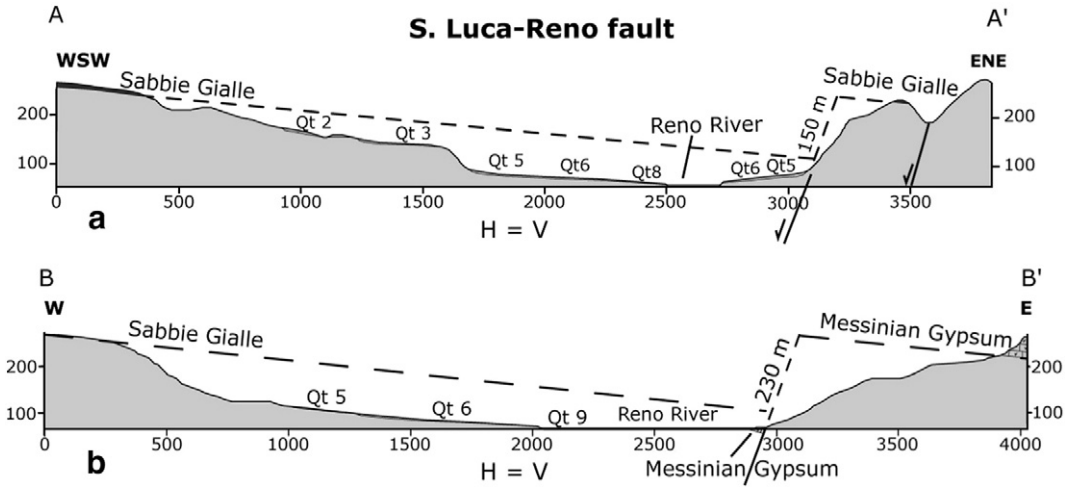

Fig. 4. Cross sections across the S. Luca–Reno fault. In a), note the stratigraphic separation of the Middle Pleistocene Sabbie Gialle. In b), the vertical throw is measured using the separation of the Messinian evaporites.

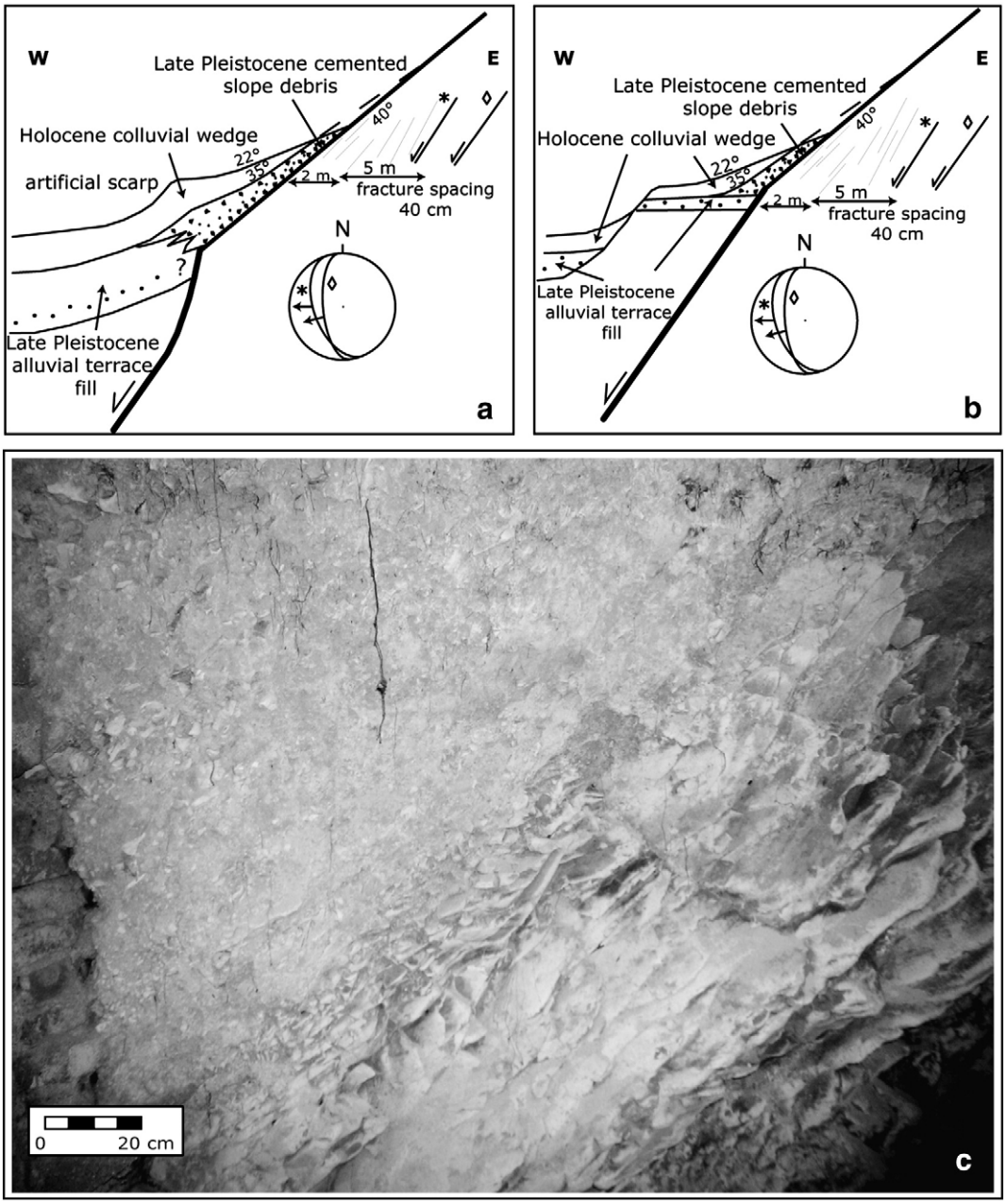

Fig. 5. A section across a triangular facet. a) and b) show two possible interpretations of the geological situation observed in the tunnel entering the base of slope of the facet. Two meso-scale faults are projected in the stereonet. Interpretation a) is that of a blind fault, where the deformation of the latest Pleistocene and Holocene is accommodated by folding of the surface units. Interpretation b) suggests that the fault cuts almost to the surface and a configuration of the alluvial terraces different than that of interpretation a). c) displays the bedrock contact of the bedded slope debris. Note the smooth surface and the tight spacing of the fracturing in the bedrock.

stratigraphic normal throw. Some 9 km to the east toward the Lamone valley, the Riolo Terme fault shows ~250 m of total separation, while cutting the Lower Pleistocene Argille Azzurre. This area (Fig. 6c, profile D–D′) displays a third fault situated to the south of the Riolo Terme fault. This latter is a south-dipping normal fault cutting through the Messinian succession. This fault disrupts the continuity of the gypsum hogback, offsetting the northern structural slope with some 100 m, which corresponds to the height of the present-day topographic escarpment.

The slip rate of the main Riolo Terme fault is 0.35 mm/yr, if we infer the onset of slip to be Middle Pleistocene, as is the case for the S. Luca–Reno fault, for example. A lower estimate of ~0.18 mm/yr is calculated if the onset of faulting is Lower Pleistocene rather than Middle Pleistocene. The Dmax/L of the Riolo fault is ~0.02–0.03 if we consider the other smaller faults as linked to the same fault system. This value falls below the normal fault line of Kim and Sanderson (2005). Either this fault has abnormally small amounts of slip for its length or we are underestimating the slip due to lack of definitive offset stratigraphic horizons.

The Riolo Terme fault effectively intercepts the subsurface fluid circulation and allows natural seepage of both formation and meteoric waters. These seeps have been used since the Middle Age for their positive effects on health and/or as a source of salt (see Fig. 6c). Similarly, there is a source of sulfur-rich water located at the most depressed point where the fault intercepts the topography, i.e. the Senio valley bottom. The formation waters, supplied by deeper Tertiary reservoirs, on the contrary, form seeps at several points along the fault, seemingly independently of the topography. The positions of these seeps suggest that the fault zone, here cutting across mudstones, acts an effective conduit to deep aquifers.

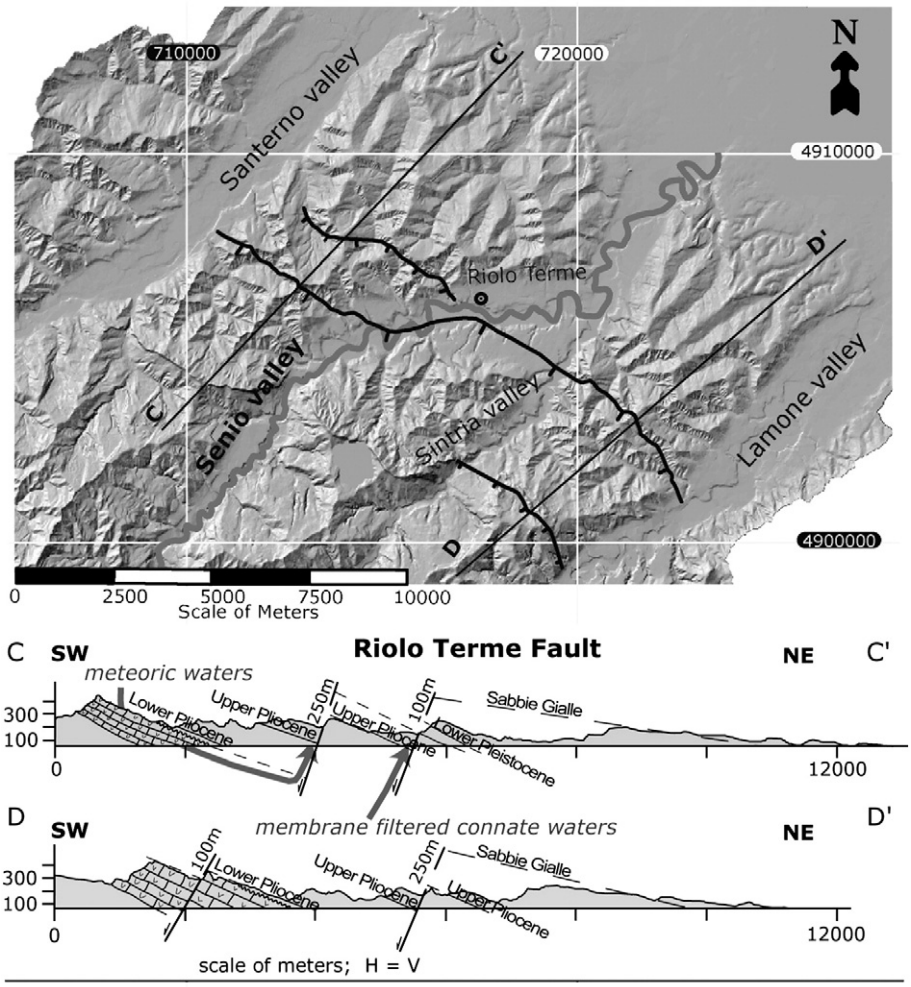

Fig. 6. The Riolo Terme fault and two cross sections showing the structures and the stratigraphic separations, documented through biostratigraphic data. Note the presence of secondary faults and of an active subsurface water circulation, effectively interrupted by the faults. The Riolo Terme fault drains essentially meteoric waters, whereas connate waters are seeping along the secondary fault.

2.3. The Ponte Ronca fault

The surface trace of the Ponte Ronca fault strikes WNW and is detectable for a distance of approximately 4 km along the mountain front. This feature has been recently identified in a high resolution high-angle reflection seismic profile, acquired during the NSF project RETREAT (REtreating TRench, Extension, and Accretion Tectonics) (see Picotti and Pazzaglia, 2008). This southwest dipping fault has a measured maximum throw of 120 m (Fig. 7; applying for a Dmax/L of 0.03) and offsets middle Pleistocene to Holocene deposits. In the seismic line, it is seen that the hangingwall of the Ponte Ronca fault is subsequently cut by several other minor faults (Fig. 7). The reflectors corresponding to the interval from the Sabbie di Imola to recent colluvium, display growth configuration in the hangingwall of the Ponte Ronca fault. Still, its middle Pleistocene activity cannot be determined, due to the absence of the Synthem Emiliano Inferiore (deposited between 600 and 400 ky, Fig. 7) that pinches out a few hundreds of meters to the north of the fault. The calculated mean long-term slip rate is ~0.13 mm/yr, with a possible increase in the slip rate during latest Pleistocene to Holocene, depending on the precise age of the undated surficial colluviums.

2.4. The Scascoli fault

The Scascoli fault (Bertotti et al., 1997) is the southernmost and the longest of the studied faults of the foothills of the Northern Apennines (Figs. 2 and 7). It has recently been crossed by the High Velocity Railway tunnel that allows for a detailed investigation of its configuration and to determine its offset that locally reaches more than 1000 m (see Figs. 2 and 8). The total fault system length is around 32 km, beginning on the west side of the Reno Valley, where it cuts the middle Pleistocene alluvial terrace Qt1 (~600 ka) (Picotti and Pazzaglia, 2008). It can be followed to the east towards the Santerno valley, traversing the Setta, Savena, Zena, Idice and Sillaro valleys with a clear topographic expression (see Fig. 2).

The Scascoli fault has Dmax/L ratio of 0.031, a value similar to the other faults, suggesting self-similarity of the deformation matrix in the northern Apennine foothills. Given a similar Dmax/L ratio, the larger displacement and length of the Scascoli fault can be interpreted to have either a rapid slip rate (~1.4 mm/yr) on a young fault initiated in the middle Pleistocene, or a slower slip rate, similar to other foothills normal faults, on a much older fault system of late Pliocene–early Pleistocene age. The slow slip is our preferred interpretation, owing that the growth rate of each fault is strongly controlled by the rheology of the upper crust. Moreover, a late Pliocene age of the Scascoli fault is in agreement with the onset of exhumation of this side of the Northern Apennines (Zattin et al., 2002) and the observation that, south of the water divide, the onset of the normal faults are late Pliocene–earliest Pleistocene, as documented by the clastic infill of the Mugello graben (see Fig. 2, Benvenuti, 1997).

The High Velocity Railway tunnel unexpectedly broke through the fault plane during construction and immediately experienced a seepage

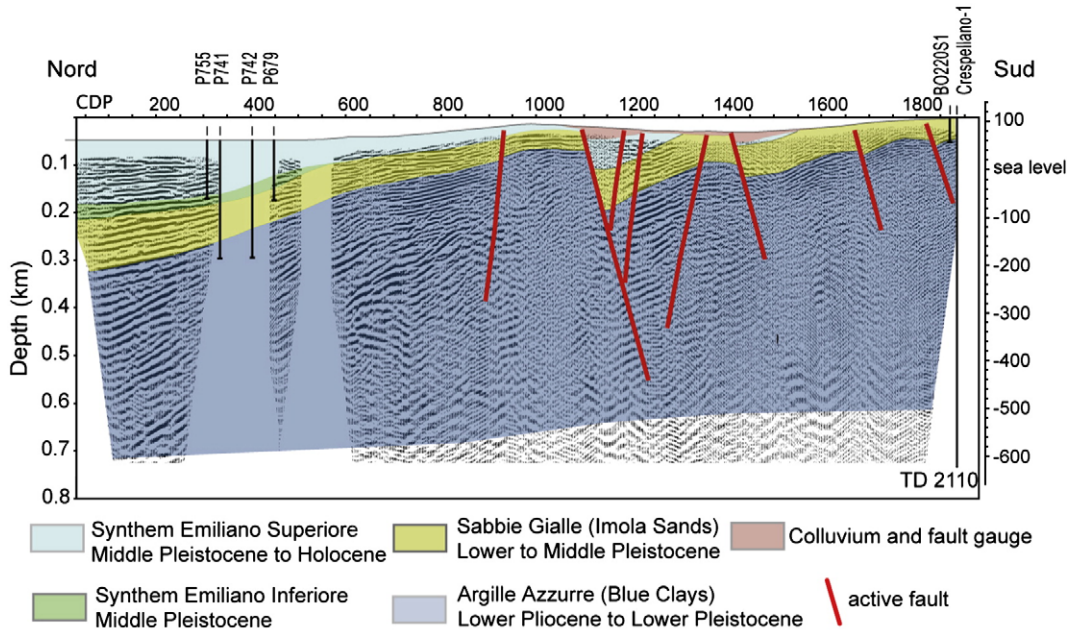

Fig. 7. A seismic profile across the Ponte Ronca fault and associated features (modified after Picotti and Pazzaglia, 2008). See Fig. 2 for location.

of oil and gas. Diffuse seepage of condensate was described first by Bertotti et al. (1997) along this fault, documenting its effective capability of this fault to tap deep hydrocarbon reservoirs, likely located in the Tertiary flysch below alloctonous less permeable units, as documented some tens of km to the west by Capozzi and Picotti (2002).

2.5. A general picture of the active faults around Bologna

The four active faults of the Bologna area described above are representative members of a much larger system of high angle normal faults of the foothills of the Northern Apennines (Fig. 2). Most of these faults do not offset Pleistocene deposits, so their strike lengths and cumulative throw are poorly known (as an example, see Capozzi and Picotti, 2006). Cumulatively, these faults represent a component of penetrative brittle shear accompanied by modest amounts of crustal stretching. One example is provided by the four active N-striking faults that traverse the lower reach of the Reno Valley (see Figs. 2 and 7 of Picotti and Pazzaglia, 2008). The cumulative displacement rate of these structures is ~0.77 mm/yr. Assuming a mean fault dip of 60°, the total horizontal stretching rate is 0.25 mm/yr, for a total net extension of 200 m since the Middle Pleistocene. The origin of this extension is partitioned among hangingwall ramp folding atop a deep buried thrust (Picotti and Pazzaglia, 2008), prevalent at the mountain front (Ponte Ronca fault), and retreating of the upper plate, i.e. the well documented extension of the Apennine crest (Scascoli fault), a process started earlier and acting at rates of several mm/yr of total stretching according to geodetic GPS measurements (Serpelloni et al., 2005, see also Picotti and Pazzaglia, 2008, for further discussion).

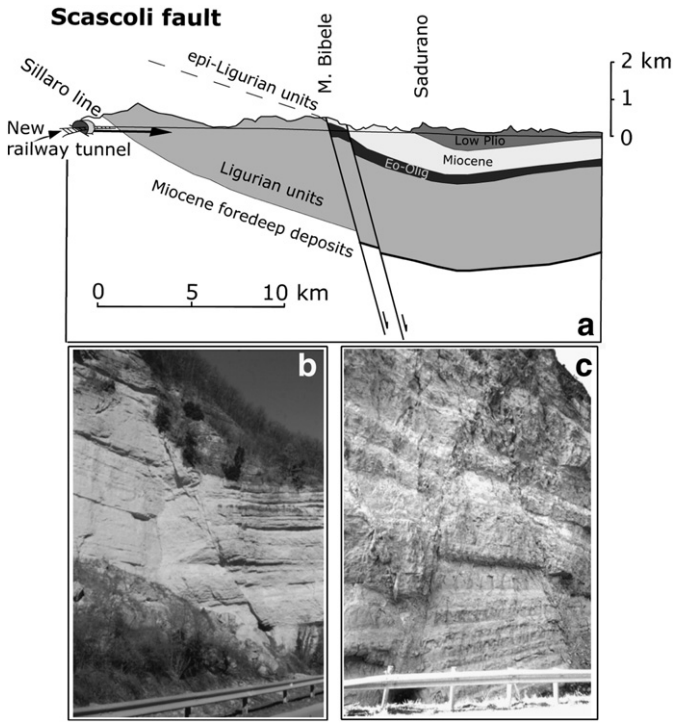

Fig. 8. A cross section through the Scascoli fault along a new tunnel of the railway (a) and minor extensional features at the Scascoli gorge (b and c), describing the deformational style of the Miocene epi-Ligurian rocks in between the two main faults.

3. Discussion

3.1. Topographic expression of active faults (Local tectonic uplift vs local erosion

Exhumation of the Northern Apennines started at around 3 Ma and has proceeded at an average rate of about 0.7 mm/yr based largely on an apatite fission track (AFT) data base (Zattin et al., 2002; Balestrieri et al., 2003). This exhumation temporally overlaps with the widely accepted notion that surface uplift and relief in the Apennines was greatly enhanced since the Middle Pleistocene (Bartolini, 2003). Data from disparate erosion rate studies either corroborate the AFT results, such as reconstructed sediment volumes (Bartolini, 2003), or suggest slightly lower rates of ~0.2–0.4 mm/yr for methods that integrate across Holocene time scales, such as measuring river suspended sediments (Simoni et al., 2003) or from basin-wide cosmogenic nuclides inventories of sand bedload in river channels (Cyr and Granger, 2008). It is interesting to note that the highest rates of erosion reported in the Cyr and Granger (2008) study come from watersheds we report to be in the uplifted footwall of active normal faults. Cyr and Granger (2008) did not consider active normal faults in

their sampling strategy so it remains a testable hypothesis to determine if the range of cosmogenically-measured erosion rates reflects uncertainties with the data, natural variations due to transients in the rate of landscape change, or a strong base level fall forcing because of the active normal faults. It is in this context of large scale uplift of the Apennines and its balance with erosional processes that the active normal faults imprint a unique signature upon the landscape.

A general observation is that there is little net subsidence of the hangingwall blocks. Also there is a non-uniform topographic expression of uplifted footwall blocks, especially where the footwall is underlain by rock type less resistant to erosion. Exceptions to this are faults affecting resistant rock types, such as limestone or the gypsum evaporites, with the latter allowing for fast karst development, therefore lowering the capability of hillslope erosion. We found triangular facets developed in limestone only, whereas fault scarps in mudstone are consequently characterized by badlands (*calanchi*) enhanced presumably because of continuous local base-level lowering at the footwall block escarpment. The general message, therefore, is that active faults, such as those found in the foothills of the Northern Apennines, are not uniformly obvious from a simple geomorphic analysis.

The key topographic fingerprints of the Apennine high angle normal faults include offset of late Pleistocene and Holocene terraces, facets in resistant rocks, and depressions filled with colluvium. The fault indicators, which provide best results even in the absence of visible traces, are the perturbations of the drainages, such as documented for the drainage density (Simoni et al., 2003). The faults in the study case interact with the catchments in several ways. The N–S faults, like the S. Luca–Reno fault, are associated with tilt of the hangingwall so that it tends to deflect the Reno channel, shifting it eastward against the footwall scarp. A similar tilt has also been described for the Lamone catchment, located some 30 km to the southeast of the S. Luca–Reno fault by Simoni et al. (2003). It appears as a widespread feature in the valley reaches developed along the N-oriented faults.

In contrast, south-dipping normal faults, such as the Riolo Terme fault, tend to uplift a footwall block as seen in the lower reach of the Senio river course. The long-term result is the progressive defection of the river along the damage zone, until the capture executed by the adjacent trunk channel (the Sintria River). The footwall block bears the record of the progressive abandoning of valley reaches, leaving prominent wind gaps (see Fig. 9). In particular, considering net uplift

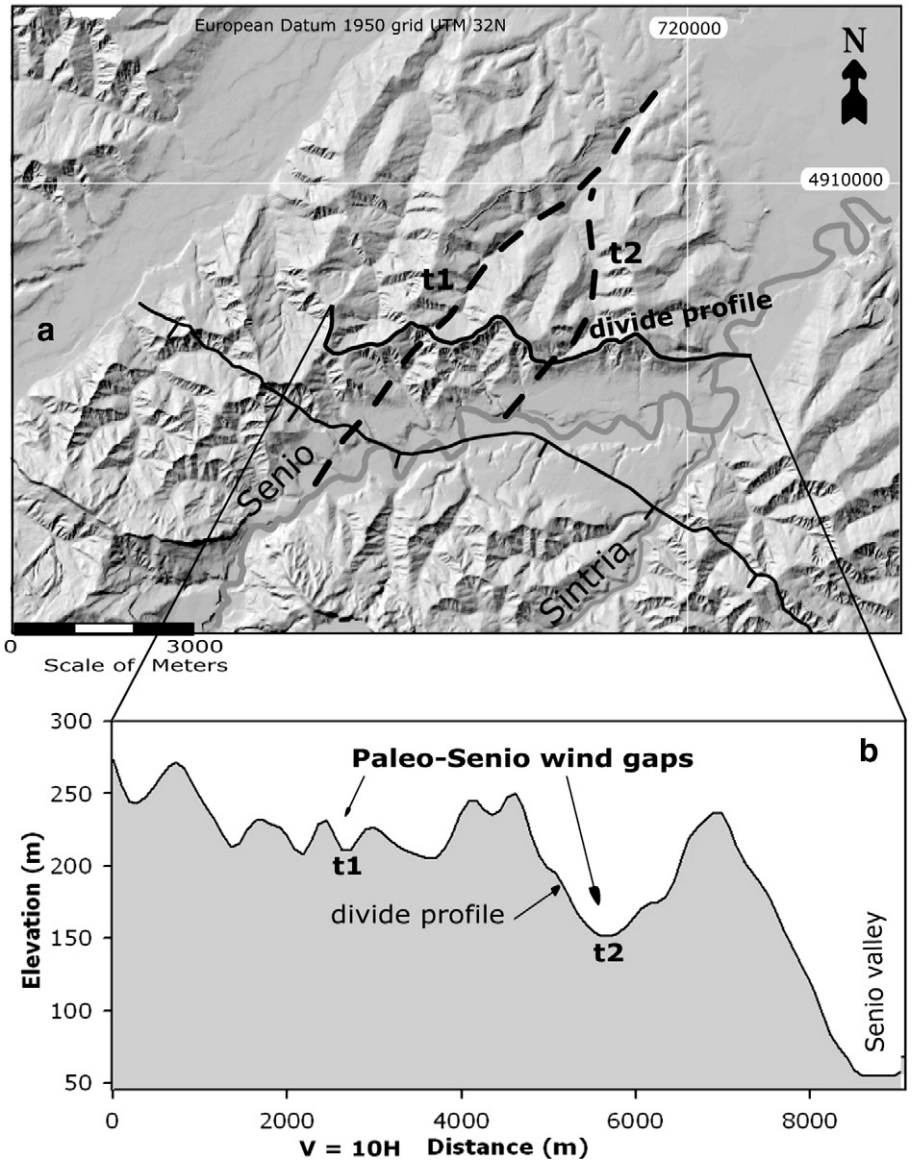

Fig. 9. The interaction of fluvial erosion and footwall uplift for the Riolo Terme fault. Prominent wind gaps are visible on the interfluve, documenting the abandonment of the previous valleys (t1 and t2 wind gaps are discussed in the text).

of the footwall and using the calculated slip rate in estimation of this uplift, it is possible to calibrate the timing of valley abandonment and the formation of the two wind gaps at 145 m (t1) and 85 m (t2) above the present Senio river. Given a constant slip rate of 0.35 mm/yr, ages of the wind gaps are ~400 ky for t1 and ~240 ky for t2. These values may be younger if it is considered the river incision into the hangingwall. Regional considerations (see Picotti and Pazzaglia, 2008; Cyr and Granger, 2008) suggest a local incision rate of about 0.2 mm/yr. Therefore, a possible corrected age for the Senio wind gaps is ~260 and ~150 ky, respectively.

For north-dipping faults, such as the Scascoli fault, there is a long slip history that brought about the juxtaposition of different rock types along strike. This led to the development of different landscape features along the fault. The most striking feature is the western defection of the Setta river and its final capture into the Reno valley. This latter is also deflected to the west when approaching the footwall uplift of the Scascoli fault (see Fig. 2), that shows pronounced obsequent tributaries due to northward tilting. The Setta river is deflected along the fault plane, possibly following the damage zone and because the hangingwall rocks are more resistant. Given the vicinity of the Setta and the Savena valleys at the capture elbow it is likely that the Setta was discharging into the Savena prior to the capture, which probably occurred early during the Pleistocene.

A classic problem in the active fault studies is the localization of slip at surface in the cases of absent seismogenic rupture (De Martini et al., 2003). Frequently, the slip is claimed along the faceted spur at the slope deposit–bedrock interface, (e.g. the Magnola fault in the central Apennines, Palumbo et al., 2004; the Avion fault in central Greece, Ganas et al., 2005, see also Roberts and Michetti, 2004). In other cases, such as the northern Apennines at Colfiorito (September, 1997 earthquake) however, geologic and geodetic studies document that the surface deformation associated to the coseismic slip occurred several km within the hangingwall (Basili et al., 1998; De Martini et al., 2003). Similarly, observations of the Gubbio normal fault revealed pronounced faceting of the spurs cut by the main fault, but virtually no evidence of activity at the bedrock–surface deposit interface (Pucci et al., 2003). These studies suggest that many of the so-called reactivation belts at the bedrock–slope deposit interface are likely erosional and the result of mass-wastage processes, therefore masking the real surface deformation associated to tectonic movements.

In the case of the S. Luca–Reno fault, there is no evidence of slip between the surficial units and the bedrock. This fact could be interpreted in two ways: the fault is no longer active, or the fault is active and the slip is not localized at the bedrock–slope deposit interface. Taking as working hypothesis the mean constant slip rate of 0.2 mm/yr, the Holocene offset should be in the order of 2 m. We have not been able to document such throw, but, in our preferred interpretation of the footslope deposits and the distribution of the alluvial units (Figs. 4a and 3), a blind fault is likely present (Fig. 5a), and the Holocene accumulated slip may be accounted for by folding of the hangingwall over a buried fault tip of unknown depth (Fig. 5a). In this interpretation, the triangular facets are mostly an erosional feature, where the footwall escarpment is high, steep, and swept clear of footslope sediments by the location of the Reno trunk channel.

3.2. Seismotectonic bearing of the studied faults

There are published contrasting views on the seismogenic nature of the high angle normal faults at the entire Bologna mountain front in general (Pondrelli et al., 2006). The recently published seismotectonic map of the Region (Boccaletti et al., 2004) represents a comprehensive synthesis. Unfortunately, however, the location of historical and instrumental events is too inaccurate to allow for a certain correlation between seismological events and the (assumed) active faults. In any event, some historical events with equivalent moment magnitudes of 5 to 5.5 (report of the last 850 years) are located to zones at or close to the S. Luca–Reno fault, as well as the Ponte Ronca and the Scascoli faults, (see Fig. 2). The expected surface rupture for similar events is zero or negligible and might be utilized to confirm our interpretation that most of recent deformation is not expressed at surface. These faults are capable of generating earthquakes every ~1000 years (Wells and Coppersmith, 1994; Keller and Pinter, 1996). This recurrence time is in agreement with the events recorded by the seismotectonic map of Boccaletti et al. (2004), where the time window of the list is almost sufficient to record seismic activity.

A different case is presented by the Riolo Terme fault that is associated to a larger and more precisely located event (1781 A.D. $M>5.5$). In the cited map of Boccaletti et al. (2004), the authors provided a reconstruction of the geometry of the inferred seismogenic source, in agreement with the orientation of the fault investigated here. The literature, however, do not report any surface rupture, that should be expected with events of such magnitudes. We can therefore only infer that the coseismic movement of the Riolo Terme fault likely did not affect the fault along its entire length, but rather in a segment located near its eastern tip in the Lamone valley, where the epicenter is also located. In case of surface rupture of the entire fault of 12 km, in fact, the equivalent magnitude, according to the available literature data (e.g. Pavlides and Caputo, 2004) would have been M 6.5, a highly destructive event for the Italian standard. No such event has been recorded. Boccaletti et al. (2004) document for magnitudes M 5.5 to M 6 the rupture of a 3 to 4 km segment of the fault, which maybe in accordance with the present observation. In conclusion, new paleoseismic data would be necessary to better assess the seismic hazard of the study area, which is densely populated. The preliminary consideration is that the seismic risk would be high, even taking into account the low seismogenic depth of the described normal faults.

4. Conclusions

The normal faults in the foothills of the Northern Apennines documented in this paper, partially known in literature (Bertotti et al., 1997), are described in their geometry, length and displacement, and slip rate. The latter is averaged for the last 700–800 ky for most faults, whereas locally the slip rate history is reconstructed through the stratigraphic separation of dated late Pleistocene to Holocene units. The results consistently indicate that the faults have a moderate activity with slip rates ranging 0.1 to 0.3 mm/yr.

The geodynamic scenario of the Northern Apennines allows interpreting the origin of the observed faults as twofold: related to the retreat of the upper plate, at least the faults closer to the watershed, such as the Scascoli fault, characterized by kilometric throw and a likely pre-Quaternary onset of its activity. The faults located closer to the foothills represent stretching of the carapace that is folding at the mountain front, due to a deep blind reverse structure (Picotti and Pazzaglia, 2008). The topographic signature of these faults is very scarce, owing the average erosion rates are systematically higher than the slip rates. The classical indicators (such as the faceted spurs) are preserved only for the resistant lithologies, not common in this part of the Apenninic belt. This fact makes it difficult to recognize active faulting in this sector, when compared with the abundant data for the carbonate-rich central Apennines. Anyway, the deformation of the drainage, such as density variations or river piracy, can reveal the long-term record of slip along the fault. This survey of the normal fault active close to a major urban area (i.e. Bologna and surroundings) can help in assessing the seismic hazard of the area. For a better knowledge, however, a paleoseismological analysis is needed, together with some micro-seismic experiments along the faults.

Acknowledgments

The authors are grateful to F. Roure and anonymous, whose thoughtful revisions greatly improved the manuscript. Grants R.F.O. (University of Bologna) are acknowledged. This work has been partly funded by GEO-EAR-0207980 (Project RETREAT) to support the collaboration between Pazzaglia and Picotti.

References

Amorosi, A., Farina, M., Severi, P., Preti, D., Caporale, L., Dio, G.D., 1996. Genetically related alluvial deposits across active fault zones: an example of alluvial fan-terrace correlation from the upper Quaternary of the southern Po Basin, Italy. Sedimentary Geology 102, 275–295.

Balestrieri, M.L., Bernet, M., Brandon, M.T., Picotti, V., Reiners, P., Zattin, M., 2003. Pliocene and Pleistocene exhumation and uplift of two key areas of the northern Apennines. In: Bartolini, C., Piccini, L., Catto, N.R. (Eds.), Uplift and Erosion; Driving Processes and Resulting Landforms; Dynamic Relations Between Crustal and Surficial Processes. Quaternary International, 101–102, 67–73.

Bartolini, C., 2003. When did the Northern Apennine become a mountain chain? In: Bartolini, C., Piccini, L., Catto, N.R. (Eds.), Uplift and Erosion; Driving Processes and Resulting Landforms; Dynamic Relations Between Crustal and Surficial Processes. Quaternary International, 101–102, 75–80.

Basili, R., Bosi, V., Galadini, F., Galli, P., Meghraoui, M., Messina, P., Moro, M., Sposato, A., 1998. The Colfiorito Earthquake sequence of September October 1997: surface breaks and seismotectonic implications for the Central Apennines (Italy). Journal of Earthquake Engineering 2 (2), 291–302.

Benvenuti, M., 1997. Physical stratigraphy of the fluvio-lacustrine Mugello Basin (Plio-Pleistocene, Northern Apennines, Italy. Giornale di Geologia 59, 91–111.

Bertotti, G., Capozzi, R., Picotti, V., 1997. Extension controls Quaternary tectonics, geomorphology, and sedimentation of the N-Apennines foothills and adjacent Po plain (Italy). Tectonophysics 282, 291–301.

Billi, A., Salvini, F., Storti, F., 2003. The damage zone-fault core transition in carbonate rocks: implication for fault growth structure and permeability. Journal of Structural Geology 25, 1777–1794.

Boccaletti, M., Bonini, M., Corti, G., Gasperini, P., Martelli, L., Piccardi, L., Tanini, C., Vannucci, G., 2004. Seismotectonic Map of the Emilia-Romagna Region, 1:250000. Regione Emilia-Romagna CNR. SELCA, Firenze.

Bull, W.B., Fadden, L.M., 1977. Tectonic geomorphology north and south of the Garlock Fault, California. In: Doehring, D.O. (Ed.), Geomorphology in Arid Regions: Binghamton, N.Y. State University of New York, Binghamton, pp. 115–138.

Capozzi, R., Picotti, V., 2002. Fluid migration and origin of a mud volcano in the Northern Apennines (Italy); the role of deeply rooted normal faults. Terra Nova 14, 363–370.

Capozzi, R., Picotti, V., 2006. Genesis of cold seeps and mud volcanoes in the Northern Apennines foothills. CIESM Workshop Monograph, Int. Comm. Sci. 25 Explor. Mediterranean Sea, Monaco, 26–29, 59–64.

Chester, F.M., Logan, J.M., 1986. Composite planar fabric of gouge from the Punchbowl Fault, California. Journal of Structural Geology 9, 621–634.

Cyr, A.J., Granger, D.G., 2008. Dynamic equilibrium among erosion, river incision, and coastal uplift in the northern Apennines, Italy. Geology 36, 2, 103–106.

De Martini, P.M., Pino, N.A., Valensise, G., Mazza, S., 2003. Geodetic and seismologic evidence for slip variability along a blind normal fault in the Umbria-Marche 1997–1998 earthquakes (central Italy). Geophysical Journal International 155, 819–829.

Elter, P., Giglia, G., Tongiorgi, M., Trevisan, L., 1975. Tensional and compressional areas in the recent (Tortonian to present) evolution of the Northern Apennines. Bollettino di Geofisica Teorica ed Applicata 17, 3–18.

Eppes, M.C., Bierma, R., Vinson, D., Pazzaglia, F.J., 2008. A soil chronosequence study of the Reno valley, Italy. Geoderma 147 (3–4), 97–104.

Ganas, A., Pavlides, S., Karastathis, V., 2005. DEM-based morphometry of range-front escarpments in Attica, central Greece, and its relation to fault slip rates. Geomorphology 65, 301–319.

Keller, E.A., Pinter, N., 1996. Active tectonics. Earthquakes, Uplift and Landscape. Prentice Hall, pp. 1–338.

Kim, Y.S., Sanderson, D.J., 2005. The relationships between displacement and length of faults: a review. Earth-Science Reviews 68, 317–334.

Kim, Y.S., Peacock, D.C.P., Sanderson, D.J., 2004. Fault damage zones. Journal of Structural Geology 26, 503–517.

McCalpin, J., Nelson, A., 1996. Introduction to paleoseismology. In: McCalpin, J.P. (Ed.), Paleoseismology. Academic Press, San Diego, California. 131pp.

Menges, C.M., 1990. Soil and geomorphic evolution of bedrock facets on a tectonically active mountain front, western Sangre de Cristo Mountains, New Mexico. Geomorphology 3, 301–332.

Morley, C.K., 2007. Development of crustal normal faults associated with deepwater fold growth. Journal of Structural Geology 29, 1148–1163.

Palumbo, L., Benedetti, L., Bourles, D., Cinque, A., Finkel, R., 2004. Slip history of the Magnola fault (Apennines, Central Italy) from 36Cl surface exposure dating: evidence for strong earthquakes over the Holocene. Earth and Planetary Science Letters 225, 163–176.

Pavlides, S., Caputo, R., 2004. Magnitude versus faults surface parameters: quantitative relationships from the Aegean Region. Tectonophysics 380, 159–188.

Picotti, V., Pazzaglia, F.J., 2008. A new active tectonic model for the construction of the Northern Apennines mountain front near Bologna (Italy). Journal of Geophysical Research 113, B08412. doi:10.1029/2007JB005307.

Picotti, V., Capozzi, R., Bertozzi, G., Mosca, F., Sitta, A., Tornaghi, M., 2007. The Miocene petroleum system of the Northern Apennines in the central Po Plain (Italy). In: Lacombe, O., Lavé, J., Roure, F., Vergés, J. (Eds.), Thrust Belts and Foreland Basins, from Fold Kinematics to Hydrocarbon System. Springer Verlag, pp. 117–131.

Pondrelli, S., Salimbeni, S., Ekstrom, G., Morelli, A., Gasperini, P., Vannucci, G., 2006. The Italian CMT dataset from 1977 to present. Physics of the Earth and Planetary Interiors 159, 286–303.

Pucci, S., Martini, P.M.D., Pantosti, D., Valensise, G., 2003. Geomorphology of the Gubbio Basin (Central Italy): understanding the active tectonics and earthquake potential. Annals of Geophysics 46 (5), 837–864.

Roberts, G.P., Michetti, A.M., 2004. Spatial and temporal variations in growth rates along active normal fault systems: an example from the Lazio-Abruzzo Apennines, central Italy. Journal of Structural Geology 26, 339–376.

Sami, M., 1992. Rilevamento geologico e biostratigrafico nella bassa valle del Lamone: dalla Fm. a Colombacci ai depositi terrazzati. Implicazioni cronologiche e paleoecologiche. Unpublished graduate thesis work, University of Bologna.

Scrocca, D., Carminati, E., Doglioni, C., Marcantoni, D., 2007. Slab retreat and active shortening along the Central-Northern Apennines. In: Lacombe, O., Roure, F., Verges, J. (Eds.), Thrust Belts and Foreland Basins, from Fold Kinematics to Hydrocarbon System. Springer Verlag, pp. 471–487.

Serpelloni, E., Anzidei, M., Baldi, P., Casula, G., Galvini, A., 2005. Crustal velocity and strain-rate fields in Italy and surrounding regions: new results from the analysis of 22 permanent and non-permanent GPS networks. Geophysical Journal International 161, 861–880.

Simoni, A., Elmi, C., Picotti, V., 2003. Late Quaternary uplift and valley evolution in the Northern Apennines; Lamone catchment. In: Bartolini, C., Piccini, L., Catto, N.R. (Eds.), Uplift and Erosion; Driving Processes and Resulting Landforms; Dynamic Relations Between Crustal and Surficial Processes. Quaternary International, 101–102, 253–267.

Viaggi, P., 1991. Biostratigrafia e Paleoclimatologia del Pliocene della sezione del Santerno. Unpublished graduate thesis work, University of Bologna, 158 pp.

Wegmann, K.W. and Pazzaglia, F.J., in review, Fluvial terrace straths as growth strata markers of late Quaternary tectonic deformation in the Emilia-Romagna and Marche Apennines, Basin Research, submitted.

Wells, D., Coppersmith, K., 1994. New empirical relationships among magnitude, rupture length, rupture width, rupture area, and surface displacement. Bulletin of the Seismological Society of America 84, 974–1002.

Zattin, M., Picotti, V., Zuffa, G., 2002. Fission-track reconstruction of the front of the northern Apennine thrust wedge and overlying Ligurian unit. American Journal of Sciences 302, 346–379.

Thrust-fold growth history at the mountain front of the Northern Apennines (Italy) from quantitative landscape analysis

Alessio Ponza (alessio.ponza@unibo.it) [a,*]

Frank J. Pazzaglia (fjp3@lehigh.edu) [b]

Vincenzo Picotti (vincenzo.picotti@unibo.it) [a]

[a] Università di Bologna, Dipartimento di Scienze del la Terra e Geologico Ambientali, Via Zamboni 67, 40126 Bologna, Italy

[b] Department of Earth and Environmental Science, Lehigh University, 31 Williams, Bethlehem, PA 18015, USA

* Corresponding author

Dr. Alessio Ponza

Dipartimento di Scienze della Terra e Geologico-Ambientali

University of Bologna

Via Zamboni, 67

40126 Bologna - Italy

Tel. +39 051 2094546; Fax +39 051 2094522

Email: alessio.ponza@unibo.it

Abstract

We document the active tectonics of growing anticlines embedded in the Northern Apennine Mountain front using a quantitative analysis of the topography. We infer rates of rock uplift for these structures using stream channel steepness and incision. Individual structures appear to be

growing more slowly than the long-term, general rate of emergence of the Apennines from the Po Plain. Topographic swath profiles and the steepness index of river longitudinal profiles that traverse the anticlines are consistent with field stratigraphic, structural mapping, aquifer geometry, and seismic reflection profiles relationships. Collectively, these data indicate that parts of the Apennine Mountain front and Po Plain, such as the Ghiardo Plateau and Castelvetro anticline, maintain a slowly deforming mid- and late-Pleistocene vestige of the style of deformation that characterized the Apennines from the Messinian through the early Pleistocene that elsewhere has mostly given way to more rapid, longer-wavelength growth of the mountain front. This contrast in deformation style is significant in that it holds implications for tectonic processes driving growth of the northern Apennines and for along-strike changes in seismic hazards for a particularly heavily populated part of Italy.

Key words: active folding, topography, tectonic geomorphology, long profile modeling, foothills of the Northern Apennines

1 Introduction

The northern Apennines and Po foreland (Fig. 1) are commonly presented as a good example of an active fold and thrust belt (Bally et al., 1986; Hill and Hayward, 1988) and a wealth of outcrop and seismic data supports this interpretation in characterizing the deformation from the Messinian through the early Pleistocene. Since the middle Pleistocene, deformation in the northern Apennines appears to be concentrated in building a mountain front and defining the southern boundary of the Po basin (Picotti and Pazzaglia, 2008) as evidence for clearly deformed middle and late Pleistocene stratigraphy and geomorphic markers are concentrated there. In this paper we present clear topographic, stratigraphic, and geomorphic evidence for active tectonic deformation consistent in

scale and style with the pre-middle Pleistocene fold and thrust-belt deformation. This deformation contrasts with larger-scale processes that are building the Apennine mountain front, but also reaffirms that the northern Apennines and Po Plain define a belt of active compression in the foreland that is paired with a belt of active extension that characterizes the hinterland and back arc of the orogen (Elter et al., 1975).

Rates of rock uplift and mountain front construction have been recently quantified for three parts of the northern Apennines relying primarily on deformed geomorphic markers, from northwest to southeast respectively, the Salsomaggiore anticline (Wilson et al., 2009), the Reno valley at Bologna (Picotti and Pazzaglia, 2008), and the Bidente River at Forli (Wegmann and Pazzaglia, 2009). We focus on the analysis of fluvial channels, Quaternary deposits, and swath topographic profiles in two zones located ~ 40 km and ~ 80 km west of the Reno valley, the Castelvetro - Vignola foothills and the Ghiardo plateau near San Polo d'Enza (Fig. 2 and 3) respectively. We focus on these areas because earlier geomorphic and structural geology studies argued for active tectonic deformation (Gasperi et al., 1999; Cremaschi and Papani, 1975) and topographic growth of low hills on the margin of the Po Plain. Our analysis is dedicated to quantifying that deformation and determining its style. The case study chosen appears particularly suitable, in that there are only minor lithologic variations with the whole foothills range being underlain by relatively soft Plio-Pleistocene mudstone, sandstone, and conglomerate. Similarly, there are no climatic gradients and the history and influence over the Late Pleistocene to Holocene denudation is fairly well known (e.g. Wegmann and Pazzaglia, 2009). As a result, our approach provides a test for establishing the lower threshold signal of channel response to active tectonics among a low-noise background of climate change and lithologic variation. In this respect, we are also able to evaluate the relative seismic hazards for a part of the Apennine mountain front in terms of the style and rate of deformation.

77 **2. Geologic setting**

78 ***2.1.The Northern Apennines***

79 The Northern Apennines are a fold and thrust belt developed as the pro-wedge of the subducting
80 Adria plate since the Oligocene. They are well-recognized example of a plate boundary
81 characterized by a retreating upper plate and lower-plate slab roll back (*sensu* Royden 1993), for
82 their coeval character of compression at the front and extension at the hinterland (Elter et al., 1975).
83 The present day mountain range is characterized by rapid Pliocene and Pleistocene uplift and
84 exhumation (Balestrieri et al., 2003; Bartolini, 2003). The northern Apennines mountain front and
85 its adjoining foothills are riddled with geologic and geomorphic evidence of active tectonics such as
86 growing folds and faults that collectively represent the near-surface structural response of ongoing
87 Adria-Europe convergence (see Picotti and Pazzaglia, 2008, with references).
88 The main mountain front of the Northern Apennines is commonly viewed as some version of a
89 continuous thrust structure (also known as Pede-Apenninic Thrust Front PTF, Boccaletti et al.,
90 1985, see Fig. 1) that offsets Quaternary deposits and locally may be emergent (e.g. Boccaletti et
91 al., 2004; Lavecchia et al., 2003; 2004; Picotti and Pazzaglia, 2008), as an out-of-sequence thrust
92 rooted deep in the wedge. In contrast, the buried front of the northern Apennines, i.e. the most
93 external thrust, is sometimes viewed as the true active front of the Northern Apennines (Scrocca,
94 2006, doglioniXXX), but this view cannot explain the rapid Quaternary growth of the main
95 geomorphic feature, i.e. the mountain front, since the thrust front creates almost no relief.
96 Near Bologna the PTF or its attendant splays do not appear to be emergent. Here the PTF is a deep,
97 steep, blind structure associated with the frontal limb of an antiform that defines the mountain front
98 (Picotti and Pazzaglia, 2008). However, locally west of Bologna (Fig. 1) in the Emilia foothills and
99 adjacent to the Po Plain, shallow splays of the PTF remain active in the Miocene - Pliocene thrust
100 belt (e.g. Scrocca et al., 2007). The geometry of the Quaternary activity is complex, suggesting
101 shortening to the northwest, obique to the pre-Quaternary direction (Gasperi et al., 1999; Picotti et
102 al., 2007).

103

104 ***2.2 Castelvetro - Vignola hills and the Ghiardo plateau.***

105 The southern flank of the Po Plain in the vicinity of Castelvetro and the Ghiardo plateau is
106 corrugated into a series of low, elongated hills and valleys that have long been associated with
107 actively growing folds (Cremaschi and Papani 1975, Gasperi et al. 1999, Carnicelli et al., 2003,
108 Figs 2, 3 and 4). The Castelvetro fold is approximately ~ 4 km in amplitude, ~ 15 km in strike
109 length, and is bound to the east by the Panaro river and to the west by the Tiepido river (Fig. 2). The
110 Castelvetro folds show evidence of the interaction of two deformation trends: a WNW (Apenninic)
111 and a NE (anti-apenninic) trend, with a final dome-and-swell geometry. The limbs of the fold are
112 formed by Plio-Pleistocene deposits and involve Pliocene to Lower Pleistocene mudstone (Argille
113 Azzurre Fm), with local coarse interbeds (Gasperi et al., 1999; Amorosi et al., 1998a), middle
114 Pleistocene beach deposits (Sabbie Gialle Fm), and two units of continental deposits, respectively
115 the Lower Emiliano-romagnolo Synthem (AEI), consisting of coastal plain facies and the Upper
116 Emiliano-romagnolo Synthem (AES), formed by alluvial plain facies (Gasperi et al., 1999) with
117 growth geometries. The youngest deposits involved in the folding are late middle Pleistocene
118 alluvial units, called AES7/7a in Gasperi et al. (1999) and mapped in this paper (Fig. 2 and 3) as
119 Qt3, following the chronostratigraphy proposed by Picotti and Pazzaglia (2008) and Wegmann and
120 Pazzaglia (2009).
121 Further to the west and between Quattro Castella and Albinea the Enza river carves a valley through
122 Quaternary sediments of the Ghiardo plateau (Fig. 3) an east-west-elongated hill that sits several
123 kilometers north of the mountain front, here defined by topographically striking flatirons underlain
124 by middle Pleistocene conglomerates. These flatirons led Bernini and Papani (1987) and Boccaletti
125 et al. (2004) to argue for emergence of the PTF, but subsequent map and seismic data show no
126 evidence of such a structure. On the contrary, the Ghiardo Plateau is the more likely surface
127 expression of actively growing folds cored by an shallow blind or emergent fault (Figs. 3 and 4).
128 Here, a syncline is infilled by fine-grained upper Pleistocene-Holocene deposits corresponding to

129 the Qt5-Qt6 chronostratigraphic units of Picotti and Pazzaglia (2008). The top of the plateau is
130 dissected by small N-S valleys cutting middle to upper Pleistocene continental deposits
131 corresponding to Qt3/Qt2 uplifted above the Holocene plain of the Enza river (Cremaschi and
132 Papani 1975).
133
134 **3 Methods**
135 ***3.1 Ks Steepness index***
136 In active tectonic settings fluvial processes are both a direct consequence of and have a dynamic
137 interaction with rock deformation (Wegmann and Pazzaglia, 2002).
138 Since Hack (1957) many studies (Flint, 1974; Snyder et al., 2000; Kirby and Whipple, 2001) have
139 already empirically observed in many geologic settings, that the channel slope along a river tends to
140 decrease inversely with the increase of the drainage area, defined by a power law in the form:
141
142 $S = k_S A^{-\theta}$ (1)
143
144 where S is the local channel gradient (m/m), A is the upstream drainage area (m^2) and considered a
145 good proxy for discharge, k_s and θ are respectively steepness and concavity, the slope and y-
146 intercept of a log-log plot of S and A. Equation (1) can be shown to be in the same form as the
147 stream power law (Sklar and Dietrich, 1998) that describes steady, uniform, detachment-limited
148 bedrock incision:
149
150 $E = KA^mS^n$ (2).
151
152 In equation (2) E is the bedrock erosion rate, K is a dimensional constant that varies with rock type,
153 climate, channel width, channel hydraulics and sediment load, A is the drainage area, usually
154 considered a good proxy for discharge, and S is the channel gradient.

155 Equation 2 is valid only assuming a linear (or nearly linear) relationship between discharge and
156 drainage area, a negligible threshold for activating erosion/transport and a channel width that scales
157 with the square root of the discharge.
158 Rearranging and solving for S equation (2) is it possible to obtain:
159
160 $S = (E/K)^{(1/n)} A^{(-m/n)}$ (3),
161
162 When the m/n ratio is equal to 1, then the erosion rate is proportional to the total stream power;
163 when m/n is equal to 0.5, the erosion rate is proportional to unit stream power, if channel width
164 varies with the square root of drainage area, or to the basal shear stress at the streambed (Whipple &
165 Tucker, 1999).
166 In the case of a steady state topography (defined as the condition where erosionrate E balances rock
167 uplift rate U everywhere along the channel profile) being the rate of change of river-bed elevation
168 (dz/dt):
169
170 $dz/dt = U - E = 0$ (4),
171
172 is it possible to sobstitute E with U in equation (3) obtaining:
173
174 $S = (U/K)^{(1/n)} A^{(-m/n)}$ (5).
175
176 Thus, the observationally-derived equation (1) and the theoretically-derived equation (5) for the
177 case of detachment-limited, steady state channels have the same general form and in an analysis of
178 stream longitudinal profiles, the relationships implied by:
179
180 $\theta = m/n$, (6)

and

$$k_S = (U/K)^{(1/n)}, \quad (7)$$

hold true if and only if (1) the river profile is in steady state with respect to current climatic and uplift conditions; and (2) both uplift rate (U) and coefficient of erosion (K) are uniform through the channel reach. Where these conditions are met, the parameters $(U/K)^{1/n}$ and m/n can be estimated directly through regressions of channel-gradient and drainage-area data (Snyder et al., 2000).

Simple models (for both detachment and transport-limited systems) predict power-law relations between channel gradient and drainage area in the form of equation 1 (e.g. Whipple and Tucker, 1999; Willgoose et al., 1991). Furthermore, these models, in the case of steady state topography predict that the concavity index (θ) is independent of rock uplift rate (U), provided U does not vary along the channel length (Whipple and Tucker 1999; Kirby and Whipple 2001) and there is a positive linear correlation between the steepness index (k_s) and rock uplift rate. A number of factors not incorporated into these models are known to influence the relation between k_s and U. These include (1) non-linearities in the incision process (Whipple and Tucker, 1999), such as thresholds for incision (Snyder et al., 2003; Tucker, 2004; Tucker and Bras, 2000), (2) adjustments in channel width and sinuosity (Duvall et al., 2004; Finnegan et al., 2005; Lave and Avouac, 2000), (3) adjustments in hydraulic roughness, grain size of bed material, and/or extent of alluvial cover (Sklar and Dietrich, 1998, 2001, 2004), (4) changes in the efficacy of erosive debris flows (Stock and Dietrich, 2003), and (5) orographic enhancement of precipitation (Roe et al., 2002, 2003). Moreover k_s can be strongly influenced by climatic factors as well as rock mass quality and strength (Duvall et al., 2004; Kobor and Roering, 2004; Moglen and Bras, 1995; Stock and Montgomery, 1999). Where lithologic properties really are or can be considered uniform through a sort of local

207 calibration of an erosion model, the steepness index can be directly affected by and contain useful
208 information about variations in rock uplift rates (Wobus et al., 2006b). Most models predict that
209 profile concavity will be independent of rock uplift (if spatially uniform) and available data suggest
210 little change in the concavity index of adjusted river profiles as a function of rock uplift rate (e.g.
211 Tucker and Whipple, 2002). In contrast, because k_s is a function of U, an along profile change in
212 rock uplift rate may be manifested as a change in concavity. In fact some studies have highlighted
213 distinct changes in concavity associated with variable uplift rate (Kirby and Whipple, 2001, Kirby
214 et al., 2003), climate (Zaprowski et al., 2001), and rock type (Spagnolo and Pazzaglia, 2005; Wilson
215 et al., 2009). Our analysis selects those parts of the channel that are most reflective of detachment-
216 limited fluvial processes and avoids the upper reaches dominated by debris flows and the lower
217 segments that have become alluvial and transport-limited.
218
219 All topographic data (profiles and indexes) are extracted from the Regione Emilia-Romagna (RER)
220 10 meters digital elevation model (DEM). The method of data extraction we apply comes directly
221 from the "New tools for Quantitative Geomorphology: Extraction and Interpretation of Stream
222 Profiles from Digital Topographic Data" (Whipple et al., 2007). Those tools provide for a dual,
223 interfaced, and user-interactive ArcGIS - Matlab environment.
224
225 We use a moving average window of 250 m in length that allows to smooth raw elevation data prior
226 to calculating channel slopes over a specified vertical interval. Regressing the slope versus area plot
227 over a user specified moving window of 0.5 km (Auto k_sn window in the tool), normalized
228 channel steepness indices k_{sn} (y-intercept of the regression fit), varying along channel segments
229 were extracted for drainage network, both small creeks and rivers, crossing the described tectonic
230 structures in the Ghiardo Plateau and at Castelvetro - Vignola foothills (Fig 9-12).
231
232 Normalized steepness indexes (k_{sn}) have been calculated for a reference channel concavity (θ_{ref})

233 required for inter-channel interpretation and comparison. We choose a value for θ_{ref} of 0.45, both
234 equal to the mean of observed concavity values in undisturbed channel segments in this study area
235 and to compare to previous studies (e.g., Duvall et al., 2004; Snyder et al., 2003; Wobus et al.,
236 2006b). In principle, however, relative differences in k_{sn} do not depend on the choice of θ_{ref} (Wobus
237 et al., 2006b). We plot the data in map-view with color-coded stream segments based on their
238 normalized k_{sn} that allows to look at patterns of steepness indices within catchments and to identify
239 transients related to continued growth of the structures.
240

241 ***3.2 Swath profile***

242 Swath-averaged topographic profiles provide a useful way to characterize the topography of
243 orogenic belts where along-strike variations are small (Isacks, 1992). The difference between the
244 maximum and minimum envelops represents a measure of the local relief at length scales of the
245 order of the swath width (Masek et al., 1994). In this technique a topographic profile is taken
246 perpendicular to the strike and all elevations within a specified swath width are projected into the
247 plane of the section. Curves may then be constructed outlining the maximum, minimum, and the
248 average elevations within the swath. Swath topographic profiles centered on and paralleling an
249 anticlinal hinge of a structure represent alternative means of assessing along-strike variations in
250 elevation that may reflect underlying fold growth. For the same reason, extended swath topographic
251 profiles oriented perpendicularly to a fold axis are constructed to reflect underlying fold growth
252 perpendicular to strike direction. We use an ArcInfo script (M. Oskin, personal communication)
253 that extracts topography data from the 10-m resolution DEM along a defined number of parallel
254 profile lines, variable from 1 to 5 km in width and spaced 20 m apart orthogonally to the folds.
255

256 **4 Morphometric data**

257 ***4.1 Tectonic setting***

258 The geologic section AA' crosses folded middle Pleistocene growth deposits (AEI, Qt1 and Qt2 in

259 Picotti and Pazzaglia, 2008 and Wegmann and Pazzaglia 2009) of the Ghiardo plateau from SW to
260 NE (Figs. 3 and 4). The strata tilt to the SW at the mountain front and to the NE on top of the
261 Ghiardo anticline, where they onlap the underlain folded Sabbie Gialle. A measured section in the
262 Enza River at San Paolo d'Enza, subsurface seismic reflection data (see Ponza et al., submitted)
263 and the SP3 borehole stratigraphy published by Carnicelli et al., (2003) have been integrated to
264 locally calibrate the thickness of the Quaternary deposits. To approximate the local uplift rate for
265 the anticline top some assumptions are needed: (1) first we assume the base and the top of the
266 coastal plain unit (AEI) as horizontal datum during the time of deposition; (2) we assume that the
267 greater thickness of the AEI sediments infilling the syncline with respect to those covering the
268 Ghiardo Plateau is due to local syn-depositional subsidence and uplift, respectively. The difference
269 in stratigraphic thickness of the AEI gives an uplift rate for the Ghiardo anticlines of ~0.28 mm/yr.
270 The current elevation of the Ghiardo Plateau surface (110 m.a.s.l.), assuming no erosion, indicates a
271 long-term uplift rate of the anticline of ~0.18 mm/yr since the close of AEI deposition.
272
273 ***4.2 Swath profiles***
274 Swath topographic profiles oriented across the anticline hinge of the Castelvetro, Villa Camilla and
275 Ghiardo anticlines (see fig 6 and fig 7) can be compared to a swath profile erected parallel to their
276 anticlinal hinges (fig 8). The mean and the maximum topography of the fold-orthogonal swaths
277 describe two folds that cede to an abrupt rise in elevation towards the SW. In contrast, the
278 minimum topography (the stream valleys actually), appear to be graded to a common elevation. The
279 minimum, mean and maximum topography envelopes of the fold-axis parallel line (Fig. 7) show a
280 general NW-SE uniform growth culminating at the intersection of the Guerro river valley, except
281 for a small pike (km 9.1) that increase in elevation ~ 2 km east of the Panaro valley (stream n 41 in
282 figure 10 and 12). Those profiles clearly show as the valley bottom of the major transverse rivers
283 (which number in figure correlates with the stream numeration in figure 10 and 12) dissecting the
284 topography, are not at the same elevation, with the valley of the Guerro standing the highest. Fig. 8

285 shows a NE-SW oriented swath profile along the Ghiardo plateau bulge where the swath axis
286 parallels the geologic section of Fig. 4, and swath area includes almost entirely the trace of this
287 section, (see location and relative kilometric profile in Fig. 3). Starting from the high topography of
288 SW the minimum mean and maximum profiles abruptly decrease in elevation describing a clear
289 synclinal shape NE into the Po Plain, whereas the mean and maximum topography growth in the
290 well known Ghiardo antiform the minimum topography (corresponding to the valley bottom of
291 stream 13) lies several meters beneath the mean and minimum values.
292
293 ***4.3 Stream profile analysis: steepness indexes***
294 We model channel profile steepness for 23 streams in the Ghiardo plateau and 18 streams at
295 Castelvetro – Vignola (see Figs. 9 and 10). Channel steepness is determined by regressions through
296 slope-area data considering 0.25-km long channel reaches (Fig. 5). This imposed length scale
297 effective sets a lower drainage are threshold for conducting our analysis. The magnitudes of k_{sn} are
298 plotted as color-coded maps Fig. 9 and 10 (see table 1 for all topographic characteristics of the
299 streams). K_{sn} coded map have been colored following a geometrical statistical distribution of the
300 values such that chromatic gradation intervals are scaled to be able to better visualize changes in k_{sn}
301 across the critical areas.
302 In both study areas, k_{sn} values tend to scale with the size of the channel (Figs 9 and 10). Large
303 channels (such as the Enza, the Moddolena, the Crostolo, the Panaro, the Teipido and the Guerro)
304 ,that have headwaters in the Emilia foothills, have higher overall k_{sn} values in comparison to
305 smaller, commonly ephemeral streams that are sourced at the mountain front or in the Po Plain.
306 Furthermore the spatial distribution of these higher values do not appear to record spatial variations
307 of rock uplift across the tectonic structures (Figs 9 and 10). For example, in the Ghiardo plateau, the
308 largest analyzed channel is a reach of the Enza river (stream 2 in table 1) ~ 32 km long. It drains an
309 area of ~ 200 km^2, with max k_{sn} value equal to 70.6 (highest registered steepness index in the area,
310 see figure 9 and table 1). The smallest stream is number 18, a tributary of stream 17, Rio Moreno

311 (see table 1), that develops ~ 3.43 km in length, with a drainage area of ~ 1.7 km^2 and with a max
312 k_{sn} value of 9.5. Similarly, in the Castelvetro - Vignola area the largest analyzed channel is a reach
313 of the Panaro river ~ 34 km long and with a maximum drainage area of ~ 103 km^2 and a maximum
314 k_{sn} value of 93.6 (absolute maximum steepness index obtained by the stream analysis in this study).
315 The smallest stream is number 40 (see Fig. 10 and table 1), a tributary of the Rio Schiaviroli ~ 1.7
316 km long, with a maximum drainage area of ~ 0.7 km^2 and highest value of k_{sn} of 15.9.
317 We focus on the subtle differences in k_{sn} in the region where the channels transverse to the
318 structures. The corresponding reaches are about 3-4 km long, straddle the fold axes, and include 14
319 and 16 rivers across the Ghiardo and Castelvetro - Vignola structures that have drainage areas in
320 excess of 170 km^2 (Figs. 11, 12 and tables 2 and 3). The general distribution of k_{sn} values is once
321 again shown by a blue color ramp where darker blue indicates steeper channels. For these channels
322 k_{sn} value ranges just from 5 to 21 in the Ghiardo Plateau and from 6.3 to 22.8 in Castelvetro –
323 Vignola.
324 A red star is plotted to show the maximum k_{sn} value calculated as a maximum for a 5-k_{sn}-value
325 moving window. A white star is plotted to show the minimum k_{sn} value calculated as a minimum
326 for a 5-k_{sn}-value moving window. In the Ghiardo Plateau, most of the red stars fall on or few
327 hundreds of meters downstream of the mapped trace of the fold hinge, mostly in the fold frontal
328 limb zone (see e.g. k_{sn} trend of stream 13 in fig. 7), while a large number of the white stars fall on
329 or near the syncline axis. We note that a reach of the Crostolo creek (stream 23) has r k_{sn} values of
330 30-52, results that are tanomalously high with respect to the regional values. (see table 2).
331 In the Castelvetro-Vignola foothills the general location of the red stars lies mostly in the zone of
332 highest topography, near or on the Villa Camilla fold axis which stands in comparison to the
333 Ghiardo plateau results. However, for 5 small streams red stars fall on or near the Castelvetro fold
334 hinge, in the frontal limb area toward the Po plain. In contrast, the greater part of the white stars
335 localize in the syncline zone, in between the the two anticlines, similarly to their position in the
336 Ghiardo area. Also similar to the Ghiardo area, stars of the smaller streams with drainage area <

337 2E+07 m^2 fall closer to the axes of the strucutres then the larger streams such as the Panaro, the
338 Guerro and the Tiepido.
339
340 **6 Discussion and Conclusions**
341
342 (1) Collectively, the mapped surface geology (Figs. 2 and 3), the structural data (Fig. 4), the swath
343 profiles (Figs. 5, 6, and 7), and the modeled channel steepness (Figs. 9, 10, 11, and 12) indicate
344 contemporary growth of folds in the Ghiardo Plateau and Castelvetro - Vignola regions. These folds
345 have a similar strike length and amplitude of older, well-recognized Mio-Pliocene fault-bend and
346 fault-propagation folds that appear to have been reactivated in part, with renewed middle
347 Pleistocene-present NW-SE oriented shortening.
348 The swath profiles in particular (Fig. 6) outline the two folds where the mean and maximum
349 envelopes match the hinge trace of both the Castelvetro and the Villa Camilla anticlines mapped in
350 Fig. 2 (see vertical dashed lines in Fig. 6). Relief in the profiles represents mature dissection of
351 the topography, implying long term activity of the structures. This suggestion of long term slow
352 growth is further supported by the smoothed and nicely graded profile of the subenvelope which is
353 consistent with a near balance between channel incision and rock uplift. . There are no obvious
354 knick points in the stream valleys.
355 In the swath along the Castelvetro anticline hinge, the small spike in the profile (see km 9.1 in Fig.
356 6) appears to locate the active topographic growth associated with the Villa Camilla anticline,
357 locally related with an active NE-SW oriented reverse fault (Ponza et al., submitted).
358 The narrow swath profile across the Ghiardo Plateau (Fig. 7) strictly matches the fold shape
359 evidenced by the geological section (Fig. 4). The mean and envelope surfaces indicate that the top
360 of the plateau has yet to incise, suggesting a relatively youthful morphology and recent growth of
361 the structure. We suggest that for these folds, morphology to the combination of two factors
362 (Burbank and Vergés, 1994): (1) the formation of a young topography that, despite the decreasing

363 uplift rates of the anticlines to 0.18 mm/yr in the last 450-620 ka (see paragraph 4.1) is probably
364 related to a contemporary decrease in background subsidence of the foreland (see Ponza et al.,
365 submitted); (2) the response to erosion and the develop of a limited drainage network into the high
366 permeable middle Pleistocene conglomerates being deformed atop of the Ghiardo plateau.
367
368 (2) Of particular interest is the spatial overlap of the k_{sn} maxima with the frontal limb zone of the
369 anticline and of the k_{sn} minima with the syncline hinge in the Girardo Plateau. Here for most
370 streams the fold-shape trend of k_{sn} values (e.g. stream 13 in Fig. 7) indicates streams sensitive to the
371 tectonic signal, decreasing in value in correspondence of the syncline and clearly increasing
372 downstream of the fold hinge in the frontal limb zone. This observation is particularly true for
373 channels characterized by a drainage area < 20 km2 at the point that the stream traverses the
374 structure (e.g. streams 1, 3, 10, 11, 13; table 2).
375 This drainage area extent of 20 km^2 seems to be the local critical threshold that allow these
376 ephemeral, small streams to incise in a detachment-limited regime, avoiding transport-limited and
377 channel width complications due to the greater sediment source and discharge of the larger
378 perennial stream. We record this threshold value in both the studied areas.
379
380 Along the Villa Camilla structure, the spatial overlap of k_{sn} maxima with the fold hinge area
381 reflects, with respect to the Ghiardo, a different adjustment of channel profiles to rock uplift. We
382 note that the rates of uplift of the three anticlines are comparable with the uplift rates of the Villa
383 Camilla measured at the fold hinge culmination near Vignola (Ponza et al., submitted) equal to 0.29
384 ± 0.05 mm/yr, averaged in the last 230 ka; the Castelvetro anticlines uplift rates have been
385 documented (Ponza et al., submitted) 0.1 – 0.2 mm/yr, while uplift rate of the Ghiardo anticline
386 vary in the Middle Pleistocene from 0.28 mm/yr to 0.18 mm/yr. We also found that the 20 km^2
387 threshold of drainage area influencing channel regime of the streams characterizes both the study
388 areas.

389 Localization of the maximum k_{sn} values at the fold hinge, together with the older age of the
390 deformed deposits (recognized ad spatially distributed along the Apennines mountain front, Gasperi
391 et al., 1999, Pizziolo et al., submitted) and with the swath profiles, suggest "mature" drainage
392 networks where channel profiles are near the steady state with the topography. In contrast the
393 regular trend of the maximum k_{sn} values located some hundreds of meters far from the Ghiardo
394 anticline hinge, together with the less developed drainage network on the plateau (see swath profile
395 of Fig. 8), indicate e the growth of the Ghiardo anticline is more recent of the Castelvetro and Villa
396 Camilla anticlines and the small ephemeral streams flowing through the Ghiardo plateau are in a
397 transient state of incision with respect to the growing topography where the k_{sn} maximum values
398 represent knickpoints migrating upstream toward the plateau bulge.
399
400 (3) The general correspondence of modeled stream steepness to other data is complicated by noise
401 that likely arises from subtle variations in rock type, bedload conditions, stream widths, and channel
402 transients. Notwithstanding this noise, in numerous studies variations of the steepness indexes along
403 stream long-profile have been demonstrated to be powerful in delineating spatial patterns and
404 variations of rock uplift rates, revealing robust and important qualitative results. The highest
405 steepness values consistently correspond to the regions with highest rock uplift and exhumation
406 rates.
407 The Mendocino triple junction region of northern California, where field area can be neatly divided
408 into high and low uplift zones, and late Pleistocene and Holocene rock-uplift rates varying over
409 nearly an order of magnitude, from 4 mm/yr to 0.5 mm/yr respectively (Merritts and Bull, 1989;
410 Merritts and Vincent, 1989; Merritts, 1996) has been analyzed by Kirby and Whipple (2001) and
411 Snyder et al. (2000). The latter study documents how channel steepness increases by a factor of ~
412 1.8 between the low and high uplift rate zones, whereas the range of concavity of streams within a
413 zone is not statistically difference. Wobus et al., (2006) investigated other study areas characterized
414 by remarkably different rock uplift rates: in the San Gabriel Mountains, where a restraining bend on

415 the San Andreas fault creates strong east-west gradients in long term exhumation rates, the field
416 area can be divided, following the apatite fission-track thermochronology (Blythe et al., 2000;
417 Spotila et al., 2002), into a western block with 2-3 mm/yr of rock uplift rate and in an eastern block
418 with 0.5mm/yr. Here, among channel profiles they reveal no systematic relation between concavity
419 index and rock uplift rates, while highest normalized steepness index ~150-175 are coincident with
420 the youngest cooling ages and highest long term erosion rates, such as lowest k_sn values ~65-80
421 with oldest cooling ages and lowest long-term erosion rates.
422 In the Siwalik Hills, central Nepal, formed by a fault-bend fold in the Himalayan foreland and
423 characterized by spatially uniform lithology, Wobus et al., (2006) reconstructed deformation rates
424 from the distribution of Holocene terraces. Uplift rates vary from ~4 mm/yr in the backlimb, to ~17
425 mm/yr at the range crest (i.e. the hinge), and back to ~0 mm/yr just south the main frontal thrust.
426 Concavity indices of channels range from 0.45 to 0.55, and steepness coefficients of strike-parallels
427 drainages, reveal a linear relation whit uplift rates, k_{sn} doubling its value from ~85 in low uplift
428 regions (~7 mm/yr) to ~200 in high uplift regions (~17 mm/yr).
429 Again, Kirby et al., (2007) evidenced that the steepness of the channel profiles incised into the
430 western flank of the Bolinas Ridge (Marin County, California) mimic changes in topographic relief
431 elevation, increasing 4-6 times from north to south of the Ridge line. Since there are little to no
432 climatic or lithologic changes along the relatively continuous sandstone body of Bolinas Ridge the
433 authors interpret the variations in channel steepness as a response to differential rock uplift across
434 the region. A subsequent model of the elastic deformation associated with a blind thrust and its
435 effects on the erosion (Johnson et al., 2009), finally demonstrated that such a structure underlying
436 the elevated region has the potential to produce topography similar to that of Marin County.
437 However, in all these different settings, the tectonic signal is strongly identifiable (difficult to hide).
438 Tectonics can be (1) independently determined, (2) it is variable at a wide regional scale and (3)
439 exhibits consistent differences, of at least an order of magnitude, between high and low uplift rates.
440

441 (4) Our analysis is distinct from those many related published studies in that the tectonic forcing of
442 these mountain front folds is gentle compared to the active tectonic areas that are typically studied.
443 In this respect, our study, which is characterized by long-term rates of incision ~ 0.1 – 0.3 mm/yr
444 (Ponza et al., submitted) is deforming an order of magnitude more slowly that comparable regions
445 deforming at ~ 1 – 2 mm/yr. The fact that we see correspondence between geology, structure, and
446 stream metrics is a contribution in its own right given the slow rates of rock uplift. This study has
447 illustrated a possible lower boundary for the k_{sn} modeling technique in identifying channel
448 responses to actively deforming landscapes.
449
450 (5) Documentation of the location and style of deformation of this part of the Apennine front helps
451 further understanding of the associated seismic hazards in that it defines the location and rates of
452 the active faults. This method helps revealing the subtle movements, often disregarded by earlier
453 field surveys. In the case study, this precise location of the active thrusts, whose slip rates can be
454 detected with incision rates (Ponza et al., submitted), helps defining a clear seismotectonic
455 framework for f the area.
456
457 **References**
458
459 Amorosi, A., L. Caporale, U. Cibin, M. L. Colalongo, G. Pasini, F. Ricci Lucchi, P. Severi, and
460 S. C. Vaiani, 1998. The Pleistocene littoral deposits (Imola Sands) of the northern Apennines
461 piedmont. Geol., 60, 83 – 118.
462
463 Balestrieri, M. L., Bernet, M., Brandon, M. T., Picotti, V., Reiners, P., Zattin, M., 2003. Pliocene
464 and Pleistocene exhumation and uplift of two key areas of the northern Apennines, in Uplift and
465 erosion; driving processes and resulting landforms; dynamic relations between crustal and
466 surficial processes, edited by Bartolini, C., L. Piccini, and N. R. Catto. Quaternary International,

101 – 102, 67 – 73.

Bally, A. W., L. Burbi, C. Cooper, and R. Ghelardoni, 1986. Balanced sections and seismic reflection profiles across the central Apennines, Mem. Soc. Geol. Ital., 35, 257 – 310.

Bartolini, C., 2003. When did the Northern Apennine become a mountain chain? In: Bartolini, C., L. Piccini, and N. R. Catto, N. R. (Eds.), Uplift and Erosion; Driving Processes and Resulting Landforms; Dynamic Relations Between Crustal and Surficial Processes. Quaternary International, 101 – 102, 75 – 80.

Bernini M., and Papani G., 1987. Alcune considerazioni sulla struttura del margine appenninico emiliano fra il T. Stirone ed il T. Enza (e sue relazioni con il Sistema del Taro), Atti Meeting "Brittle deformation analysis in neotectonics", Firenze, 17 aprile 1986, L'Ateneo Parmense.

Blythe, A.E., Burbank, D.W., Farley, K.A., and Fielding, E.J., 2000. Structural and topographic evolution of the central Transverse Ranges, California, from apatite fission-track, (U-Th)/He and digital elevation model analyses: Basin Research, 12, 97–114, doi: 10.1046/j.1365-2117.2000.00116.x.

Boccaletti, M., M. Coli, C. Eva, G. Ferrari, G. Giglia, A. Lazzarotto, A. Merlanti, F. Nicolich, R. Papani, and G. Postpischl, 1985. Considerations on the seismotectonics of the Northern Apennines, Tectonophysics, 117, 7 – 38.

Boccaletti, M., Bonini, M., Corti, G., Gasperini, P., Martelli, L., Piccardi, L.,Tanini, C., Vannucci, G., 2004. Seismotectonic Map of the Emilia-Romagna Region, 1:250000. Regione Emilia- Romagna CNR. SELCA, Firenze.

493

494 Burbank, D., and J. Vergés, 1994. Reconstruction of topography and related depositional
495 systems during active thrusting, J. Geophys. Res., 99, 20281–20297.

496

497 Carnicelli, S., Caporale, L., Marchi, N., Iasio, C., Ferrari, G. A., Guermandi, M., Tarocco, P.,
498 2003. Paleosoils of the margin, a case of study in the Reggio-Emilia province; notes for field
499 excursion. Pre-congress field trip, 4th Cartography European Congress, Bologna, Italy.
500 http://www.regione.emilia-
501 romagna.it/wcm/geologia/canali/convegni_e_seminari/congresso_europeo/congresso_04/Pre_Co
502 ngress_Field_Trip.pdf

503

504 Cremaschi, M., and Papani, G., 1975. Contributo preliminare alla neotettonica del margine
505 padano dell'appennino: le forme terrazzate comprese tra Cavriago e Quattro Castella (Reggio
506 E.), Acta Naturalia, Ateneo Parmense, 11, 335–371.

507

508 Duvall, A., E. Kirby, and D. Burbank, 2004. Tectonic and lithologic controls on bedrock channel
509 profiles in coastal California, J. Geophys. Res., 109, F03002, doi:10.1029/2003JF000086.

510

511 Elter, P., G. Giglia, M. Tongiorgi, and L. Trevisan, 1975. Tensional and compressional areas in
512 the recent (Tortonian to present) evolution of the Northern Apennines, Boll. Geofis. Teor. Appl.,
513 17, 3 – 18.

514

515 Finnegan, N. J., Roe, G., Montgomery, D.R., Hallet, B., 2005. Controls on the channel width of
516 rivers: Implications for modeling of fluvial incision of bedrock, Geology, 33, 229 – 232.

517

518 Flint, J. J., 1974. Stream gradient as a function of order, magnitude and discharge. Water

519 Resources Research, 10, 969 – 973.
520
521 Gasperi, G., Cremaschi, G., Mantovani, M., Uguzzoni, M. P., Cardarelli, A., Cattani, M. and
522 Labate D., 1987. Evoluzione plio-quaternaria del margine appenninico modenese e
523 dell'antistante pianura. note illustrative alla carta geologica, Mem. Soc. Geol. It., 39, 375 – 431.
524
525 Gasperi, G., Bettelli, G., Panini, F., Pizziolo, M., 1999. Note illustrative alla Carta Geologica d'
526 Italia a scala 1:50000 Foglio n 219 Sassuolo. Servizio Geologico d'Italia.
527
528 Hack, J. T., 1957. Studies of longitudinal profiles in Virginia and Maryland. U. S. Geological
529 Survey Professional Paper 294-B, 45 – 97.
530
531 Hill, K., and Hayward, A., 1988. Structural constraints on the Tertiary plate tectonic evolution of
532 Italy, Mar. Pet. Geol., 5, 2 – 16.
533
534 Isacks, B. L., 1992. Long term land surface processes: Erosion, tectonics and climate history in
535 mountain belts. In TERRA-1: Understanding the terrestrial environment, ed. P. M. Mather, pp.
536 21-36. London: Taylor and Francis.
537
538 Johnson, C. B., Furlong, K. P., Kirby, E., 2009. Integrated geomorphic and geodynamic
539 modeling of a potential blind thrust in the San Francisco Bay, Tectonophysics, 471, 319–
540 328,doi:10.1016/j.tecto.2009.03.002
541
542 Kirby, E.,. Johnson, C. B, Furlong, K. P., Heimsath, A., 2007. Transient channel incision along
543 Bolinas Ridge, California: Evidence for differential rock uplift, adjacent to the San Andreas
544 fault, J. Geophys. Res., 112 (F03S07).

545

546 Kirby, E., Whipple, K., Tang, W., and Chen, Z., 2003. Distribution of active rock uplift along
547 the eastern margin of the Tibetan Plateau: Inferences from bedrock channel longitudinal profiles,
548 Journal of Geophysical Research, v. 108, no. B4, doi: 10.1029/2001JB000861.

549

550 Kirby, E., Whipple, K. X., 2001. Quantifying differential rock-uplift rates via stream profile
551 analysis. Geology, 29, 415 – 418.

552

553 Kobor, J. S., and J. J. Roering, 2004. Systematic variation of bedrock channel gradients in the
554 central Oregon Coast Range: Implications for rock uplift and shallow landsliding,
555 Geomorphology, 62, 239 – 256.

556

557 Lavé, J., and J. P. Avouac, 2000. Active folding of fluvial terraces across the Siwalik Hills,
558 Himalayas of central Nepal, J. Geophys. Res., 105, 5735 – 5770.

559

560 Lavecchia, G., P. Boncio, and N. Creati, 2003a. A lithospheric-scale seismogenic thrust in
561 central Italy, J. Geodyn., 36, 79 – 94.

562

563 Lavecchia, G., P. Boncio, N. Creati, and F. Brozzetti, 2004. Stile strutturale, stato termo-
564 meccanico e significato sismogenetico del thrust Adriatico; dati e spunti da una revisione del
565 profilo CROP 03 integrata con l'analisi di dati sismologici, Boll. Soc. Geol. Ital., 123, 111 – 125.

566

567 Masek, J. G., Isacks, B. L., Gubbels, T. L., Fielding, E. J., 1994. Erosion and tectonics at the
568 margins of continental plateaus. Journal of Geophysical Research 99, NO. B7, 941–956.

569

570 Merritts, D.J., 1996. The Mendocino triple junction: Active faults, episodic coastal emergence,

571 and rapid uplift: Journal of Geophysical Research, 101, 6051 – 6070, doi: 10.1029/95JB01816.
572
573 Merritts, D.J., and Bull, W.B., 1989. Interpreting Quaternary uplift rates at the Mendocino triple
574 junction, northern California, from uplifted marine terraces: Geology, 17, 1020 – 1024.
575
576 Merritts, D., and Vincent, K.R., 1989. Geomorphic response of coastal streams to low,
577 intermediate, and high rates of uplift, Mendocino junction region, northern California:
578 Geological Society of America Bulletin, 101, 1373 – 1388.
579
580 Moglen, G. E., and R. L. Bras, 1995. The effect of spatial heterogeneities on geomorphic
581 expression in a model of basin evolution, Water Resour. Res., 31, 2613 – 2623.
582
583 Picotti, V., R. Capozzi, G. Bertozzi, F. Mosca, A. Sitta, and M. Tornaghi,, 2007. The Miocene
584 petroleum system of the Northern Apennines in the central Po Plain (Italy), in Thrust Belts and
585 Foreland Basins, From Fold Kinematics to Hydrocarbon System, edited by O. Lacombe et F.
586 Rome., pp. 117 – 131, Springer Verlag, Berlin.
587
588 Picotti, V., Pazzaglia, F. J., 2008. A new active tectonic model for the construction of the
589 Northern Apennines mountain front near Bologna (Italy). Journal of Geophysical Research. V.
590 113 (B8), 1-24.
591
592 Pizziolo, M., Segadelli, S., Vaiani S. C., submitted. Note illustrative alla Carta Geologica d'
593 Italia a scala 1:50000 Foglio n 200 Reggio nell'Emilia. Servizio Geologico d'Italia.
594
595 Ponza, A., Picotti, V., Pondrelli, S., Pazzaglia, F. J., Berti, C., submitted. The active deep
596 mountain front of the Northern Apennines: seismicity and geomorphology, Tecton

Ics.

Roe, G. H., et al., 2002. Effects of orographic precipitation variations on the concavity of steady-state river profiles, Geology, 30, 143 – 146.

Roe, G. H., D. R. Montgomery, B. Hallet, 2003. Orographic precipitation and the relief of mountain ranges, J. Geophys. Res., 108(B6), 2315, doi:10.1029/2001JB001521.

Royden, L., 1993. Evolution of retreating subduction boundaries formed during continental collision, Tectonics, 12, 629 – 638.

Scrocca, D., 2006. Thrust front segmentation induced by differential slab retreat in the Apennines (Italy), Terra Nova, 18, 154 – 161.

Scrocca, D., E. Carminati, C. Doglioni, and D. Marcantoni, 2007. Slab retreat and active shortening along the Central-Northern Apennines, in: Thrust Belts and Foreland Basins, From Fold Kinematics to Hydrocarbon System, edited by O. Lacombe and F. Roure, pp. 471 – 487, Springer Verlag, Berlin.

Sklar, L., Dietrich, W. E., 1998. River longitudinal profiles and bedrock incision models: Stream power and the influence of sediment supply. in Tinkler, K.J., and Wohl, E.E., eds., Rivers over rock: Fluvial processes in bedrock channels: Washington, D.C., American Geophysical Union 10.1146/annurev.earth.32.101802.120356, 237–260.

Sklar, L., and W. E. Dietrich, 2001. Sediment and rock strength controls on river incision into bedrock, Geology, 29, 1087 – 1090.

623 Sklar, L. S., and W. E. Dietrich, 2004. A mechanistic model for river incision into bedrock by
624 saltating bed load, Water Resour. Res., 40, W06301, doi:10.1029/2003WR002496.
625
626 Snyder, N., Whipple, K., Tucker, G., Merritts, D., 2000. Landscape response to tectonic forcing:
627 DEM analysis of stream profiles in the Mendocino triple junction region, northern California.
628 Geological Society of America Bulletin 112, 1250–1263.
629
630 Snyder, N.P., Whipple, K.X, Tucker, G.E., and Merrits, D.J., 2003a. Channel response to
631 tectonic forcing: Field analysis of stream morphology and hydrology in the Mendocino triple
632 junction region, northern California: Geomorphology, 53, 97–127, doi: 10.1016/S0169-
633 555X(02)00349-5.
634
635 Snyder, N.P., Whipple, K.X, Tucker, G.E., and Merrits, D.J., 2003b. Importance of a stochastic
636 distribution of floods and erosion thresholds in the bed rock river incision problem: Journal of
637 Geophysical Research, v. 39, doi: 10.1029/2001WR001057.
638
639 Spagnolo, M. and Pazzaglia F. J., 2005. Testing the geological influences on the evolution of
640 river profiles: a case from the Northern Apennines (Italy), Geogr. Fis. Dinam. Quat. 28, 103 –
641 113.
642
643 Spotila, J.A., House, M.A., Blythe, A., Niemi, N.A., and Bank, G.C., 2002. Controls on the
644 erosion and geomorphic evolution of the San Bernardino and San Gabriel Mountains, southern
645 California, in Barth, A.P., ed., Contributions to crustal evolution of the southwestern United
646 States: Geological Society of America Special Paper 365, 205–230.
647
648 Stock, J., and W. E. Dietrich, 2003. Valley incision by debris flows: Evidence of a topographic

649 signature, Water Resour. Res., 39(4), 1089, doi:10.1029/2001WR001057.
650
651 Stock, J. D., and D. R. Montgomery, 1999. Geologic constraints on bed- rock river incision
652 using the stream power law, J. Geophys. Res., 104, 4983 – 4993.
653
654 Tucker, G.E., and Bras, R.L., 2000. A stochastic approach to modeling the role of rainfall
655 variability in drainage basin evolution: Water Resources Research, 36, 1953–1964, doi:
656 10.1029/2000WR900065.
657
658 Tucker, G.E., and Whipple, K.X, (2002). Topographic outcomes predicted by stream erosion
659 models: Sensitivity analysis and intermodel comparison, Journal of Geophysical Research, 107,
660 B9, doi:10.1029/2001JB000162.
661
662 Tucker, G.E., 2004. Drainage basin sensitivity to tectonic and climatic forcing: Implications of a
663 stochastic model for the role of entrainment and erosion thresholds: Earth Surface Processes and
664 Landforms, 29, 185–205, doi: 10.1002/esp.1020.
665
666 Wegmann, K. W., Pazzaglia, F. J., 2002. Holocene strath terraces, climate change, and active
667 tectonics: The Clearwater river basin, Olympic peninsula, Washington State. Geological Society
668 of America Bull, 114, 731 – 744.
669
670 Wegmann, K. W., Pazzaglia, F. J., 2009. Late Quaternary fluvial terraces of the Romagna and
671 Marche Apennines, Italy: Climatic, lithologic, and tectonic controls on terrace genesis in an
672 active orogen. Quaternary Science Reviews 28, 1-2, 137-165. doi
673 10.1016/j.quascirev.2008.10.006
674

675 Whipple, K. X., Tucker, G. E., 1999. Dynamics of the stream-power river incision model:
676 Implications for height limits of mountain ranges, landscape response timescales, and research
677 needs. Journal of Geophysical Research 104, 17661 – 17674.
678
679 Whipple, K. X., Tucker, G. E., 2002. Implications of sediment-flux-dependent river incision
680 models for landscape evolution. Journal of Geophysical Research 107, no. B9, doi:
681 10.1029/2001JB000162.
682
683 Whipple, K. X., Wobus. C., Krosby, B., Kirby, E., Sheehan, D., 2007. New Tools for
684 Quantitative Geomorphology: Extraction and Interpretation of Stream Profiles from Digital
685 Topographic Data. GSA Short Course: #506.
686
687 Willgoose, G., Bras, R.L., and Rodriguez-Iturbe, I., 1991. A coupled channel network growth
688 and hillslope evolution model: I. Theory: Water Resources Research, v. 27, no. 7, 1671–1684,
689 doi: 10.1029/91WR00935.
690
691 Wilson L.F., Pazzaglia F. J., Anastasio D. J., 2009. A fluvial record of active fault-propagation
692 folding, Salsomaggiore anticline, northern Apennines, Italy. J. Geophys. Res. 114 (B8), doi
693 10.1029/2008JB005984.
694
695 Wobus, C., Whipple, K. X., Kirby, E., Snyder, N., Johnson, J., Spyropolou, K., Crosby, B.,
696 Sheehan, D., 2006. Tectonics from topography: Procedures, promise, and pitfalls. Geological
697 Society of America Special Paper 398, 55w–74.
698
699 Zaprowski, B.J., Evenson, E.B., Pazzaglia, F.J., Epstein, J., 2001. Knickzone propagation in the
700 Black Hills and northern High Plains; a different perspective on the late Cenozoic exhumation of

the Laramide Rocky Mountains. Geology 29 (6), 547 – 550.

Figures Captions

Figure 1.: *Location of the studied areas (colored boxes) in the foothills of the Northern Apennines at the boundary between the extensional and the compressional realms.*

Figure 2. *Geologic map, modified from Gasperi et al., 1999, Carta Geologica d'Italia, scale 1:50000, foglio Sassuolo and partially compiled from R.E.R. Dashed blue box shows the surfaces of swath profile in figure 6 and 7.Quaternary fluvial terraces chronostratigraphy follows Picotti and Pazzaglia 2008 and Wegmann and Pazzaglia 2009.*

Figure 3. *Geologic map modified Carnicelli et al., (2003) and partially compiled from R.E.R. Quaternary fluvial terraces chronostratigraphy in accordance with Picotti and Pazzaglia 2008 and Wegmann and Pazzaglia 2009. Geologic structure traces are adjusted on the base of well stratigraphy and seismic lines.*

Figure 4. *Geological section across the Ghiardo plateau, modified from Carnicelli et al., (2003): Pleistocene terrace deposits chronostratigraphy in accordance with Picotti and Pazzaglia (2008) and Wegmann and Pazzaglia (2009).*

Figure 5. *Channel 13 plot as exits from Whipple et al., (2007) tool: Long profile (a), Drainage Area vs. Distance from mouth (b) and Log Slope vs. Log Area (c). (a) Raw elevations are in green, smoothed in pink. The dark blue lines are the profiles predicted by the regressed channel concavity; the cyan lines are for the specified reference concavity, $\theta_{ref.}$ (c) K_{sn} values extracted from channel*

reaches: slope of log S vs. log A scaling is the concavity index, where blue and cyan colors show the regressed and reference concavities respectively; y-intercept is the steepness index k_{sn}. Red squares are log- bin averages of the Slope –Area data.

Figure 6. *Swath profile of topography perpendicular to anticlinal hinge of the Castelvetro and the Villa Camilla anticline, vertical exaggeration 15x. Maximum (shaded line), minimum (white line), and mean (black line) elevations extracted from a 5 km wide and 9 km long swath (location and kilometric profile are shown in the blue dashed box A in Figure 2). Vertical dashed lines correspond to locations of anticlinal hinge of Villa Camilla and Castelvetro anticlines from Gasperi et al., (1999). Data source is a RER 10 m Elevation Dataset.*

Figure 7. *Swath profile of topography parallel to anticlinal hinge of Castelvetro anticline, vertical exaggeration 20x. Maximum (shaded line), minimum (white line), and mean (black line) elevations extracted from a 1 km wide and 12 km long swath (location is shown as blue dashed box B in Figure 2). Data source is a RER 10 m Elevation Dataset. Guerro river (Gu), Tiepido river (Tie), Panaro river (Pa). Numbers correspond to stream numeration in k_{sn} analysis shown in figure 10 and 12.*

Figure 8: *Swath topographic profile perpendicular to anticlinal hinge of Ghiardo anticline, vertical exaggeration 20x. The 1 km wide and 11 km long area of swath profile is dashed in figure 3: its relative kilometric profile runs in the box middle. Black circle highlights, in correspondence of the fold frontal limb, a zone of increasing in k_sn steepness index (see fig 9).*

Figure 9. *Map of k_{sn} index color-coded to magnitude in a hillshaded topography of Ghiardo Plateau. Light azure to dark blue color scales from lowest to highest K_{sn} value. Dashed box shows an example of stream reaches about 3–4 km long straddling the fold axes and examined in tables 2*

753 *and 3.*

754 Figure 10. *Layout of color-coded stream segments based on their normalized steepness indices in*
755 *Castelvetro – Vignola foothills. Light blue to dark blue color scales from lowest to highest* K_{sn}
756 *value. Dashed box shows an example of stream reaches about 3–4 km long straddling the fold axes*
757 *and examined in tables 2 and 3.*

758 Figure 11. *Selected channel reaches crossing the active strucutres in the Ghiardo plateau: light*
759 *blue to blue color-coded to magnitude spectum have been here regularly graduated from* k_{sn} *5 to*
760 *21, while greater values (comprised between 21 and 52.5) maintain the same dark blue color. Red*
761 *stars mark maximum values of* k_{sn} *smoothed for a 5-*k_{sn} *-value moving window, while white stars*
762 *mark minimum values of* k_{sn} *smoothed for a 5-*k_{sn} *-value moving window. Drainage areas of the*
763 *examined stream reaches straddling the fold axes not exceed 170* km^2.

764

765 Figure12. *Selected channel reaches crossing the active strucutres in in the Castelvetro – Vignola*
766 *foothills: light blue to blue color-coded to magnitude spectrum is here regularly graduated from* k_{sn}
767 *6 to 23, while greater values (from 23 to 40.6) result constricted to darkest blue color (see table 3).*
768 *Red stars mark maximum values of* k_{sn} *smoothed for a 5-*k_{sn} *-value moving window, while white*
769 *stars mark minimum values of* k_{sn} *smoothed for a 5-*k_{sn} *-value moving window. Drainage areas of*
770 *the examined stream reaches straddling the fold axes not exceed 170* km^2.

771

772

773 Table 1. *Topographic characteristics of channels profiles in the studied areas*[c].

774 [a] *Spatial reference of data Projection: European Datum 1950 Transverse Mercator, fuse 32N*

775 [b] *Main local rivers and creeks*

776 [c]*Read 1.6E + 07 as* 1.6×10^7

777 [d]*Calculated with* $\theta_{ref} = 0.45$

778

779 Table 2. *Variations of k_{sn} along selected channel reaches, crossing the active tectonic structures*

780 *on the Ghiardo plateau.*

781 [a] *Spatial reference of data Projection: European Datum 1950 Transverse Mercator, fuse 32N,*

782 *false Northing -4000000 m.*

783 [b] *Drainage area expressed in m^2*

784 [c]*Read 3.2E + 06 as 3.2 x 10^{6}*[d]*Calculated with $\theta_{ref} = 0.45$*

785

786 Table 3. *Variations of k_{sn} along selected channel reaches crossing the active tectonic structures*

787 *in the Castelvetro – Vignola foothills.*

788 [a] *Spatial reference of data Projection: European Datum 1950 Transverse Mercator, fuse 32N,*

789 *false Northing -4000000 m.*

790 [b] *Drainage area expressed in m^2*

791 [c]*Read 2.7E + 07 as 2.7 x 10^{7}*

792 [d]*Calculated with $\theta_{ref} = 0.45$*

793

Figure

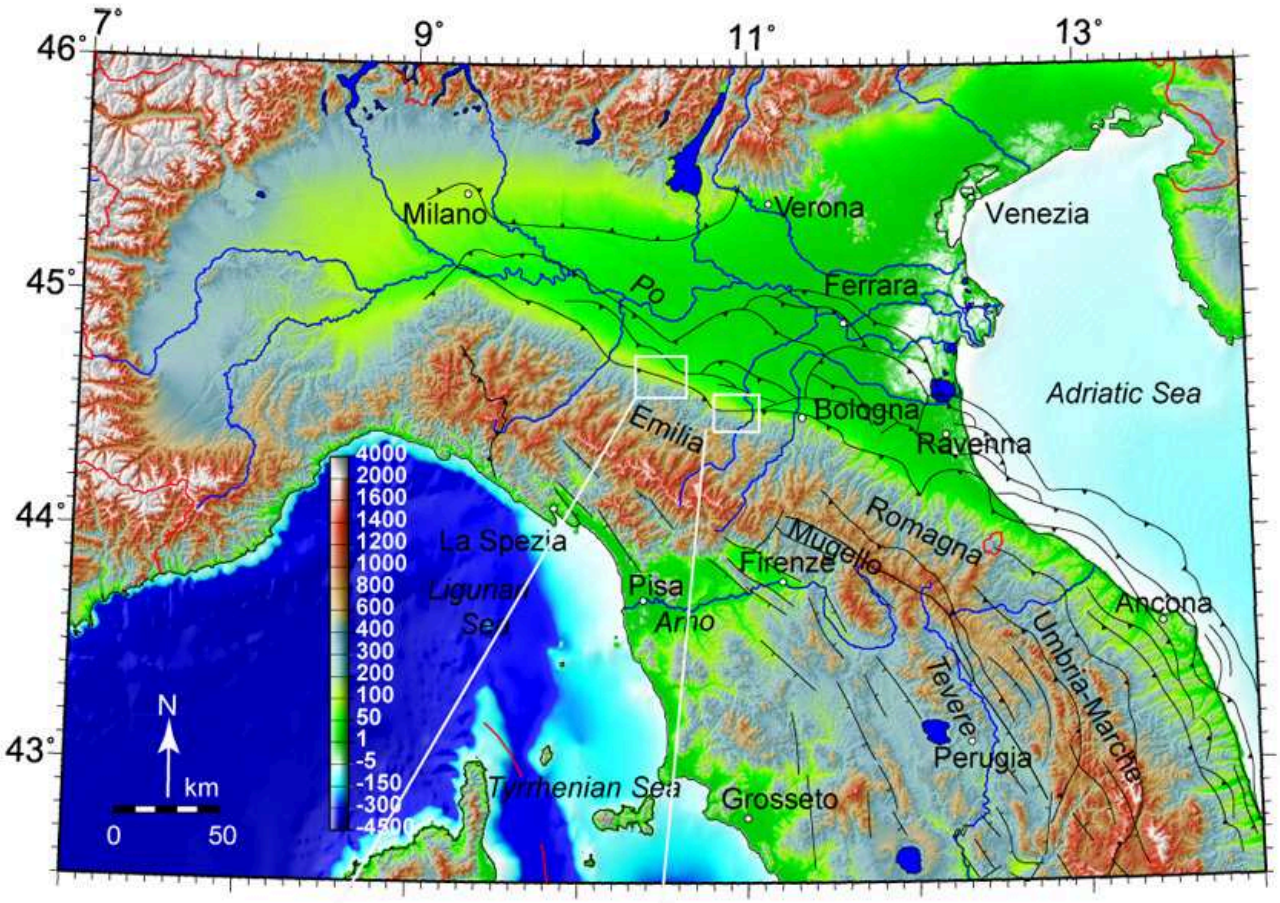
7°
9°
11°
13°
46°
45°
44°
43°
Milano
Verona
Venezia
Po
Ferrara
Adriatic Sea
Emilia
Bologna
Ravenna
Romagna
Mugello
Firenze
La Spezia
Ligurian Sea
Pisa
Arno
Ancona
Umbria-Marche
Tevere
Perugia
Tyrrhenian Sea
Grosseto
4000
2000
1600
1400
1200
1000
800
600
400
300
200
100
50
1
-5
-150
-300
-450
N
km
0
50

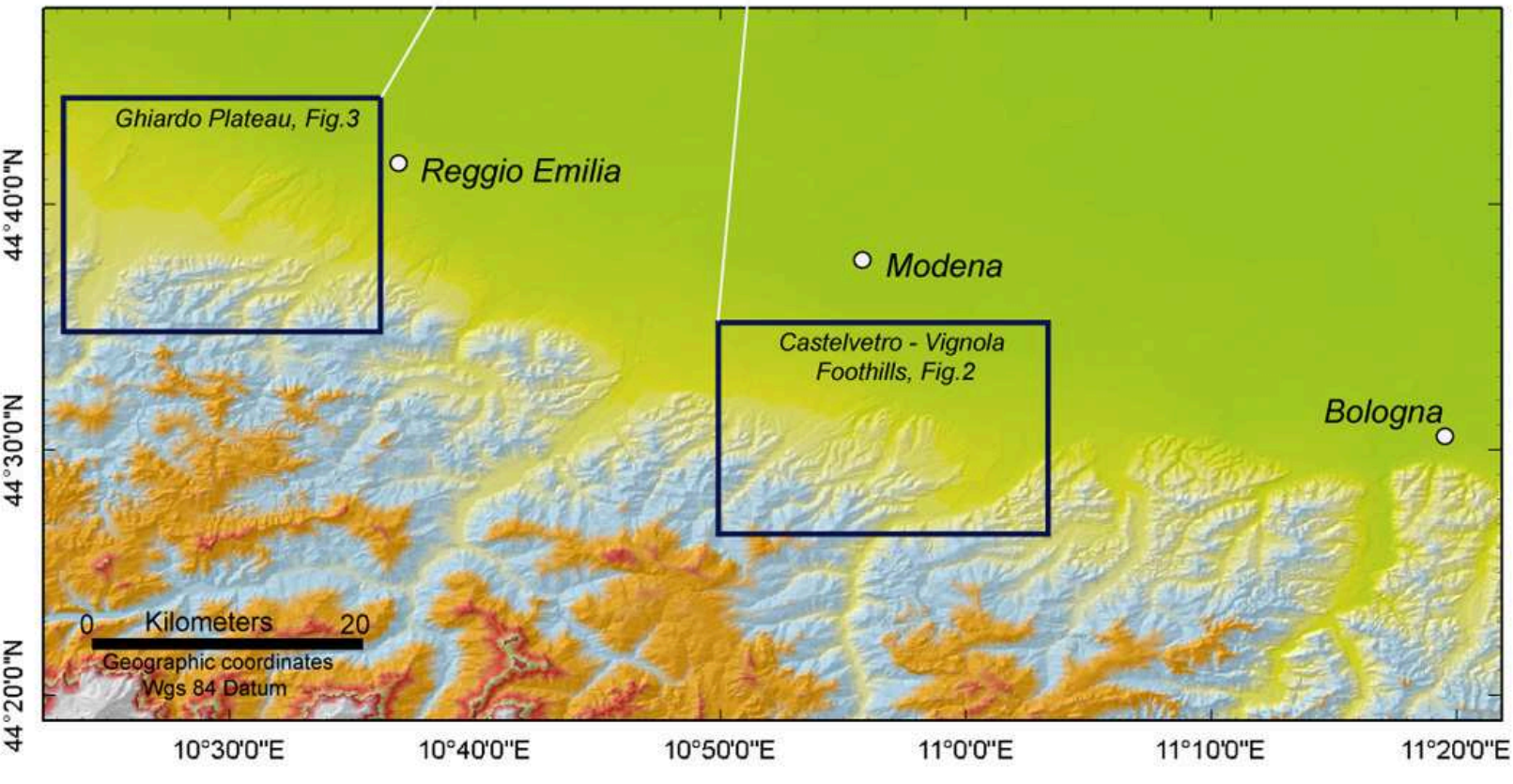
Ghiardo Plateau, Fig.3
Reggio Emilia
Modena
Castelvetro - Vignola
Foothills, Fig.2
Bologna
0
Kilometers
20
Geographic coordinates
Wgs 84 Datum
44°40'0"N
44°30'0"N
44°20'0"N
10°30'0"E
10°40'0"E
10°50'0"E
11°0'0"E
11°10'0"E
11°20'0"E

Figure

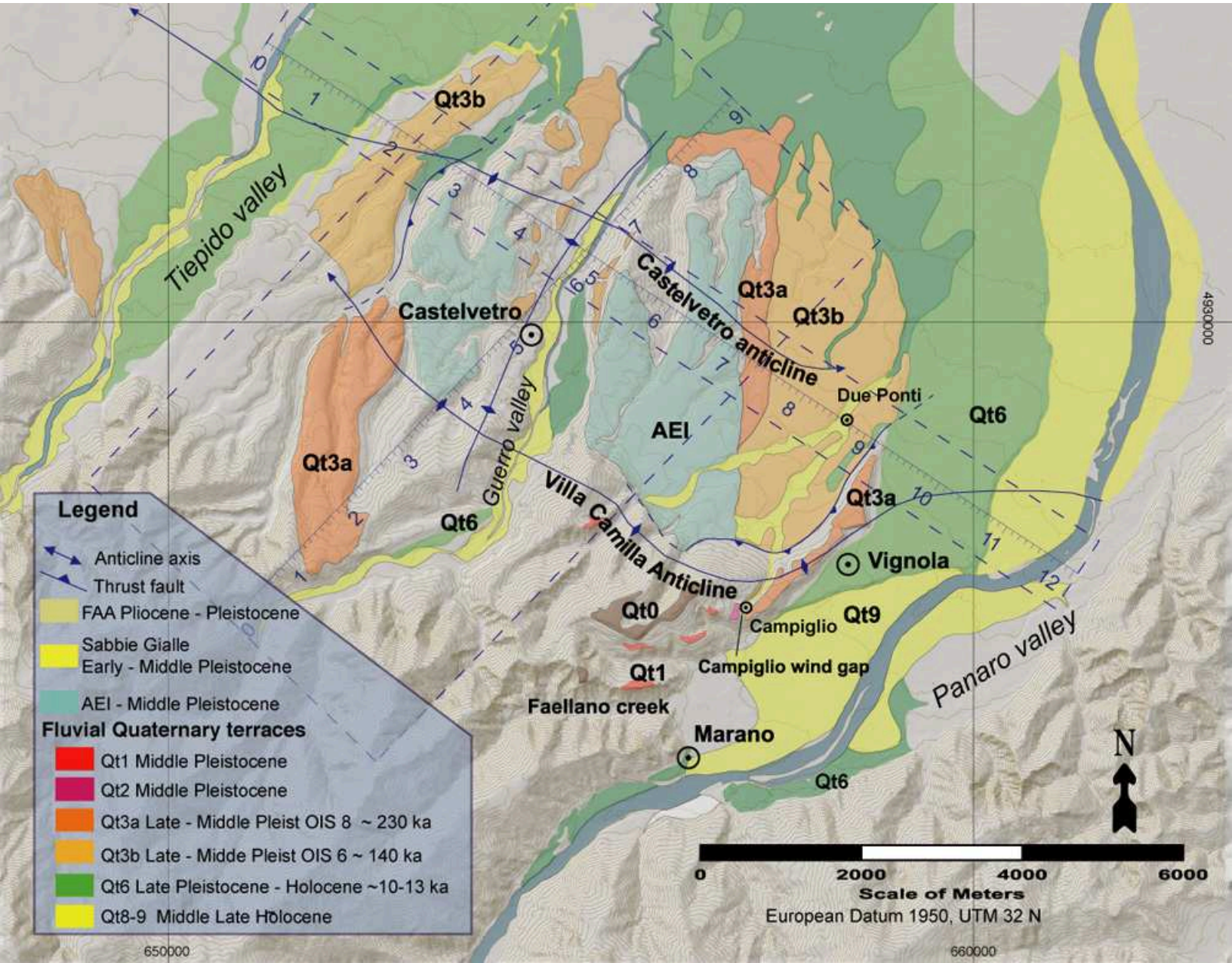
Qt3b
Tiepido valley
Castelvetro
Castelvetro anticline
Qt3a
Qt3b
Due Ponti
Qt6
AEl
Qt3a
Guerro valley
Villa Camilla Anticline
Qt6
Qt3a
Vignola
Qt0
Campiglio
Qt9
Qt1
Campiglio wind gap
Faellano creek
Panaro valley
Marano
Qt6
N
0
2000
4000
6000
Scale of Meters
European Datum 1950, UTM 32 N
650000
660000
4930000
Legend
Anticline axis
Thrust fault
FAA Pliocene - Pleistocene
Sabbie Gialle
Early - Middle Pleistocene
AEl - Middle Pleistocene
Fluvial Quaternary terraces
Qt1 Middle Pleistocene
Qt2 Middle Pleistocene
Qt3a Late - Middle Pleist OIS 8 ~ 230 ka
Qt3b Late - Midde Pleist OIS 6 ~ 140 ka
Qt6 Late Pleistocene - Holocene ~10-13 ka
Qt8-9 Middle Late Holocene

Figure

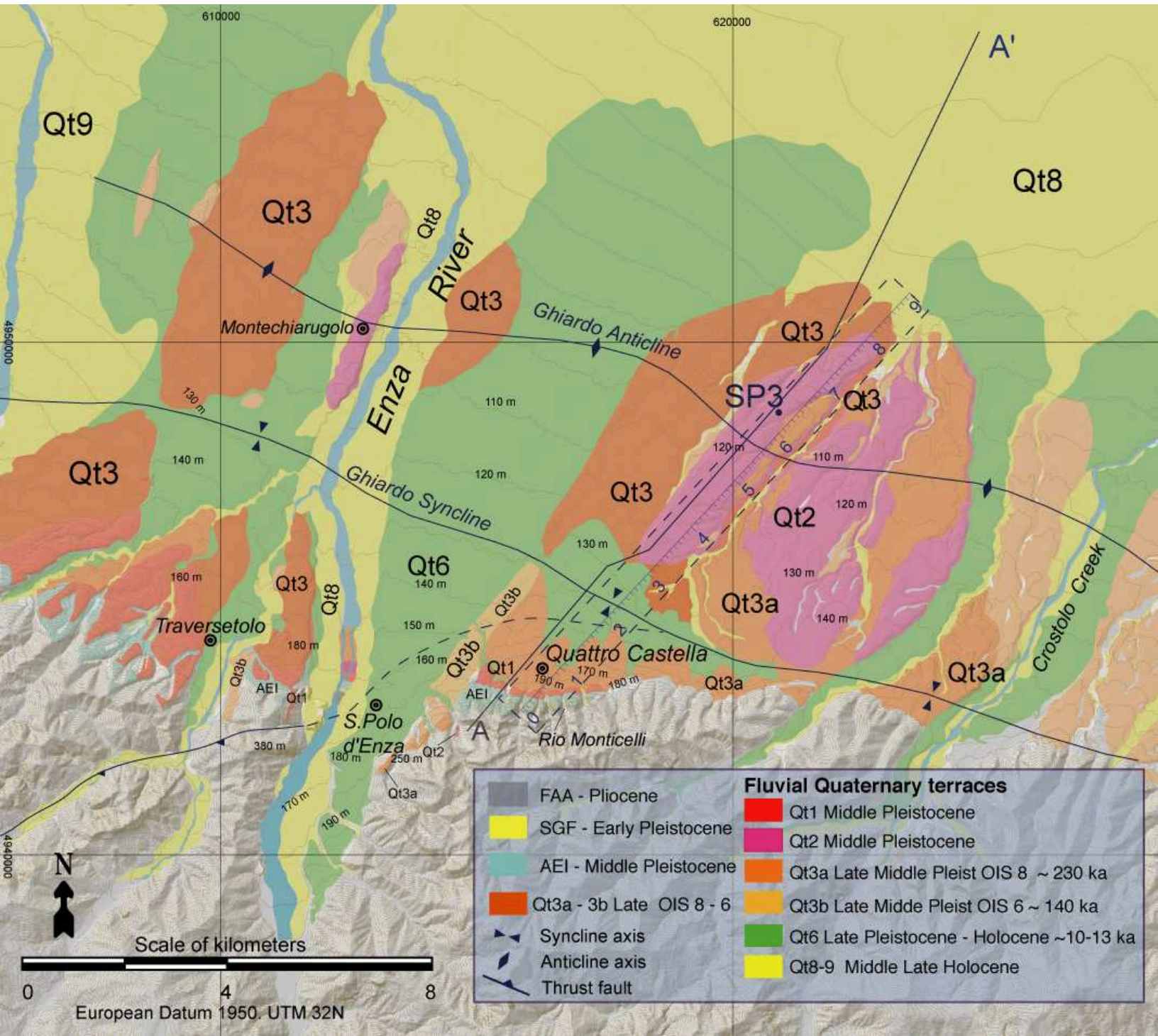
610000
620000
4950000
4940000
A'
A
Qt9
Qt8
Qt3
Qt6
Qt2
Qt3a
Qt1
Qt3b
AEI
Montechiarugolo
Ghiardo Anticline
Ghiardo Syncline
Enza River
Traversetolo
S.Polo d'Enza
Quattro Castella
Rio Monticelli
Crostolo Creek
SP3
130 m
140 m
110 m
120 m
160 m
150 m
180 m
380 m
250 m
170 m
190 m
N
Scale of kilometers
0
4
8
European Datum 1950. UTM 32N
FAA - Pliocene
SGF - Early Pleistocene
AEI - Middle Pleistocene
Qt3a - 3b Late OIS 8 - 6
Syncline axis
Anticline axis
Thrust fault
Fluvial Quaternary terraces
Qt1 Middle Pleistocene
Qt2 Middle Pleistocene
Qt3a Late Middle Pleist OIS 8 ~ 230 ka
Qt3b Late Midde Pleist OIS 6 ~ 140 ka
Qt6 Late Pleistocene - Holocene ~10-13 ka
Qt8-9 Middle Late Holocene

Figure

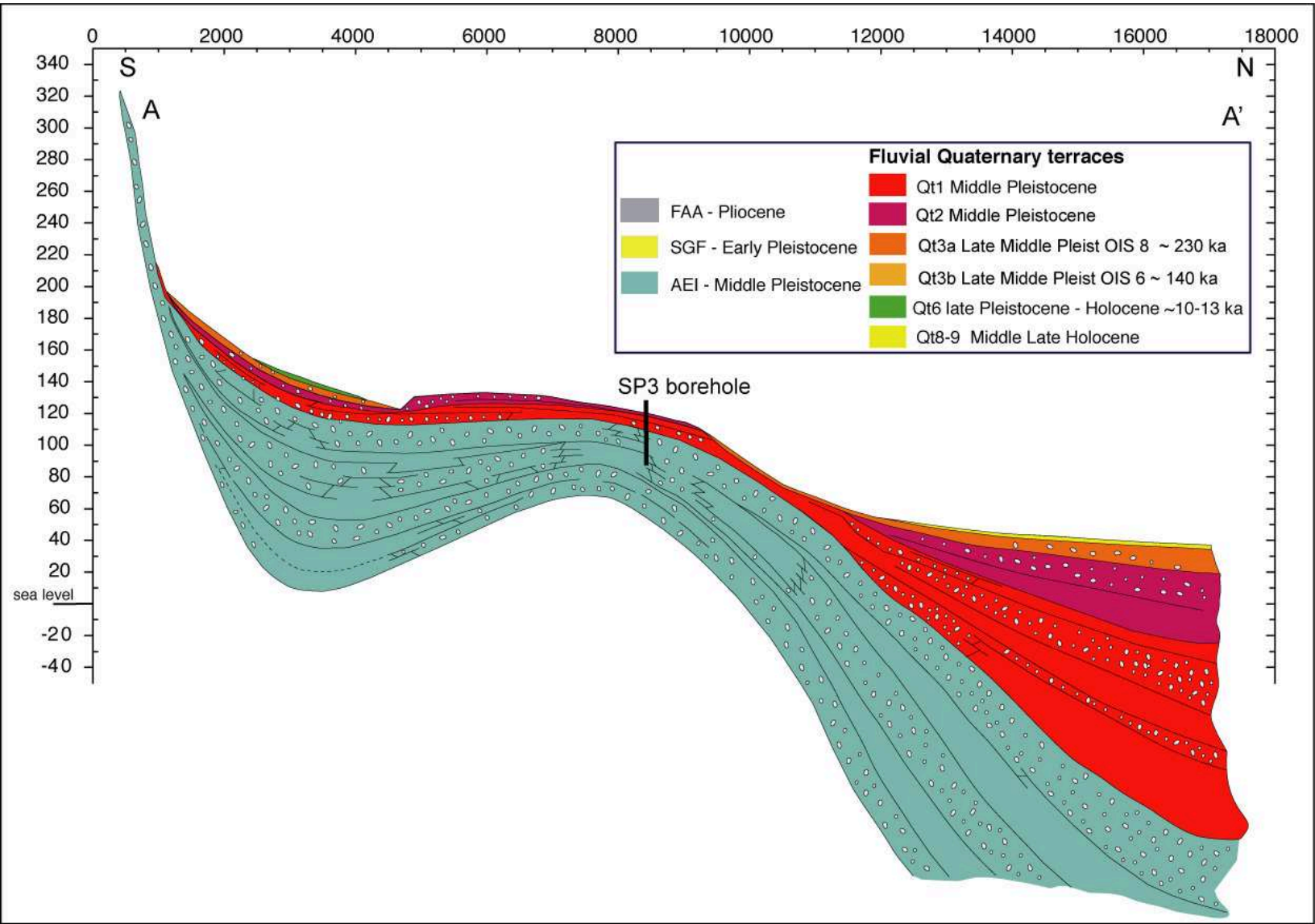
0
2000
4000
6000
8000
10000
12000
14000
16000
18000
340
320
300
280
260
240
220
200
180
160
140
120
100
80
60
40
20
sea level
-20
-40
S
A
N
A'
Fluvial Quaternary terraces
Qt1 Middle Pleistocene
Qt2 Middle Pleistocene
Qt3a Late Middle Pleist OIS 8 ~ 230 ka
Qt3b Late Midde Pleist OIS 6 ~ 140 ka
Qt6 late Pleistocene - Holocene ~10-13 ka
Qt8-9 Middle Late Holocene
FAA - Pliocene
SGF - Early Pleistocene
AEI - Middle Pleistocene
SP3 borehole

Figure

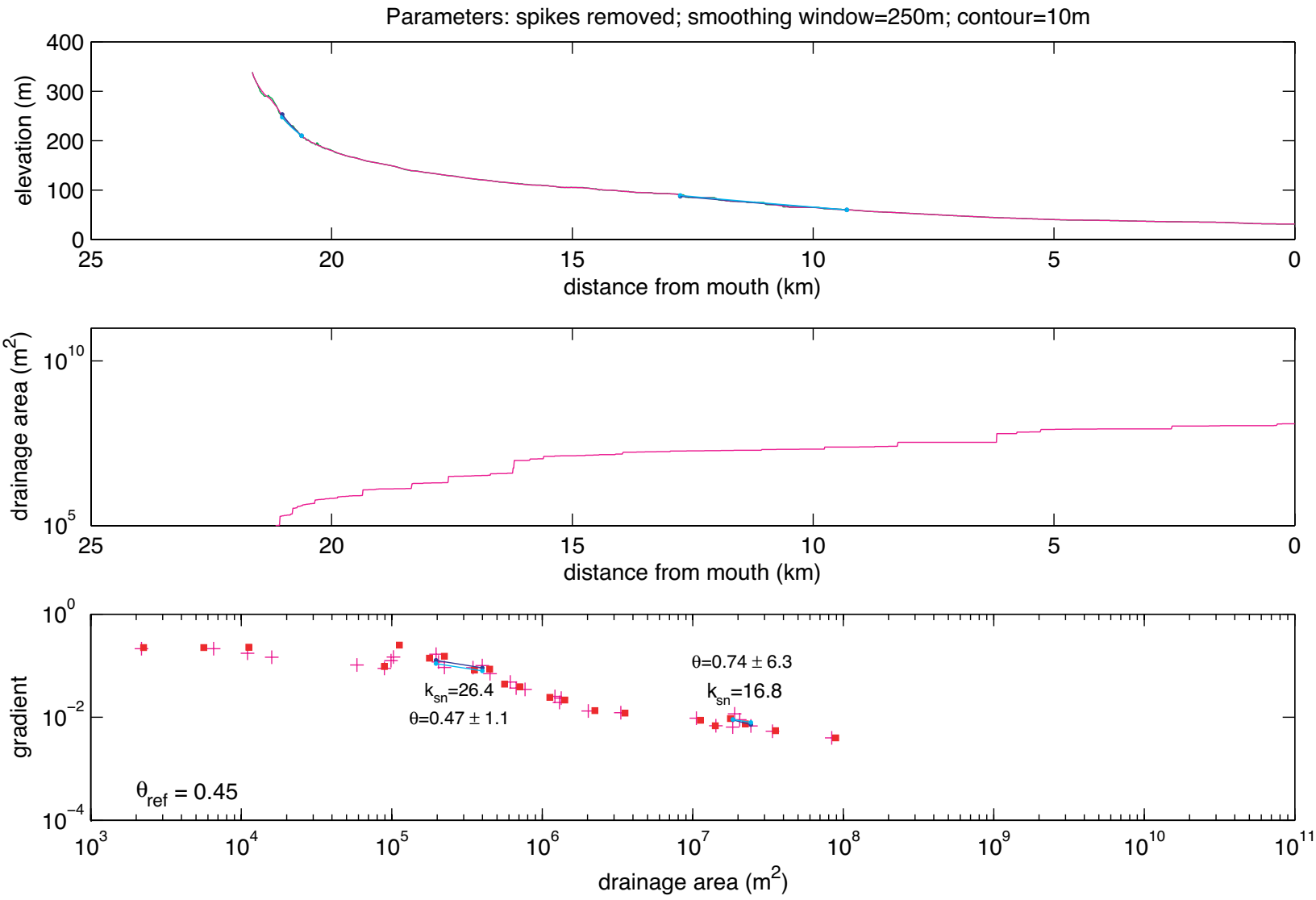
Parameters: spikes removed; smoothing window=250m; contour=10m
elevation (m)
400
300
200
100
0
25
20
15
10
5
0
distance from mouth (km)
drainage area (m^2)
10^{10}
10^{5}
25
20
15
10
5
0
distance from mouth (km)
gradient
10^{0}
10^{-2}
10^{-4}
k_{sn}=26.4
θ=0.47 ± 1.1
θ=0.74 ± 6.3
k_{sn}=16.8
θ_{ref} = 0.45
10^{3}
10^{4}
10^{5}
10^{6}
10^{7}
10^{8}
10^{9}
10^{10}
10^{11}
drainage area (m^2)

Figure

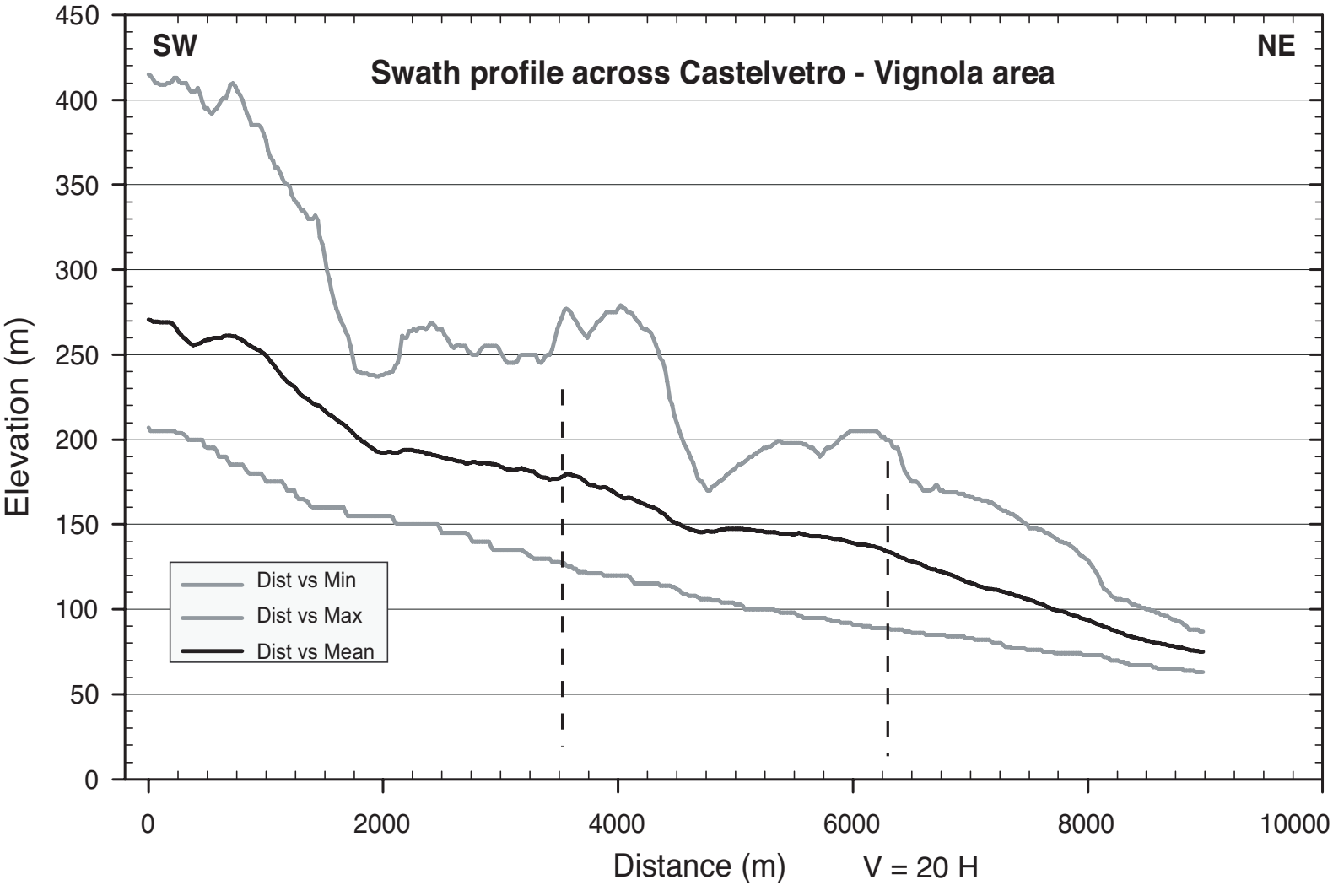
SW
NE
Swath profile across Castelvetro - Vignola area
Elevation (m)
Distance (m)
V = 20 H
Dist vs Min
Dist vs Max
Dist vs Mean
450
400
350
300
250
200
150
100
50
0
0
2000
4000
6000
8000
10000

Figure

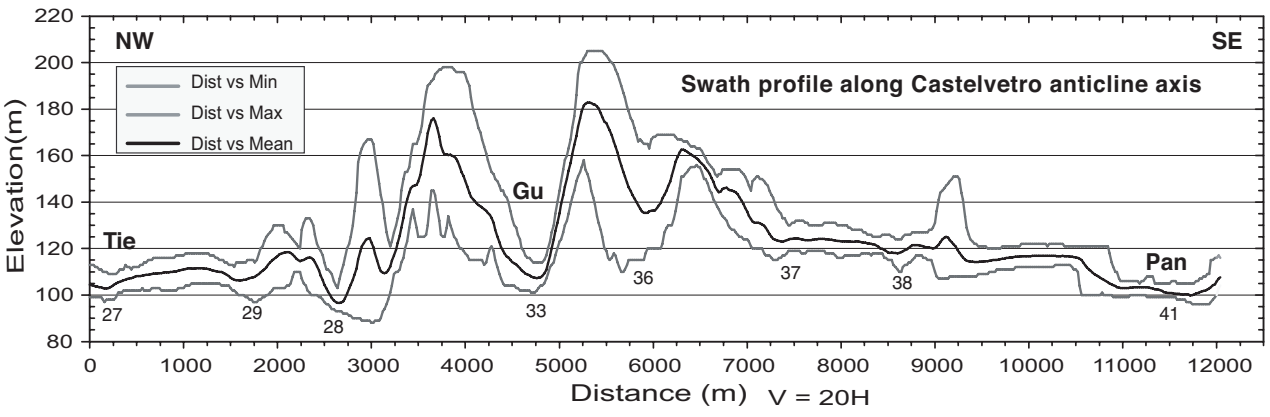
NW
SE
Swath profile along Castelvetro anticline axis
Dist vs Min
Dist vs Max
Dist vs Mean
Elevation(m)
Distance (m)
V = 20H
Tie
Gu
Pan
27
29
28
33
36
37
38
41
220
200
180
160
140
120
100
80
0
1000
2000
3000
4000
5000
6000
7000
8000
9000
10000
11000
12000

Figure

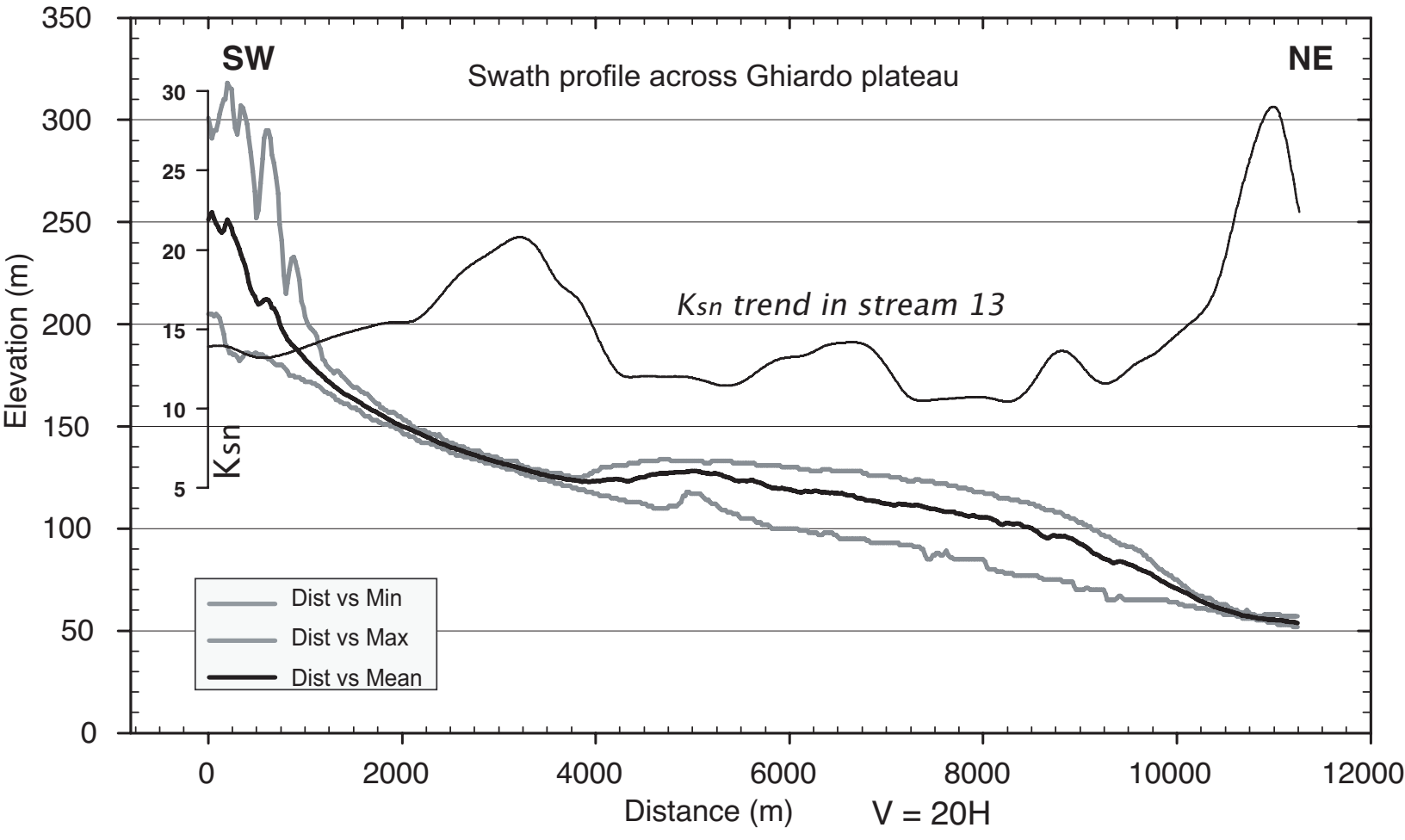
SW
NE
Swath profile across Ghiardo plateau
Ksn trend in stream 13
Ksn
30
25
20
15
10
5
Dist vs Min
Dist vs Max
Dist vs Mean
Elevation (m)
350
300
250
200
150
100
50
0
0
2000
4000
6000
8000
10000
12000
Distance (m)
V = 20H

Figure

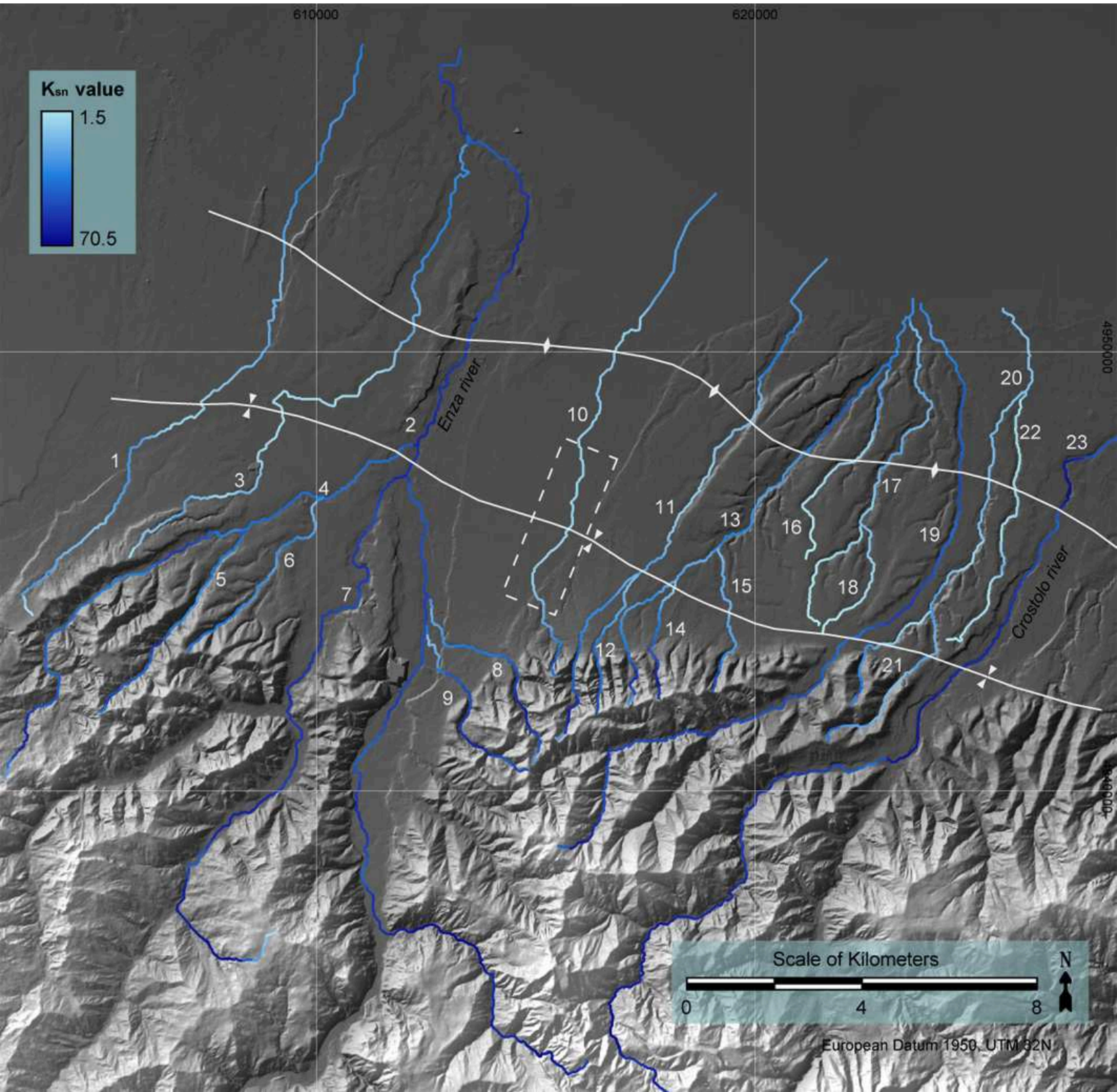
610000
620000
4950000
Ksn value
1.5
70.5
Enza river
Crostolo river
1
2
3
4
5
6
7
8
9
10
11
12
13
14
15
16
17
18
19
20
21
22
23
Scale of Kilometers
0
4
8
N
European Datum 1950, UTM 32N

Figure

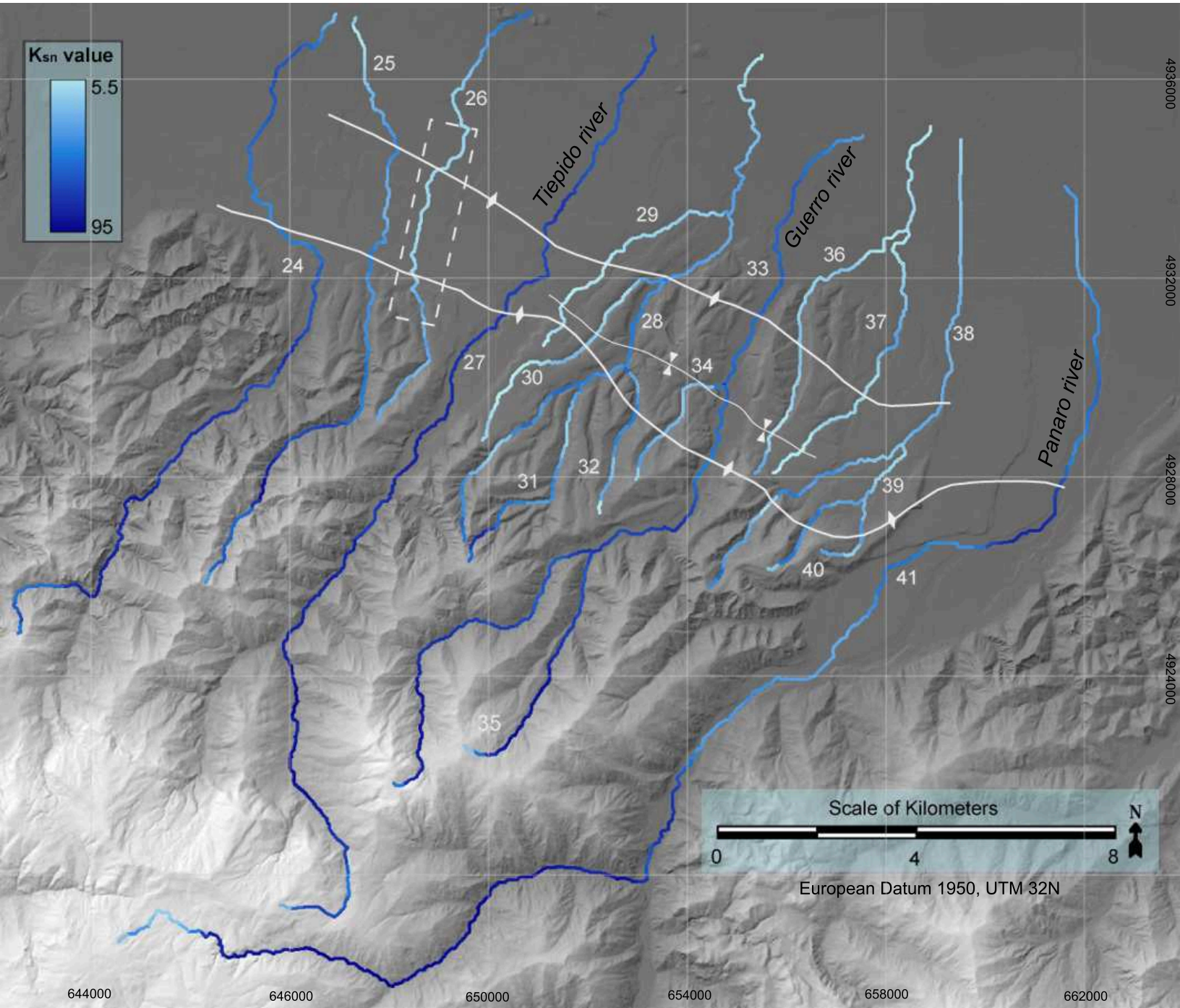
Ksn value
5.5
95
25
26
Tiepido river
29
Guerro river
36
33
24
28
37
38
27
34
30
Panaro river
32
31
39
40
41
35
Scale of Kilometers
0
4
8
N
European Datum 1950, UTM 32N
4936000
4932000
4928000
4924000
644000
646000
650000
654000
658000
662000

Figure

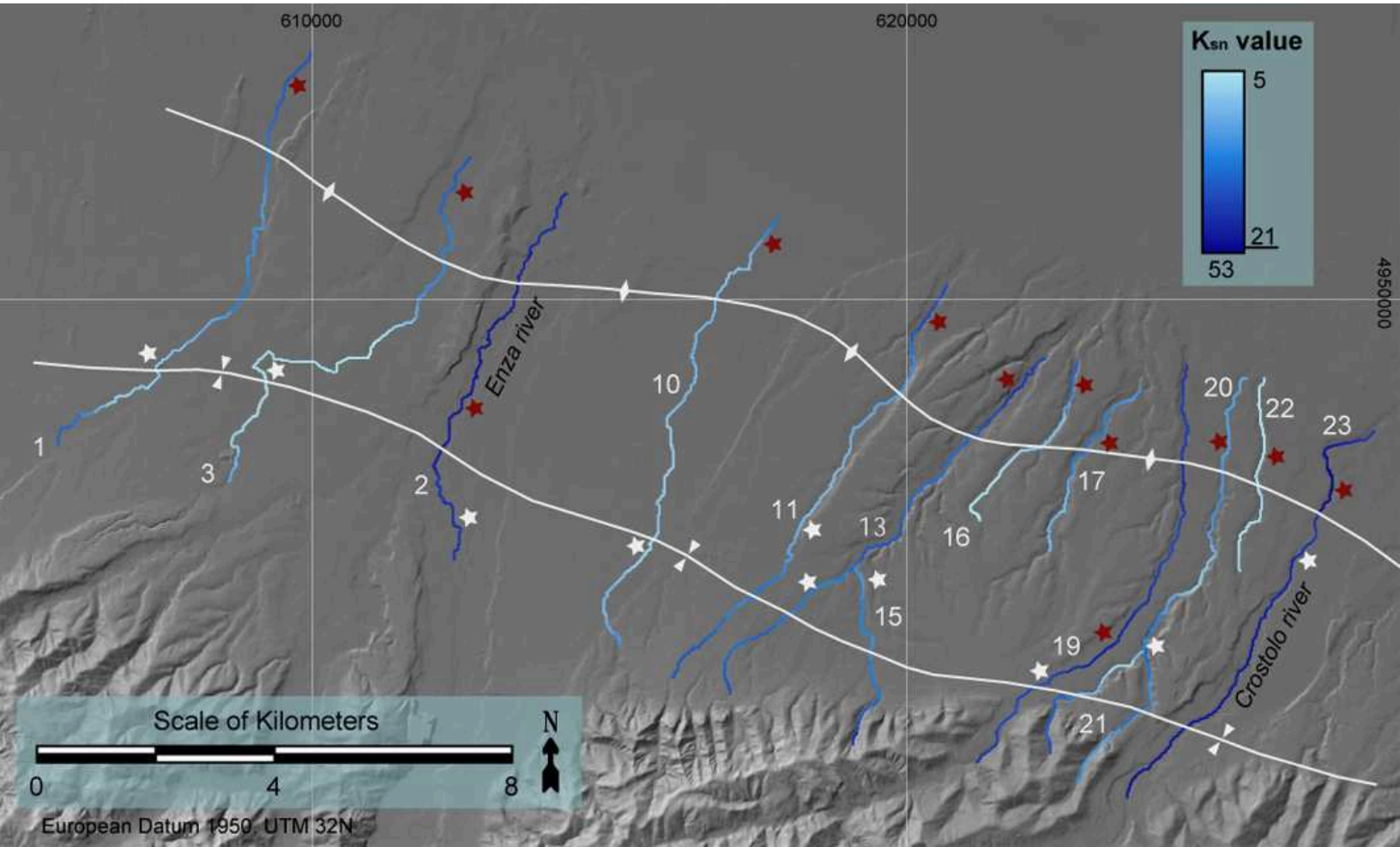
610000
620000
4950000
Ksn value
5
21
53
Enza river
Crostolo river
1
2
3
10
11
13
15
16
17
19
20
21
22
23
Scale of Kilometers
0
4
8
N
European Datum 1950, UTM 32N

Figure

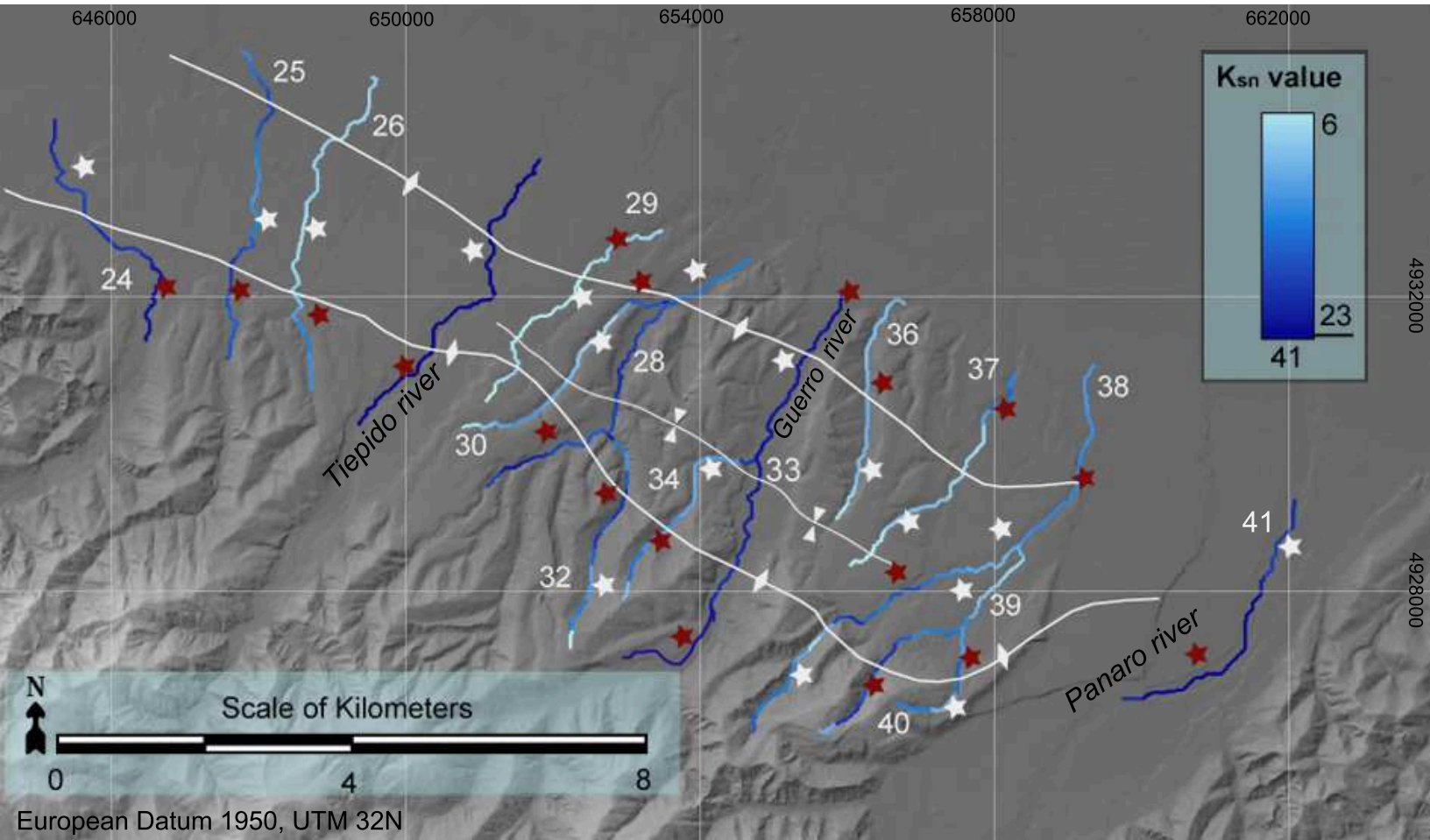
646000
650000
654000
658000
662000
4932000
4928000
Ksn value
6
23
41
25
26
24
29
28
30
Tiepido river
Guerro river
36
37
38
34
33
32
39
41
40
Panaro river
N
Scale of Kilometers
0
4
8
European Datum 1950, UTM 32N

Table

GHIARDO K_{sn} Analysis										
Stream	Easting_headwater[a]	Northing_headwater[a]	Easting_mouth[a]	Northing_mouth[a]	Max Area (m^2)	Min Area (m^2)	Max_k_{sn}[d]	Min_k_{sn}[d]	Length (km)	Name
1	603341.4	4944206.5	611001.4	4956786.5	1.55E+07	2.60E+04	14.9	6.6	17.78	
2[b]	616031.4	4933686.5	612811.4	4956206.5	1.98E+08	3.91E+04	70.6	17.7	32.80	Enza river
3	605821.4	4945546.5	613401.4	4954726.5	2.03E+07	2.16E+04	17.7	5.2	16.74	Rio Zola
4	602951.4	4940506.5	612171.4	4947896.5	2.53E+07	4.17E+04	37.2	11.2	15.39	Masdone creek
5	605171.4	4941956.5	608281.4	4945786.5	3.94E+06	2.46E+04	25.9	12.2	5.97	Madolo creek
6	607181.4	4943376.5	609961.4	4946576.5	5.54E+06	6.19E+04	18.1	9.5	5.48	Rio Lama
7	608841.4	4936706.5	611971.4	4947176.5	6.44E+07	4.48E+04	20.9	9.4	17.84	Termina creek
8	614591.4	4940476.5	612511.4	4943556.5	2.58E+06	4.03E+04	34.3	8.7	5.23	
9	615021.4	4940856.5	612581.4	4944376.5	3.80E+06	5.19E+04	37.6	9.7	5.86	
10	615351.4	4942836.5	618921.4	4953446.5	1.15E+07	2.52E+04	21.6	6.3	13.77	Rio Montebellone
11	615621.4	4941306.5	621451.4	4951946.5	1.23E+07	1.04E+04	33.2	7.4	14.78	Rio della Moia
12	616411.4	4942006.5	617311.4	4944916.5	1.21E+06	3.50E+04	22.6	9.1	3.78	Rio Monticelli
13	617201.4	4942176.5	623591.4	4950976.5	3.38E+07	2.89E+04	28.7	10.4	13.78	Rio Quaresimo
14	617801.4	4942346.5	618151.4	4944666.5	1.07E+06	9.62E+04	34.9	8.3	16.52	
15	619101.4	4942516.5	619201.4	4945386.5	5.55E+06	3.04E+04	22.4	9.5	3.92	
16	621251.4	4945486.5	623031.4	4949586.5	3.21E+06	1.16E+04	15.5	1.9	5.97	Rio Caviolo
17	621301.4	4943936.5	623531.4	4950676.5	8.38E+06	1.40E+04	13.0	2.0	9.65	Rio Moreno
18	621591.4	4943806.5	622561.4	4945976.5	1.72E+06	2.83E+04	9.5	1.9	3.43	
19[b]	615741.4	4938716.5	623871.4	4950896.5	2.71E+07	2.65E+04	43.1	11.9	20.53	Moddolena creek
20	622291.4	4942156.5	625801.4	4950866.5	1.29E+07	3.85E+04	19.0	5.9	12.26	
21	621701.4	4941366.5	624041.4	4944076.5	2.22E+06	4.11E+04	17.0	9.1	4.81	
22	624571.4	4943486.5	626061.4	4948926.5	2.94E+06	2.19E+04	9.7	3.3	7.21	
23[b]	618131.4	4933076.5	628261.4	4948076.5	8.42E+07	1.03E+04	68.8	16.3	25.70	Crosotolo creek

Castelvetro - Vignola K_{sn} Analysis										
Stream	Easting_headwater[a]	Northing_headwater[a]	Easting_mouth[a]	Northing_mouth[a]	Max_Area (m^2)	Min_Area (m^2)	Max_k_{sn}[d]	Min_k_{sn}[d]	Length (km)	Name
24	640576.1	4925148.0	646786.1	4937228.0	5.76E+07	4.85E+04	50.8	12.7	19.54	Fossa creek
25	644386.1	4926178.0	647276.1	4937168.0	1.34E+07	4.06E+04	65.1	7.2	14.47	Grizzaga creek
26	647816.1	4929448.0	650696.1	4937348.0	9.66E+06	5.07E+04	21.7	8.5	10.76	
27[b]	646006.1	4919438.0	653336.1	4936718.0	5.09E+07	2.63E+04	80.1	13.3	24.30	Tiepido river
28	649636.1	4926628.0	655326.1	4936428.0	2.57E+07	4.06E+04	37.5	7.6	15.02	Nizzola creek
29	651686.1	4931818.0	654706.1	4933388.0	3.63E+06	2.27E+04	14.9	6.3	5.42	
30	649946.1	4929038.0	653466.1	4932068.0	2.14E+06	1.56E+04	21.1	5.5	5.62	
31	650086.1	4928618.0	651666.1	4929928.0	3.24E+06	2.69E+04	23.2	9.9	4.47	
32	652246.1	4927598.0	652816.1	4930198.0	2.04E+06	2.83E+04	22.8	12.0	3.13	
33[b]	648276.1	4921918.0	657326.1	4934898.0	3.44E+07	4.57E+04	61.6	14.8	20.53	Guerro creek
34	653006.1	4928258.0	654716.1	4929928.0	2.14E+06	1.20E+04	33.1	11.1	3.05	
35	649666.1	4922568.0	652056.1	4926558.0	7.78E+06	2.25E+04	60.7	20.7	5.58	
36	654586.1	4926028.0	659486.1	4934638.0	9.20E+06	3.49E+04	21.5	8.3	12.28	Rio Schiaviroli
37	655476.1	4928338.0	658786.1	4934938.0	1.18E+07	4.02E+04	13.4	7.3	9.27	
38	655876.1	4928318.0	658426.1	4933088.0	4.43E+06	4.46E+04	15.5	6.4	6.77	Rio Pissarotta
39	655806.1	4926338.0	658376.1	4928588.0	3.10E+06	4.37E+04	19.8	9.0	4.18	
40	656876.1	4926538.0	657546.1	4927638.0	7.01E+05	3.74E+04	15.9	10.4	1.75	
41[b]	642726.1	4918908.0	661736.1	4933768.0	1.03E+08	2.81E+04	93.6	9.9	34.54	Panaro river

Table

Stream	Easting[a]	Northing[a]	Min_Area[b]	Max_Area[b]	k_{sn}		Easting[a]	Northing[a]	Min_Area[b]	Max_Area[b]	k_{sn}
1	606071.4	948056.5	3.2E+06	3.3E+06	9.95		609031.4	951046.5	9.7E+06	9.7E+06	9.81
1	606301.4	948096.5	3.3E+06	3.3E+06	8.23		609061.4	951196.5	9.7E+06	9.8E+06	9.54
1	606511.4	948216.5	3.3E+06	3.3E+06	6.95		609161.4	951356.5	9.8E+06	9.9E+06	9.30
1	606671.4	948346.5	3.3E+06	3.4E+06	6.69		609151.4	951596.5	9.9E+06	1.2E+07	9.45
1	606901.4	948406.5	3.4E+06	3.5E+06	6.87		609201.4	951826.5	1.2E+07	1.2E+07	9.84
1	607091.4	948536.5	3.5E+06	3.9E+06	7.08		609201.4	952076.5	1.2E+07	1.3E+07	10.36
1	607291.4	948606.5	3.9E+06	3.9E+06	7.18		609241.4	952306.5	1.3E+07	1.4E+07	10.86
			Syncline		►◄				Anticline		◄►
1	607381.4	948786.5	3.9E+06	4.2E+06	7.38		609241.4	952546.5	1.4E+07	1.4E+07	11.27
1	607451.4	948966.5	4.2E+06	4.3E+06	7.68		609251.4	952786.5	1.4E+07	1.4E+07	11.81
1	607641.4	949136.5	4.3E+06	4.3E+06	7.97		609331.4	952996.5	1.4E+07	1.4E+07	12.25
1	607841.4	949246.5	4.3E+06	4.4E+06	8.26	#	609391.4	953216.5	1.4E+07	1.4E+07	12.89
1	608031.4	949396.5	4.4E+06	4.4E+06	8.57		609511.4	953416.5	1.4E+07	1.4E+07	13.41
1	608211.4	949576.5	4.4E+06	4.5E+06	8.70		609531.4	953666.5	1.4E+07	1.4E+07	13.97
1	608411.4	949686.5	4.5E+06	4.5E+06	9.24		609701.4	953836.5	1.4E+07	1.4E+07	14.46

Stream	Easting[a]	Northing[a]	Min_Area[b]	Max_Area[b]	k_{sn}		Easting[a]	Northing[a]	Min_Area[b]	Max_Area[b]	k_{sn}
2	612381.4	945626.5	6.7E+07	6.7E+07	21.18		612771.4	948826.5	1.6E+08	1.6E+08	29.03
2	612451.4	945846.5	6.7E+07	6.8E+07	21.01		612811.4	949046.5	1.6E+08	1.6E+08	28.83
2	612471.4	946086.5	6.8E+07	6.8E+07	20.88		612891.4	949196.5	1.6E+08	1.6E+08	28.60
2	612371.4	946236.5	6.8E+07	6.8E+07	20.78		612941.4	949356.5	1.6E+08	1.6E+08	28.22
2	612361.4	946476.5	6.8E+07	6.9E+07	20.66		613041.4	949566.5	1.6E+08	1.6E+08	27.57
2	612211.4	946606.5	6.9E+07	6.9E+07	20.42		613211.4	949706.5	1.6E+08	1.6E+08	26.57
2	612141.4	946826.5	6.9E+07	6.9E+07	20.53		613351.4	949876.5	1.6E+08	1.6E+08	25.27
2	612111.4	947026.5	6.9E+07	1.3E+08	24.01		613411.4	950106.5	1.6E+08	1.6E+08	24.10
			Syncline		►◄				Anticline		◄►
2	612041.4	947236.5	1.3E+08	1.3E+08	27.39		613461.4	950316.5	1.6E+08	1.7E+08	23.44
2	612141.4	947456.5	1.3E+08	1.3E+08	27.51		613531.4	950526.5	1.7E+08	1.7E+08	22.77
2	612281.4	947636.5	1.3E+08	1.3E+08	28.55		613641.4	950726.5	1.7E+08	1.7E+08	22.02
2	612301.4	947876.5	1.3E+08	1.6E+08	29.83		613701.4	950916.5	1.7E+08	1.7E+08	21.50
2	612381.4	948076.5	1.6E+08	1.6E+08	29.95		613831.4	951096.5	1.7E+08	1.7E+08	21.26
2	612511.4	948246.5	1.6E+08	1.6E+08	29.79		614041.4	951196.5	1.7E+08	1.7E+08	21.11
2	612651.4	948396.5	1.6E+08	1.6E+08	29.50		614111.4	951396.5	1.7E+08	1.7E+08	21.78

Stream	Easting[a]	Northing[a]	Min_Area[b]	Max_Area[b]	k_{sn}		Easting[a]	Northing[a]	Min_Area[b]	Max_Area[b]	k_{sn}
3	608681.4	947176.5	1.8E+06	1.8E+06	8.08		611281.4	949476.5	7.9E+06	8.6E+06	6.93
3	608731.4	947396.5	1.8E+06	2.3E+06	7.07		611491.4	949576.5	8.6E+06	1.0E+07	7.67
3	608641.4	947576.5	2.3E+06	2.4E+06	6.48		611711.4	949676.5	1.0E+07	1.0E+07	8.63
3	608741.4	947776.5	2.4E+06	2.4E+06	5.98		611761.4	949896.5	1.0E+07	1.1E+07	9.61
3	608881.4	947936.5	2.4E+06	2.6E+06	5.69		611871.4	950096.5	1.1E+07	1.1E+07	10.11
3	609061.4	948096.5	2.6E+06	3.4E+06	5.48		612001.4	950256.5	1.1E+07	1.2E+07	10.20
3	609141.4	948316.5	3.4E+06	3.6E+06	5.22		612161.4	950426.5	1.2E+07	1.2E+07	10.25
3	609211.4	948516.5	3.6E+06	4.5E+06	5.34				Anticline		◄►
			Syncline		►◄		612201.4	950656.5	1.2E+07	1.2E+07	10.29
3	609181.4	948756.5	4.5E+06	4.6E+06	5.81		612251.4	950856.5	1.2E+07	1.3E+07	10.31
3	609001.4	948886.5	4.6E+06	6.0E+06	6.12		612341.4	951036.5	1.3E+07	1.3E+07	10.33
3	609181.4	949066.5	6.0E+06	6.0E+06	6.04		612261.4	951256.5	1.3E+07	1.3E+07	11.16
3	609341.4	949036.5	6.0E+06	6.2E+06	5.95		612171.4	951446.5	1.3E+07	1.6E+07	12.26
3	609551.4	948966.5	6.2E+06	6.2E+06	5.78		612221.4	951666.5	1.6E+07	1.7E+07	12.76
3	609801.4	948946.5	6.2E+06	6.2E+06	5.72		612331.4	951856.5	1.7E+07	1.7E+07	13.23
3	610041.4	948946.5	6.4E+06	6.8E+06	5.90		612391.4	952056.5	1.7E+07	1.7E+07	13.64
3	610241.4	948816.5	6.8E+06	7.7E+06	6.02		612521.4	952226.5	1.7E+07	1.7E+07	14.04
3	610401.4	948866.5	7.7E+06	7.7E+06	6.02						
3	610561.4	949006.5	7.7E+06	7.7E+06	5.73						
3	610811.4	949016.5	7.7E+06	7.9E+06	5.27						

Stream	Easting[a]	Northing[a]	Min_Area[b]	Max_Area[b]	k_{sn}		Easting[a]	Northing[a]	Min_Area[b]	Max_Area[b]	k_{sn}
10	615161.4	944206.5	1.3E+06	1.3E+06	9.55		616371.4	948496.5	5.9E+06	6.1E+06	7.90
10	615071.4	944386.5	1.3E+06	1.4E+06	8.73		616451.4	948716.5	6.1E+06	6.2E+06	8.03
10	614941.4	944576.5	1.4E+06	1.4E+06	7.91		616421.4	948946.5	6.2E+06	6.2E+06	8.14
10	614911.4	944816.5	1.4E+06	1.4E+06	7.74		616421.4	949166.5	6.2E+06	6.2E+06	8.26
10	614961.4	945036.5	1.5E+06	2.0E+06	7.82		616451.4	949406.5	6.2E+06	6.3E+06	8.31
10	615101.4	945226.5	2.0E+06	2.0E+06	7.12		616611.4	949596.5	6.4E+06	6.5E+06	8.16
10	615271.4	945406.5	2.0E+06	2.1E+06	6.54		616751.4	949756.5	6.5E+06	6.5E+06	7.98
10	615461.4	945566.5	2.1E+06	2.2E+06	6.29				Anticline		◄►
			Syncline		►◄		616781.4	949996.5	6.5E+06	6.5E+06	7.74
10	615621.4	945746.5	2.2E+06	2.9E+06	6.38		616891.4	950196.5	6.5E+06	6.6E+06	7.54
10	615701.4	945936.5	2.9E+06	2.9E+06	6.85		617001.4	950396.5	6.6E+06	6.9E+06	7.48
10	615821.4	946136.5	2.9E+06	4.4E+06	7.26		617181.4	950526.5	6.9E+06	7.5E+06	7.52
10	615821.4	946386.5	4.4E+06	4.4E+06	7.20		617361.4	950586.5	7.5E+06	7.5E+06	7.87
10	615801.4	946606.5	4.4E+06	5.2E+06	7.04		617401.4	950816.5	7.5E+06	8.9E+06	8.99
10	615911.4	946786.5	5.2E+06	5.3E+06	6.84		617561.4	951006.5	8.9E+06	9.0E+06	10.16
10	615931.4	947026.5	5.3E+06	5.4E+06	6.72		617691.4	951196.5	9.0E+06	9.2E+06	11.06

Stream	Easting[a]	Northing[a]	Min_Area[b]	Min_Area[b]	ksn	Easting[a]	Northing[a]	Min_Area[b]	Min_Area[b]	k_{sn}
11	616441.4	944146.5	1.5E+06	1.6E+06	13.48	618951.4	947286.5	6.2E+06	6.3E+06	7.86
11	616621.4	944286.5	1.6E+06	1.6E+06	12.62	619051.4	947486.5	6.3E+06	6.5E+06	8.05
11	616801.4	944456.5	1.6E+06	1.7E+06	11.66	619061.4	947726.5	6.5E+06	6.6E+06	8.21
11	616951.4	944636.5	1.7E+06	1.7E+06	10.52	619201.4	947876.5	6.6E+06	6.6E+06	8.45
11	617111.4	944826.5	1.7E+06	1.7E+06	10.17	619381.4	948046.5	6.8E+06	6.9E+06	8.72
11	617311.4	944946.5	1.7E+06	3.0E+06	10.98	619511.4	948236.5	6.9E+06	7.0E+06	9.02
11	617511.4	945066.5	3.0E+06	3.0E+06	11.30	619721.4	948306.5	7.0E+06	7.2E+06	9.33
			Syncline		►◄			Anticline		◄►
11	617671.4	945236.5	3.0E+06	3.2E+06	10.74	619901.4	948446.5	7.2E+06	7.3E+06	9.56
11	617871.4	945356.5	3.2E+06	3.3E+06	10.07	620011.4	948646.5	7.3E+06	7.4E+06	9.72
11	617961.4	945556.5	3.3E+06	3.4E+06	9.31	620091.4	948856.5	7.4E+06	7.5E+06	10.11
11	618011.4	945736.5	3.4E+06	3.6E+06	8.49	620111.4	949066.5	7.5E+06	7.6E+06	11.37
11	618111.4	945936.5	3.7E+06	3.9E+06	8.10	620111.4	949286.5	7.6E+06	9.8E+06	13.51
11	618191.4	946156.5	3.9E+06	4.3E+06	7.81	620171.4	949486.5	9.8E+06	1.0E+07	15.66
11	618301.4	946356.5	4.3E+06	4.4E+06	7.59	620321.4	949676.5	1.0E+07	1.0E+07	16.57
11						620451.4	949866.5	1.0E+07	1.0E+07	16.17

Stream	Easting[a]	Northing[a]	Min_Area[b]	Max_Area[b]	k_{sn}	Easting[a]	Northing[a]	Min_Area[b]	Max_Area[b]	k_{sn}
13	617011.4	944016.5	1.2E+06	1.3E+06	11.70	620041.4	946526.5	1.4E+07	1.4E+07	11.69
13	617161.4	944186.5	1.3E+06	1.3E+06	11.88	620151.4	946716.5	1.4E+07	1.4E+07	11.42
13	617371.4	944286.5	1.3E+06	1.3E+06	13.32	620311.4	946896.5	1.4E+07	1.7E+07	11.76
13	617581.4	944376.5	1.3E+06	1.9E+06	13.34	620511.4	946986.5	1.7E+07	1.7E+07	11.99
13	617771.4	944516.5	1.9E+06	2.0E+06	11.47	620631.4	947166.5	1.7E+07	1.7E+07	11.98
13	617921.4	944656.5	2.0E+06	2.0E+06	10.43	620761.4	947366.5	1.7E+07	1.8E+07	12.01
13	618121.4	944766.5	2.0E+06	3.2E+06	10.63	620931.4	947526.5	1.8E+07	1.8E+07	12.15
			Syncline		►◄			Anticline		◄►
13	618271.4	944936.5	3.2E+06	3.2E+06	10.69	621071.4	947716.5	1.8E+07	1.8E+07	14.26
13	618431.4	945126.5	3.2E+06	3.3E+06	10.59	621241.4	947816.5	1.8E+07	1.9E+07	16.85
13	618641.4	945206.5	3.3E+06	3.7E+06	10.49	621421.4	947996.5	1.9E+07	1.9E+07	17.96
13	618851.4	945266.5	3.8E+06	3.8E+06	10.77	621591.4	948176.5	1.9E+07	1.9E+07	20.12
13	619011.4	945446.5	3.8E+06	9.5E+06	12.56	621731.4	948356.5	1.9E+07	1.9E+07	20.77
13	619191.4	945606.5	9.5E+06	9.5E+06	13.96	621901.4	948526.5	1.9E+07	1.9E+07	20.07
13	619311.4	945786.5	9.5E+06	1.1E+07	14.14	622021.4	948716.5	1.9E+07	1.9E+07	19.24

Stream	Easting[a]	Northing[a]	Min_Area[b]	Max_Area[b]	k_{sn}	Easting[a]	Northing[a]	Min_Area[b]	Max_Area[b]	k_{sn}
15	619101.4	942516.5	3.0E+04	1.8E+05	22.25	621081.4	946466.5	5.9E+05	6.8E+05	4.79
15	619171.4	942726.5	1.9E+05	2.8E+05	16.81	621211.4	946666.5	6.8E+05	7.7E+05	4.69
15	619211.4	942946.5	2.8E+05	3.5E+05	13.32	621371.4	946816.5	7.7E+05	1.1E+06	4.99
15	619351.4	943136.5	3.5E+05	4.4E+05	12.35	621531.4	947006.5	1.1E+06	1.2E+06	5.64
15	619531.4	943286.5	4.5E+05	7.0E+05	11.52	621651.4	947196.5	1.2E+06	1.4E+06	6.17
15	619481.4	943496.5	7.0E+05	7.5E+05	10.90	621831.4	947376.5	1.4E+06	1.4E+06	6.55
15	619431.4	943716.5	7.5E+05	1.4E+06	10.67	622041.4	947476.5	1.4E+06	1.5E+06	7.01
15	619391.4	943916.5	1.4E+06	1.4E+06	9.78			Anticline		◄►
			Syncline		►◄	622271.4	947526.5	1.9E+06	2.1E+06	7.48
15	619421.4	944156.5	1.4E+06	2.9E+06	9.83	622421.4	947676.5	2.1E+06	2.2E+06	7.45
15	619391.4	944346.5	2.9E+06	3.0E+06	10.30	622581.4	947866.5	2.2E+06	2.3E+06	7.60
15	619251.4	944506.5	3.0E+06	5.2E+06	10.45	622671.4	948076.5	2.3E+06	2.4E+06	9.17
15	619271.4	944716.5	5.2E+06	5.3E+06	10.32	622741.4	948296.5	2.4E+06	2.6E+06	11.39
15	619241.4	944936.5	5.3E+06	5.4E+06	9.91	622791.4	948526.5	2.6E+06	2.6E+06	12.16
15	619261.4	945166.5	5.4E+06	5.5E+06	9.52	622821.4	948766.5	2.7E+06	2.8E+06	12.38
15	619201.4	945386.5	5.5E+06	5.6E+06	9.83					

Stream	Easting[a]	Northing[a]	Min_Area[b]	Max_Area[b]	k_{sn}	Easting[a]	Northing[a]	Min_Area[b]	Max_Area[b]	k_{sn}
19	621161.4	942206.5	1.8E+07	1.8E+07	20.88	624451.4	945746.5	2.1E+07	2.1E+07	17.33
19	621331.4	942366.5	1.8E+07	1.8E+07	20.24	624521.4	945946.5	2.1E+07	2.1E+07	17.57
19	621511.4	942526.5	1.8E+07	1.8E+07	19.38	624581.4	946156.5	2.1E+07	2.1E+07	19.11
19	621521.4	942756.5	1.8E+07	1.9E+07	18.20	624681.4	946376.5	2.1E+07	2.2E+07	21.04
19	621681.4	942946.5	1.9E+07	1.9E+07	17.76	624631.4	946606.5	2.2E+07	2.2E+07	22.62
19	621851.4	943086.5	1.9E+07	1.9E+07	17.45	624671.4	946826.5	2.2E+07	2.3E+07	22.45
19	621911.4	943306.5	1.9E+07	1.9E+07	16.93	624671.4	947056.5	2.3E+07	2.3E+07	21.30
19	622101.4	943456.5	1.9E+07	1.9E+07	16.42			Anticline		◄►
			Syncline		►◄	624651.4	947306.5	2.3E+07	2.3E+07	20.05
19	622321.4	943536.5	1.9E+07	1.9E+07	16.95	624691.4	947536.5	2.3E+07	2.3E+07	19.05
19	622481.4	943656.5	1.9E+07	1.9E+07	19.00	624741.4	947766.5	2.3E+07	2.4E+07	18.59
19	622701.4	943736.5	1.9E+07	2.0E+07	21.57	624701.4	947976.5	2.4E+07	2.4E+07	18.84
19	622921.4	943806.5	2.0E+07	2.0E+07	23.36	624651.4	948196.5	2.4E+07	2.4E+07	19.31
19	623131.4	943916.5	2.0E+07	2.0E+07	23.99	624671.4	948436.5	2.4E+07	2.4E+07	19.87
19	623311.4	944066.5	2.0E+07	2.0E+07	24.22					

Stream	Easting[a]	Northing[a]	Min_Area[b]	Max_Area[b]	k_{sn}	Easting[a]	Northing[a]	Min_Area[b]	Max_Area[b]	k_{sn}
20	622291.4	942156.5	3.9E+04	1.8E+05	18.97	625171.4	945676.5	6.0E+06	6.3E+06	8.12
20	622431.4	942356.5	1.8E+05	2.8E+05	15.66	625141.4	945876.5	6.3E+06	6.4E+06	9.10
20	622401.4	942576.5	3.1E+05	4.4E+05	13.58	625101.4	946106.5	6.5E+06	6.6E+06	9.60
20	622391.4	942806.5	4.5E+05	5.4E+05	12.90	625161.4	946336.5	6.6E+06	6.7E+06	9.82
20	622471.4	943026.5	5.4E+05	5.9E+05	13.04	625251.4	946546.5	6.7E+06	6.8E+06	9.73
20	622501.4	943256.5	5.9E+05	8.4E+05	12.67	625301.4	946766.5	6.8E+06	6.9E+06	9.58
20	622691.4	943286.5	8.4E+05	9.8E+05	10.40			Anticline		◄►
			Siyncline		►◄	625321.4	947006.5	6.9E+06	7.1E+06	9.55
20	622891.4	943366.5	9.8E+05	1.3E+06	8.35	625331.4	947246.5	7.1E+06	7.2E+06	9.46
20	623121.4	943376.5	1.3E+06	1.5E+06	8.02	625411.4	947446.5	7.2E+06	7.3E+06	9.43
20	623271.4	943536.5	1.6E+06	1.7E+06	7.33	625441.4	947686.5	7.3E+06	7.6E+06	9.45
20	623411.4	943726.5	1.7E+06	1.7E+06	6.18	625411.4	947926.5	7.6E+06	7.7E+06	9.38
20	623621.4	943836.5	1.7E+06	2.0E+06	5.95	625391.4	948136.5	7.7E+06	7.8E+06	9.17
20	623831.4	943926.5	2.0E+06	2.0E+06	7.81	625511.4	948326.5	7.8E+06	7.9E+06	8.93
20	623991.4	944096.5	2.0E+06	4.4E+06	10.56	625631.4	948526.5	7.9E+06	8.0E+06	8.76
20	624041.4	944306.5	4.4E+06	4.9E+06	11.55					

Stream	Easting[a]	Northing[a]	Min_Area[b]	Max_Area[b]	k_{sn}	Easting[a]	Northing[a]	Min_Area[b]	Max_Area[b]	k_{sn}
23	623731.4	941626.5	6.9E+07	6.9E+07	37.91	626231.4	944986.5	7.6E+07	7.6E+07	22.16
23	623771.4	941856.5	7.0E+07	7.0E+07	37.95	626401.4	945166.5	7.6E+07	7.7E+07	22.17
23	623921.4	942036.5	7.0E+07	7.0E+07	37.57	626481.4	945386.5	7.7E+07	7.7E+07	21.93
23	624121.4	942166.5	7.0E+07	7.2E+07	36.42	626511.4	945626.5	7.7E+07	7.7E+07	21.17
23	624291.4	942336.5	7.2E+07	7.2E+07	34.98	626671.4	945776.5	7.7E+07	7.7E+07	19.93
23	624451.4	942506.5	7.2E+07	7.3E+07	33.46	626841.4	945946.5	7.7E+07	7.8E+07	18.49
23	624581.4	942696.5	7.3E+07	7.3E+07	31.00	626881.4	946156.5	7.8E+07	7.8E+07	20.85
			Syncline		►◄			Anticline		◄►
23	624761.4	942836.5	7.3E+07	7.4E+07	29.63	626921.4	946386.5	7.8E+07	7.8E+07	33.38
23	624951.4	942936.5	7.4E+07	7.4E+07	29.72	627051.4	946566.5	7.8E+07	8.1E+07	48.75
23	625141.4	943036.5	7.4E+07	7.4E+07	30.03	627161.4	946776.5	8.1E+07	8.1E+07	52.52
23	625281.4	943186.5	7.4E+07	7.5E+07	30.48	627181.4	947016.5	8.1E+07	8.2E+07	49.27
23	625431.4	943376.5	7.5E+07	7.5E+07	30.58	627091.4	947236.5	8.2E+07	8.2E+07	42.87
23	625551.4	943576.5	7.5E+07	7.5E+07	29.46	627061.4	947456.5	8.2E+07	8.2E+07	37.65
23	625651.4	943776.5	7.5E+07	7.5E+07	28.62	627251.4	947556.5	8.2E+07	8.2E+07	30.20
23						627481.4	947596.5	8.2E+07	8.3E+07	22.31
23						627701.4	947626.5	8.3E+07	8.4E+07	20.35

Stream	Easting[a]	Northing[a]	Max_Area[b]	k_{sn}
22	625621.4	945446.5	8.5E+05	6.63
22	625601.4	945686.5	9.4E+05	5.29
22	625611.4	945936.5	1.1E+06	5.56
22	625721.4	946126.5	1.2E+06	5.95
22	625881.4	946286.5	1.4E+06	6.38
22	625961.4	946446.5	1.5E+06	6.53
22	625981.4	946686.5	1.7E+06	6.39
			Anticline	◄►
22	625921.4	946906.5	1.8E+06	6.20
22	625921.4	947136.5	2.0E+06	5.90
22	626001.4	947346.5	2.0E+06	5.61
22	626031.4	947576.5	2.1E+06	5.49
22	626011.4	947816.5	2.2E+06	5.47
22	625961.4	948036.5	2.3E+06	5.48
22	625941.4	948256.5	2.3E+06	5.66

Stream	Easting[a]	Northing[a]	Max_Area[b]	k_{sn}
17.0	622401.4	945786.5	1.6E+06	7.84
17.0	622391.4	946016.5	3.4E+06	8.66
17.0	622431.4	946226.5	3.5E+06	8.30
17.0	622581.4	946416.5	4.1E+06	7.85
17.0	622681.4	946596.5	4.2E+06	8.09
17.0	622721.4	946836.5	4.3E+06	8.99
17.0	622801.4	947046.5	4.4E+06	10.11
17.0	622821.4	947276.5	4.5E+06	10.90
		Anticline		◄►
17.0	622981.4	947416.5	4.7E+06	11.29
17.0	623101.4	947616.5	4.9E+06	10.89
17.0	623271.4	947706.5	5.0E+06	10.63
17.0	623351.4	947906.5	5.1E+06	10.45
17.0	623421.4	948126.5	5.4E+06	9.92
17.0	623601.4	948256.5	5.5E+06	9.62
17.0	623811.4	5497400	5.5E+06	9.49

Table

Stream	Easting[a]	Northing[a]	Min_Area[b]	Max_Area[b]	k_{sn}
24	646456	931548	2.7E+07	2.7E+07	25.57
24	646496	931778	2.7E+07	2.7E+07	25.39
24	646496	931988	2.7E+07	2.7E+07	24.62
24	646556	932178	2.7E+07	2.7E+07	23.98
24	646646	932388	2.7E+07	2.7E+07	22.45
24	646536	932558	2.7E+07	2.7E+07	20.40
24	646406	932718	2.7E+07	2.8E+07	19.08
24	646196	932798	2.8E+07	2.8E+07	19.36
24	645986	932878	3.5E+07	3.5E+07	19.89
			Villa Camilla anticline		⟷
24	645806	933058	3.5E+07	3.5E+07	18.69
24	645636	933228	3.5E+07	3.6E+07	18.13
24	645606	933468	3.6E+07	3.6E+07	17.96
24	645466	933588	3.6E+07	3.6E+07	18.45
24	645266	933708	3.6E+07	3.7E+07	19.19
24	645276	933888	3.7E+07	3.7E+07	19.62
24	645186	934098	3.7E+07	3.7E+07	20.19

Stream	Easting[a]	Northing[a]	Min_Area[b]	Max_Area[b]	k_{sn}
25	647586	931538	6.7E+06	6.8E+06	16.08
25	647676	931748	6.8E+06	6.9E+06	15.73
25	647586	931948	6.9E+06	7.0E+06	16.58
25	647586	932178	7.0E+06	7.0E+06	18.78
			Villa Camilla anticline		⟷
25	647616	932418	7.0E+06	7.0E+06	19.41
25	647656	932648	7.0E+06	7.3E+06	17.94
25	647806	932808	7.3E+06	7.3E+06	16.22
25	647876	932948	7.3E+06	7.4E+06	14.29
25	647966	933158	7.4E+06	7.4E+06	13.08
25	647896	933368	7.4E+06	7.6E+06	12.84
25	647956	933598	7.6E+06	7.6E+06	13.18
25	647996	933828	7.6E+06	7.6E+06	13.70
25	647946	934048	7.6E+06	8.0E+06	14.75
25	647966	934288	8.0E+06	8.0E+06	16.62
25	648036	934508	8.0E+06	8.2E+06	18.22
			Castelvetro anticline		⟷
25	648176	934698	8.2E+06	8.2E+06	17.73
25	648106	934928	8.3E+06	8.3E+06	16.20
25	647976	935128	8.3E+06	8.5E+06	15.00
25	647876	935308	8.5E+06	8.7E+06	13.59
25	647746	935468	8.7E+06	1.1E+07	13.08

Stream	Easting[a]	Northing[a]	Min_Area	Max_Area	k_{sn}
26	648686	931138	1.1E+06	1.1E+06	13.30
26	648656	931368	1.1E+06	1.2E+06	14.09
26	648636	931608	1.2E+06	1.4E+06	13.68
26	648516	931808	1.4E+06	2.4E+06	12.48
			Villa Camilla anticline		⟷
26	648536	931988	2.4E+06	2.5E+06	10.38
26	648466	932178	2.5E+06	2.5E+06	9.35
26	648516	932378	2.5E+06	2.6E+06	9.10
26	648456	932598	2.6E+06	3.0E+06	8.92
26	648536	932818	3.0E+06	3.1E+06	8.58
26	648586	933048	3.1E+06	3.2E+06	8.52
26	648636	933278	3.2E+06	4.6E+06	9.06
26	648706	933498	4.6E+06	4.7E+06	9.39
26	648786	933718	4.7E+06	5.0E+06	9.27
26	648736	933938	5.0E+06	5.0E+06	9.16
			Castelvetro anticline		⟷
26	648846	934138	5.0E+06	5.1E+06	9.12
26	649016	934278	5.1E+06	5.2E+06	9.10
26	649196	934408	5.2E+06	5.3E+06	9.04
26	649366	934538	5.3E+06	5.6E+06	9.02
26	649486	934718	5.6E+06	5.6E+06	9.11
26	649496	934958	5.6E+06	6.0E+06	9.28

Stream	Easting[a]	Northing[a]	Min_Area[b]	Max_Area[b]	k_{sn}
27	649466	930608	4.3E+07	4.3E+07	34.02
27	649626	930778	4.3E+07	4.4E+07	33.69
27	649816	930928	4.4E+07	4.4E+07	33.41
27	650006	931078	4.4E+07	4.5E+07	33.02
27	650156	931208	4.5E+07	4.5E+07	32.25
			Villa Camilla anticline		⟷
27	650316	931368	4.5E+07	4.5E+07	31.71
27	650356	931608	4.5E+07	4.5E+07	31.31
27	650466	931788	4.5E+07	4.5E+07	30.90
27	650646	931938	4.5E+07	4.5E+07	30.63
27	650866	932018	4.5E+07	4.5E+07	30.22
27	651086	932098	4.5E+07	4.6E+07	29.32
27	651166	932258	4.6E+07	4.6E+07	28.42
27	651126	932498	4.6E+07	4.7E+07	27.62
			Castelvetro anticline		⟷
27	651156	932698	4.7E+07	4.7E+07	27.27
27	651126	932908	4.7E+07	4.7E+07	28.26
27	651136	933138	4.7E+07	4.7E+07	30.68
27	651326	933268	4.7E+07	4.8E+07	32.44
27	651436	933458	4.8E+07	4.8E+07	32.42
27	651526	933668	4.8E+07	4.8E+07	30.90
27	651706	933808	4.8E+07	4.8E+07	29.15

Stream	Easting[a]	Northing[a]	Min_Area[b]	Max_Area[b]	k_{sn}
28	651466	929828	3.1E+06	3.2E+06	22.25
28	651666	929928	3.2E+06	7.0E+06	20.56
28	651896	929998	7.0E+06	7.2E+06	18.67
28	652096	930128	7.2E+06	7.2E+06	16.95
			Villa Camilla anticline		⟷
28	652306	930148	7.2E+06	8.7E+06	15.91
28	652476	930228	8.7E+06	8.9E+06	16.12
28	652676	930328	8.9E+06	1.1E+07	17.59
28	652806	930438	1.1E+07	1.1E+07	18.68
28	652846	930668	1.1E+07	1.2E+07	19.67
28	652876	930898	1.2E+07	1.2E+07	20.06
28	652876	931118	1.2E+07	1.2E+07	19.66
28	652996	931278	1.2E+07	1.3E+07	19.18
28	653106	931478	1.3E+07	1.3E+07	18.42
28	653206	931688	1.3E+07	1.3E+07	17.37
28	653366	931828	1.3E+07	1.3E+07	16.41
			Castelvetro anticline		⟷
28	653506	932008	1.3E+07	1.5E+07	15.96
28	653686	932118	1.5E+07	1.5E+07	15.65
28	653916	932148	1.5E+07	1.6E+07	15.24
28	654106	932308	1.6E+07	1.6E+07	14.85
28	654296	932408	1.6E+07	1.7E+07	14.54

Stream	Easting[a]	Northing[a]	Min_Area[b]	Max_Area[b]	k_{sn}
29	651196	930918	2.3E+04	8.1E+04	8.31
29	651366	931058	8.7E+04	1.3E+05	9.27
29	651516	931228	1.3E+05	1.5E+05	8.28
29	651436	931448	1.5E+05	3.1E+05	7.77
29	651556	931638	3.1E+05	4.3E+05	6.50
29	651686	931818	4.3E+05	5.1E+05	6.29
29	651906	931888	5.1E+05	1.1E+06	7.06
29	652096	932008	1.1E+06	1.1E+06	6.96
29	652286	932168	1.1E+06	1.5E+06	7.20
			Villa Camilla anticline		⟷
29	652356	932388	1.5E+06	1.7E+06	7.82
29	652486	932578	1.7E+06	2.0E+06	8.55
29	652706	932648	2.0E+06	2.1E+06	9.22
29	652806	932838	2.1E+06	2.3E+06	9.26
29	653026	932918	2.3E+06	2.4E+06	9.16

Stream	Easting[a]	Northing[a]	Min_Area[b]	Max_Area[b]	k_{sn}
30	650986	930408	6.3E+05	9.0E+05	9.62
30	651186	930428	9.2E+05	1.1E+06	11.70
30	651396	930408	1.1E+06	1.2E+06	12.89
30	651606	930478	1.2E+06	1.3E+06	12.65
30	651806	930608	1.3E+06	1.4E+06	11.74
			Villa Camilla anticline		⟷
30	651986	930768	1.4E+06	1.4E+06	10.98
30	652146	930948	1.4E+06	1.6E+06	10.15
30	652276	931148	1.6E+06	1.7E+06	9.57
30	652346	931368	1.7E+06	1.8E+06	9.00
30	652516	931548	1.8E+06	1.9E+06	8.31
30	652696	931688	1.9E+06	1.9E+06	8.06
30	652846	931878	2.0E+06	2.0E+06	12.01
30	653026	932058	2.0E+06	2.1E+06	15.95
			Castelvetro anticline		⟷
30	653236	932018	2.1E+06	2.1E+06	16.73
30	653466	932068	2.1E+06	2.1E+06	21.09

Stream	Easting[a]	Northing[a]	Min_Area[b]	Max_Area[b]	k_{sn}
32	652246	927598	2.8E+04	6.0E+04	13.50
32	652296	927808	6.0E+04	2.5E+05	14.65
32	652436	928008	2.6E+05	3.5E+05	12.67
32	652496	928228	3.6E+05	5.4E+05	12.02
32	652506	928478	5.4E+05	7.0E+05	15.72
32	652536	928708	7.0E+05	8.9E+05	19.04
32	652616	928928	9.0E+05	9.8E+05	17.01
32	652776	929118	9.8E+05	1.1E+06	19.32
			Villa Camilla anticline		⟷
32	652916	929298	1.2E+06	1.3E+06	19.64
32	652976	929528	1.3E+06	1.4E+06	16.00
32	652996	929768	1.4E+06	1.6E+06	12.88
32	652966	930008	1.6E+06	1.7E+06	14.47
32	652816	930198	1.7E+06	2.0E+06	22.78

Stream	Easting[a]	Northing[a]	Min_Area[b]	Max_Area[b]	k_{sn}
33	653446	927038	2.0E+07	2.0E+07	33.30
33	653656	927038	2.0E+07	2.3E+07	34.76
33	653846	927138	2.3E+07	2.3E+07	32.43
33	653996	927318	2.3E+07	2.3E+07	28.35
33	654116	927518	2.3E+07	2.3E+07	25.97
33	654166	927748	2.3E+07	2.4E+07	23.00
33	654126	927968	2.4E+07	2.4E+07	20.12
33	654246	928168	2.4E+07	2.5E+07	19.36
			Villa Camilla anticline		⟷
33	654376	928348	2.5E+07	2.5E+07	19.82
33	654496	928538	2.5E+07	2.5E+07	20.27
33	654566	928748	2.5E+07	2.6E+07	20.78
33	654616	928948	2.6E+07	2.6E+07	21.51
33	654666	929138	2.6E+07	2.6E+07	21.96
33	654666	929368	2.6E+07	2.6E+07	22.55
33	654766	929538	2.6E+07	2.7E+07	23.10

Stream	Easting[a]	Northing[a]	Min_Area[b]	Max_Area[b]	k_{sn}
33	654796	929768	2.7E+07	2.9E+07	23.47
33	654766	929998	2.9E+07	2.9E+07	23.45
33	654886	930188	2.9E+07	3.0E+07	22.86
33	654896	930388	3.0E+07	3.0E+07	22.16
33	655016	930588	3.0E+07	3.0E+07	21.93
33	655186	930768	3.0E+07	3.0E+07	22.04
33	655296	930968	3.0E+07	3.0E+07	22.13
			Castelvetro anticline		⟷
33	655306	931198	3.0E+07	3.1E+07	22.28
33	655446	931388	3.1E+07	3.1E+07	22.62
33	655576	931568	3.1E+07	3.1E+07	23.16
33	655726	931738	3.1E+07	3.1E+07	23.59
33	655856	931938	3.1E+07	3.2E+07	23.99
33	655916	932168	3.2E+07	3.2E+07	23.98
33	655856	932388	3.2E+07	3.2E+07	23.74

Stream	Easting[a]	Northing[a]	Min_Area[b]	Max_Area[b]	k_{sn}
34	653006	928258	1.2E+04	1.4E+05	15.18
34	653056	928488	1.4E+05	2.7E+05	14.81
34	653186	928678	2.7E+05	3.5E+05	13.11
34	653346	928858	3.6E+05	4.3E+05	12.57
			Villa Camilla anticline		⟷
34	653536	928978	4.3E+05	8.4E+05	13.07
34	653696	929138	8.4E+05	9.3E+05	12.13
34	653866	929308	9.3E+05	9.6E+05	11.12
34	653906	929538	9.6E+05	1.0E+06	11.08
34	653916	929778	1.0E+06	1.4E+06	11.71
34	654056	929938	1.4E+06	1.8E+06	12.26
34	654296	929948	1.8E+06	2.1E+06	12.76
34	654506	929918	2.1E+06	2.1E+06	19.35
34	654716	929928	2.1E+06	2.1E+06	33.12

Stream	Easting[a]	Northing[a]	Min_Area[b]	Max_Area[b]	k_{sn}
38	654736	926458	4.1E+05	5.4E+05	14.19
38	654886	926638	5.4E+05	6.4E+05	15.28
38	655076	926788	6.4E+05	8.7E+05	14.23
38	655196	926958	8.8E+05	9.8E+05	13.49
38	655266	927178	9.8E+05	1.8E+06	11.76
38	655456	927328	1.8E+06	1.9E+06	8.31
38			Villa Camilla anticline	⟷	68.95
38	655606	927518	1.9E+06	2.0E+06	11.15
38	655786	927698	2.0E+06	2.0E+06	18.03
38	655986	927798	2.0E+06	2.4E+06	19.76
38	656196	927708	2.4E+06	2.5E+06	15.77
38	656376	927868	2.5E+06	2.6E+06	14.62
38	656566	928018	2.6E+06	3.3E+06	16.84
38	656736	928148	3.3E+06	3.7E+06	17.26
38	656956	928198	3.7E+06	3.8E+06	15.37

Stream	Easting[a]	Northing[a]	Min_Area[b]	Max_Area[b]	k_{sn}
38	657786	928448	4.2E+06	4.3E+06	10.89
38	657986	928478	4.3E+06	4.4E+06	10.65
38	658146	928628	4.4E+06	7.5E+06	12.00
38	658336	928778	7.6E+06	7.6E+06	13.32
38	658496	928958	7.7E+06	7.7E+06	13.49
38	658686	929098	7.7E+06	7.8E+06	13.62
38	658866	929278	7.8E+06	7.9E+06	13.63
			Castelvetro anticline		⟷
38	659026	929428	7.9E+06	8.0E+06	13.65
38	659106	929648	8.0E+06	8.1E+06	13.67
38	659136	929888	8.1E+06	8.1E+06	13.48
38	659196	930108	8.1E+06	8.4E+06	13.21
38	659316	930308	8.4E+06	8.5E+06	13.03
38	659256	930538	8.5E+06	8.5E+06	12.81
38	659226	930768	8.5E+06	8.8E+06	12.77

Stream	Easting[a]	Northing[a]	Min_Area[b]	Max_Area[b]	k_{sn}
36	655846	929138	6.1E+05	7.8E+05	7.38
36	655986	929338	7.8E+05	9.0E+05	8.94
36	656086	929548	9.1E+05	1.0E+06	10.16
36	656136	929778	1.0E+06	1.2E+06	10.31
36	656206	929988	1.2E+06	1.3E+06	10.46
36	656246	930218	1.3E+06	1.6E+06	10.87
36	656256	930458	1.6E+06	1.6E+06	11.02
36			Castelvetro anticline	⟷	
36	656256	930708	1.6E+06	2.0E+06	10.93
36	656256	930938	2.0E+06	2.2E+06	10.63
36	656236	931178	2.2E+06	2.3E+06	10.36
36	656246	931418	2.3E+06	2.4E+06	10.34
36	656346	931618	2.4E+06	2.6E+06	10.34
36	656456	931828	2.6E+06	2.6E+06	10.30
36	656556	932018	2.6E+06	2.7E+06	10.42
36	656756	932058	2.7E+06	2.7E+06	11.22

Stream	Easting[a]	Northing[a]	Min_Area[b]	Max_Area[b]	k_{sn}
37	656226	928578	2.8E+05	4.6E+05	6.41
37	656366	928768	4.6E+05	5.9E+05	7.73
37	656496	928968	6.0E+05	7.1E+05	9.33
37	656676	929118	7.1E+05	8.3E+05	10.34
37	656876	929258	8.3E+05	9.1E+05	10.29
37	657106	929298	9.1E+05	9.5E+05	9.74
37	657316	929388	9.5E+05	1.4E+06	9.30
37			Villa Camilla anticline		⟷
37	657396	929598	1.4E+06	1.8E+06	9.05
37	657556	929758	1.8E+06	1.8E+06	9.08
37	657656	929958	1.8E+06	2.6E+06	8.62
37	657826	930148	2.7E+06	2.7E+06	9.05
37	657836	930388	2.7E+06	2.8E+06	12.56
37	657916	930588	2.8E+06	3.0E+06	15.49
37	658116	930698	3.0E+06	3.3E+06	15.27
37	658216	930888	3.3E+06	3.3E+06	14.34

Stream	Easting[a]	Northing[a]	Min_Area[b]	Max_Area[b]	k_{sn}
39	655806	926338	4.4E+04	1.4E+05	19.78
39	656016	926438	1.4E+05	2.3E+05	19.82
39	656156	926618	2.3E+05	3.5E+05	16.76
39	656256	926828	3.5E+05	4.4E+05	15.62
			Villa Camilla anticline		⟷
39	656346	927038	4.4E+05	5.2E+05	19.38
39	656506	927228	5.4E+05	6.4E+05	19.43
39	656636	927418	6.4E+05	6.8E+05	15.86
39	656846	927518	6.8E+05	7.7E+05	13.88
39	657056	927598	7.9E+05	8.1E+05	14.38
39	657286	927608	8.1E+05	1.3E+06	15.24
39	657476	927618	1.3E+06	2.1E+06	13.71
39	657626	927788	2.1E+06	2.2E+06	11.33
39	657766	927938	2.2E+06	2.5E+06	10.31
39	657876	928108	2.7E+06	2.8E+06	9.86
					60.45

Stream	Easting[a]	Northing[a]	Min_Area[b]	Max_Area[b]	k_{sn}
40	656876	926538	3.7E+04	1.4E+05	14.62
40	657096	926528	1.4E+05	2.1E+05	10.44
40	657316	926548	2.1E+05	2.5E+05	10.98
			Villa Camilla anticline		⟷
40	657456	926738	2.5E+05	3.4E+05	15.33
40	657486	926958	3.4E+05	4.2E+05	15.91
40	657516	927198	4.2E+05	5.1E+05	12.55
40	657546	927408	5.1E+05	7.0E+05	12.74
40	657546	927638	7.0E+05	7.0E+05	13.55

Stream	Easting[a]	Northing[a]	Min_Area[b]	Max_Area[b]	k_{sn}
41	660196	926768	8.5E+07	8.5E+07	36.38
41	660436	926788	8.5E+07	8.6E+07	40.55
41	660646	926898	8.6E+07	9.0E+07	40.31
41	660846	927008	9.0E+07	9.6E+07	38.80
41	661086	927038	9.6E+07	9.6E+07	37.13
41	661246	927218	9.6E+07	9.6E+07	34.50
41	661386	927408	9.6E+07	9.6E+07	32.41
			Villa Camilla anticline	⟷	193.16
41	661396	927658	9.6E+07	9.7E+07	30.41
41	661466	927878	9.7E+07	9.7E+07	27.53
41	661586	928078	9.7E+07	9.7E+07	23.05
41	661636	928308	9.7E+07	9.8E+07	18.79
41	661756	928508	9.8E+07	9.8E+07	18.29
41	661806	928738	9.8E+07	9.8E+07	18.95
41	661956	928928	9.8E+07	1.0E+08	19.67

The active deep mountain front of Northern Apennines: seismicity and geomorphology

Alessio Ponza (alessio.ponza@unibo.it) [a*]

Vincenzo Picotti (vincenzo.picotti@unibo.it)[a]

Silvia Pondrelli (pondrelli@bo.ingv.it)[b]

Frank J. Pazzaglia (fjp3@lehigh.edu)[c]

Claudio Berti (clb208@lehigh.edu)[c]

[a]Università di Bologna, Dipartimento di Scienze del la Terra e Geologico Ambientali, Via Zamboni 67, 40126 Bologna, Italy

[b]Sezione di Bologna, Istituto Nazionale di Geofisica e Vulcanologia, Via D. Creti 12, 40128 Bologna, Italy

[c]Department of Earth and Environmental Science, Lehigh University, 31 Williams, Bethlehem, PA 18015, USA

*Corresponding author

Dr. Alessio Ponza

Dipartimento di Scienze della Terra e Geologico-Ambientali

University of Bologna

Via Zamboni, 67

40126 Bologna - Italy

Tel. +39 051 2094546; Fax +39 051 2094522

Email: alessio.ponza@unibo.it

Abstract

The Northern Apennines (NA) mark the active plate margin between Europe and Adria. Given the low convergence rates, moderate seismic activity, and rapid sedimentation in the Po atop the buried compressional front ambiguities still occur in defining a seismotectonic and geodynamic framework, a problem we address with progressively-deformed geomorphic markers, reflection seismology, and the seismicity of M>4 earthquakes over the last 30 years for the mountain front located between the Panaro and Enza river valleys. Focal mechanisms indicate a clear stratification of extensional earthquakes above 15 km, and compressional earthquakes below 15 km (see Fig.4). This strain distribution implies a mountain front cut by normal faults and deep, blind thrust as has been proposed for the Bologna segment with a tip ~17 km deep and thought to be a crustal-scale structure that soles into the subduction boundary. Since the pole of rotation of this subduction is close to the western part of the NA, the northeast verging strain accounted by the deep thrust decreases to the west, and a regional northwest verging strain field indicated by Adria GPS velocities starts to be more recognizable. As a consequence, the continuity of the subduction boundary is less defined, the shape of the mountain front is more irregular and affected by local dome and swell interference structures, and the deep focal mechanisms increasing indicate strike-slip earthquakes.

Two of domal structures between the Panaro and Enza Rivers have been studied in detail (Castelvetro – Vignola foothills and Ghiardo plateau). These shallow compressional structures do not appear to be connected to the deep blind thrust but, rather, are local reactivations of shallow-dipping late Neogene thrusts, or new northwest-vergent structures. The geometry and uplift rates of the anticlines constrain a simple trishear fault propagation folding model that inverts for blind thrust ramp depth, dip, and slip.

1 - Introduction

The mountain fronts of fold and thrust belts have been long recognized to result from at least four possible structural geometries (Vann et al., 1986), the interpretation of which is difficult to discern from isolated studies of geomorphic markers, seismology, or geodesy. The problem is compounded for cases where the deformation front does not correspond to the topographic growth of a mountain. Such is the case for the northern Apennines, Italy, where it appears that the mountain front has formed as an out-of sequence structure recently in the development of the range. This mountain front we intend to study in this paper has been the object of several different interpretations (see review in Picotti and Pazzaglia, 2008), the most popular proposing an emergent thrust called the Pedeapenninic Thrust Front (PTF, e.g. Boccaletti et al., 2004 with references) that ruptures the base of the foothills. Some authors interpret this surficial thrust as rooted at the base of the deformed wedge, whereas other proposed it as a structure cutting the whole lithosphere. Other research does not consider the PTF as the main active structure, but rather appeals to a deep, blind thrust that is uplifting and deforming a formerly active thin-skinned fold and thrust belt (see review in Picotti and Pazzaglia, 2008).

In any case, the interpretations for construction of the northern Apennine mountain front make predictions regarding kinematic processes and the associated seismic hazards for a part of Italy that has not been characterized by repeated, historic catastrophic earthquakes. The dense infrastructure and population centers situated along the Apennine front in northern Italy make it a attractive candidate for better seismic hazard prediction. In this respect, rates of activity and the depth of seismogenic layer (s) are crucial to constrain the seismic risk. Paleoseismologic and GPS geodetic studies (De Martini et al., 2003) are commonly used to address these issues but in the case of the Northern Apennines they have proven to be problematic due to the paucity of clear surface ruptures that can be trenched as the slow and complicated rates of horizontal deformation (Serpelloni et al., 2005).

We surmount these problems by integrating progressively deformed geomorphic markers, a type of geologic geodesy with historic seismicity and high-resolution reflection seismology. Our goal is the

78 localization of active structures and a hierarchy of the seismic risk, based on an assessment of their
79 rates of slip. In the process, we will be able to compare the data against the various possible
80 mountain front structural geometries and propose or modify existing models for development of the
81 northern Apennines.
82
83 **2 - Geological framework**
84 The Northern Apennines (Fig. 1) are a fold-and thrust belt evolved during the Tertiary as a response
85 to the subduction of the Adriatic plate under the European lithosphere. Since the Oligocene, the
86 flexuring of the foreland lithosphere created deep subsiding foreland basins filled with thick
87 foredeep deposits, progressively imbricated into the thrust wedge along with underlying Mesozoic
88 basement by underplating and frontal accretion. The Apenninic wedge extends down to the
89 subduction interface and is ~50 thick beneath the topographic crest. The wedge has a structural lid,
90 the Liguran nappe, a Cretaceous-Eocene mélange that represents part of a large, pre-Apenninic
91 wedge that formed far to the west and has been subsequently translated passively to the east with
92 the rollback of Adria subduction. The Ligurian unit and its epi-Ligurian forearc basins have
93 progressively over-ridden Apenninic foredeeps from the Oligocene through the Early Pliocene. This
94 structural lid is intact through much of the Emilia segment of the northern Apennines, but has been
95 largely removed by erosion for the Romagna section as well as along the topographic crest of the
96 range exposing the underlying foredeep turbidites (Zattin et al., 2002).
97 The current Apennine mountain front sharply overprints the thin-skinned fold and thrust belt
98 represented by the imbricated foredeeps and their Ligurian cover. A feature of the recently
99 emergent mountain front is that it is riddled with small, but pervasive high-angle normal faults
100 (Picotti et al., 2009) that are embedded in a larger-wavelength foreland –dipping flexure, clearly
101 documented by progressively deformed alluvial fan and river terrace growth strata (Picotti and
102 Pazzaglia, 2008). Commensurate with the growth of the mountain front has been the apparent
103 deactivation, or at least significant slowing of shortening at the thrust front, which is buried beneath
104 the Po Plain.

105 The evolution of the paleostress shows a complex interaction of northeast and northwest
106 compressional axes, overlapping through time and space (Bernini and Papani, 1987). Constant
107 northeast-oriented σ_1 is documented from the late Messinian to the Middle Pleistocene at the
108 Stirone river section of the mountain front, whereas between the Taro and Baganza valleys some 20
109 km to the southeast, there is a mix of northwest- and northeast-trending σ_1. Further to the southeast
110 at the Enza River, only the northwest-oriented σ_1 are documented. Similar juxtapositioning of
111 northeast- and northwest-directed σ_1 directions are reported for other portions of the mountain front
112 (Morelli and Costa, 1997; Ghiselli and Martelli, 1997).
113
114 ***2.1 Geologic and geomorphic setting of the study areas (Castelvetro - Vignola hills and the***
115 ***Ghiardo plateau).***
116 The southern flank of the Po Plain between the Enza and Parano rivers including the Ghiardo
117 plateau and Castelvetro-Vignola is folded into a series of low, elongated hills and valleys that have
118 long been recognized as actively growing structures (Cremaschi and Papani 1975, Gasperi et al.
119 1999, Carnicelli 2003, Pizziolo et al., submitted, see Figs. 2 and 3).
120 Downstream of San Polo d'Enza and Quattro Castella, the Enza River carves a valley through
121 Quaternary sediments of the Ghiardo plateau (Fig. 2) an east-west-elongated hill that sits several
122 kilometers north of the mountain front, here defined by topographically striking flatirons underlain
123 by middle Pleistocene conglomerate. These flatirons led Bernini and Papani (1987) and Boccaletti
124 et al. (2004) to argue for local emergence of the PTF, but subsequent map and seismic data show no
125 evidence of an emergent thrust. Rather, the Ghiardo Plateau is the more likely an actively growing
126 fold cored by a blind thrust fault (Figs. 2 and 7). Here the hanging wall syncline is infilled by fine-
127 grained upper Pleistocene-Holocene deposits corresponding to the Qt5-Qt6 chronostratigraphic
128 units of Picotti and Pazzaglia (2008). The top of the plateau is dissected by a small N-S valleys
129 cutting middle to upper Pleistocene continental deposits corresponding to Qt3/Qt2 uplifted above
130 the Holocene plain of the Enza river (Cremaschi and Papani 1975).
131 Southeast along the mountain front, the Castelvetro fold is approximately 5 km in amplitude, 15 km

in strike length, and situated between the Panaro and Tiepido rivers (Fig. 3). This structure shows evidence of the interaction of both a northwest-(apenninic) and a northeast- (anti-apenninic) deformational trends, resulting in a final dome-and-swell geometry. The limbs of the fold are formed by Plio-Pleistocene deposits and involve Pliocene to Lower Pleistocene mudstone (Argille Azzure Fm), with local coarse interbeds (Gasperi et al., 1999; Amorosi et al., 1998a), middle Pleistocene beach deposits (Sabbie Gialle Fm), and two units of continental deposits, respectively the Lower Emiliano-romagnolo Synthem (AEI), consisting of alternating coarse and fine-grained coastal plain and lacustrine facies and the Upper Emiliano-romagnolo Synthem (AES), formed by coarse-grained alluvial fan and fluvial facies (Gasperi et al., 1999). Growth geometries are evident for all Plio-Pleistocene deposits. The youngest deposits involved in the folding are late middle Pleistocene alluvial units, called AES7/7a in Gasperi et al. (1999) and mapped in this paper (Figs. 2 and 3) as Qt3, following the chronostratigraphy proposed by Picotti and Pazzaglia (2008) and Wegmann and Pazzaglia (2009), (Fig. 6).

A few kilometers south of the Castelvetro structure, a second asymmetric anticline, the so called "flexure of Villa Camilla" (Gasperi et al., 1999) has an northeast-oriented axial trace that near Vignola begins bending to the NW (Fig. 3). Around Campiglio (Fig. 3), Messinian mudstone and sandstones of the Colombacci formation and the Ligurian scaly shales outcrop at the Villa Camilla fold culmination. Along the fold hinge, near Campiglio, a wind gap is carved into the bedrock and dissecting the overlaying Quaternary deposits Qt3 (AES7) on both sides of the small Campiglio valley. Late Pleistocene alluvial terraces are not preserved, downstream of the Campiglio wind gap.

3 - Seismic activity

The recent seismic activity of the northern Apennines is mainly characterized by moderate magnitude events ($M < 4.0$), but if we take a look to the past we can see that historical records (Fig. 4) indicate several potentially great events ($M > 6$). Because pre-instrumented events are poorly located, the large earthquakes may have occurred in the extending backarc of the Apennine wedge in Toscana. For example, the 1920 Garfagnana event, Mw 6.5 and Imax X or the 1919 Mugello,

159 Mw 6.2 and Imax IX (the two northernmost historical events of Figure 4; Gruppo di Lavoro CPTI,
160 2004). Earlier large magnitude events are thought to have originated in the central Apennines close
161 to area shaken by the 1997-1998 Umbria-Marche seismic sequence (Amato et al., 1998).
162 The instrumental seismicity recorded in the last several decades shows its greatest concentration at
163 or near the crest of the chain (Fig 4; De Luca et al., 2009, Castello et al, 2006). These events are
164 mostly shallow ruptures ~10 km in depth, with less frequent events down to 30 km. Those with
165 greater hypocentral depth are mostly located on the Adriatic flank of the chain (red dots on the map
166 of Fig. 4).
167 Seismicity in the last 30 years beneath the northern Apennine mountain front include the 1996
168 Reggio Emilia earthquake (hypo depth 12-18 km; Selvaggi et al., 1996), the 2000 Forli'-Faenza
169 earthquake (8-13 km; Calderoni et al., 2009), the 2003 Monghidoro earthquake (about 20 km;
170 Piccinini et al., 2006) and the last 2008 Reggio Emilia-Parma earthquake sequence (Ercolani et al.,
171 2009). All of these are characterized by a thrust and strike-slip seismicity.
172 Available focal mechanisms show that extensional and compressional earthquakes are vertically
173 stratified (Pondrelli et al., 2006). Extensional events are mainly in the inner part of chain (Fig. 4,
174 blue focal mechanisms), while compressional and strike-slip events are located on the flanks. This
175 lateral change of deformation style (Frepoli and Amato, 1997) can now be updated with newly-
176 located, more recent seismic moment tensors allowing for visualization of the 3D distribution of the
177 seismicity (Fig.4). The CSI1.1 Catalog (20 years of instrumental seismicity (Chiarabba et al., 2005;
178 Castello et al., 2006) is plotted with symbols dimension proportional to the magnitude (from lowest
179 value of 2.0) and with colors for different hypocentral depth where yellow are depths less than 30
180 km and red are depths greater than 30 km. This boundary value has been selected on the basis of
181 Moho depth, and thus crustal thickness, determined for the Northern Apennines by receiver
182 functions (Piana Agostinetti et al., 2002). The shallower seismicity shows a great density and
183 frequency along the maximum height of the chain and in the Romagna area, south of Bologna.
184 Northward, it appears still more present in the chain but more sparse than southward. Along the
185 Bologna segment, there is an apparent seismic gap Earthquakes with deeper hypocentral depth (red

186 dots in Fig. 4) occur more frequently on the outer part of the chain and beneath the chain itself.
187 Fig. 4 plots all moment tensors available for the seismicity with magnitude Mw between 4.1 to 5.4
188 for the last 30 years (including some events of the recent Reggio Emilia-Parma, December 2008
189 seismic sequence), including CMTs (Dziewonski et al., 1981; Dziewonski et al., 2001;
190 HYPERLINK "http://www.globalcmt.org" www.globalcmt.org). The different colors given to
191 different styles of reported moment tensors help in describing the change in the trend of
192 deformation in the Northern Apennines. A lateral separation between thrust and strike-slip events
193 (red and green in Fig. 4) with respect to extensional (blue) events is evident in this map. Thrusts are
194 located exclusively in the Adriatic side of the chain while extensional earthquakes are only within
195 the chain, in the context of extensional basins that constitute the inner part of the range.
196 In general, thrust and strike-slip events are systematically deeper (below 15 km of depth) than the
197 extensional events. It is also worthy to note that (1) strike-slip events appear mainly in the
198 northernmost section of the studied area (section A in Fig. 4); (2) in the central part of the area
199 contains the Bologna seismic gap and thrust events are only beneath the mountain front, not in the
200 foreland, and (3) in the Romagna area the mutual distribution of extensional and thrust events is
201 maintained along the chain (sections C and D) going southward.
202 The different deformations styles are separated not only laterally as reported in previous studies
203 (e.g. Frepoli and Amato, 1997), but also vertically. This leads to the idea that the extensional
204 deformation pervades the shallower part of the wedge of Northern Apennines, while at a depth that
205 on average is around 25 km, thrust earthquakes are nucleating along one or more deep blind thrusts.
206

207 **4 - Tectonic geomorphology methods and approach for using terraces to measure river**
208 **incision.**

209 ***4.1 Terrace straths vs. treads as tectonic indicators***

210 River terraces are commonly used to measure the rate of vertical stream incision, typically
211 interpreted as the rate of base level fall, inclusive of rock uplift and associated crustal deformation.
212 River terraces are the geomorphic and sedimentologic expression of unsteady vertical channel

213 incision (e.g. Schumm et al., 1987; Bridgland, 2000). Terrace deposits are unconsolidated
214 allostratigraphic units with a basal unconformity called a ‘‘strath’’ typically cut across bedrock and
215 a constructional bench-like top called a ‘‘tread’’. The deposit can vary vertically and longitudinally
216 in texture, stratification, and thickness. When it is thin (<3 m), it represents the mobile alluvial
217 cover of a bedrock channel (Pazzaglia and Brandon, 2001) and the landform is correctly called a
218 ‘‘strath terrace’’ (Bull, 1991). The initial gradient of the strath is the gradient of the channel that cut
219 it, approximated in most cases by the modern channel gradient so long as the modern channel has a
220 thin mobile alluvial bed in contact with bedrock. In contrast, thick alluvial deposits represent
221 periods of valley aggradation when the channel is vertically raised above its strath; where these
222 thick fills underlie the terrace landform, they are termed ‘‘fill terraces’’ (Bull, 1991). In both cases,
223 knowing where the strath lies in the landscape, when it was carved, and when it was abandoned by
224 incision to form the base of a terrace are the pertinent observations leading to a useful terrace
225 genesis model, particularly one that is portable to tectonic problems. Attempting to utilize terrace
226 treads in a similar way requires caution. The depositional slope of the tread does not always mimic
227 the slope of the underlying strath. Treads are also commonly modified by post-depositional
228 colluvial and tributary alluvial fan burial or fluvial dissection that cumulatively increase their
229 modifications with terrace age (Eppes et al., 2008). However for fill terraces a minimum strath age
230 can be determined by the age of the stratigraphically lowest (oldest) alluvium directly atop the
231 strath, assuming no reoccupation of the strath by a younger channel. Subsequent incision of the
232 terrace fill deposit and underlying strath surface is approximated by the age of the youngest
233 conformable terrace alluvium in the fill sequence.
234
235 ***4.2 Strath genesis and applications***
236 Straths occur in mountainous regions across a wide range of channel incision rates. Where incision
237 is around 1 mm/yr, they are commonly paired and extensive (e.g. Olympic Mountains, Pazzaglia
238 and Brandon, 2001; Nepalese Himalaya, Lavé and Avouac, 2001; New Zealand, Bull and Knuepfer
239 1987 and the Apennines, Picotti and Pazzaglia, 2008), while for rivers in rapidly uplifting regions

240 of ~ 10 mm/yr (Burbank et al., 1996; Hartshorn et al., 2002), strahts tend to be unpaired and have
241 limited down-valley extent (<1 km).
242 The combination of complementary factors such as relatively non-resistant bed, oscillatory fluxes of
243 sediment and water, moderate-to-low rates of rock uplift, and a threshold drainage basin size
244 appears to be necessary to give the formation of straths (see Wegmann and Pazzaglia with
245 references).
246 We utilize fluvial incision rate (I) for a specific locality along the channel as a proxy for base level
247 fall (rock uplift), that following Lambeck et al. (2004), is given by:
248 $I = H_S/T_S$ (1),
249 where H_S(m) is the vertical separation between the uplifted bedrock strath and the modern channel
250 bedrock, and T_S is the timing (ka) of strath preservation in the landscape. The uncertainty in
251 incision rate ($\sigma 1$) is given by the standard deviation
252 $\sigma 1 = [\sigma^2_{Hs}/T_s^2 + (H_s/T^2_s)^2 \sigma^2_{Ts}]^{1/2}$ (2),
253 where σ_{Hs} is the uncertainty in measured strath height (m) and σ_{Ts} is the uncertainty in the timing of
254 strath preservation. Values of σ_{Hs} are generally ≤ 1 m for straths ≤10 m above the modern channel,
255 1-5 m for terraces ≤ 50 m above the channel, and 10 m for staths > 50 m above the channel. Values
256 of σ_{Ts} are based upon the numeric age uncertainty for radiocarbon dates or from correlation to the
257 Marine Isotope Stage (described below).
258 Strath deformation can be described as the vertical uplift or subsidence with respect to a regional
259 datum that is defined by sea level and the local channel or depositional system gradients across a
260 tenths km-long baseline, assumed to have been more or less constant over the stratigraphic age of
261 the deformed horizons (Wegmann and Pazzaglia 2009).
262 Two kinds of surfaces underlie the alluvial deposits across the mountain front, where the intra-
263 montane valley grades into the foreland (Fig. 5). The first is found within the intra-montane valley
264 where terraces are carved within the bedrock and the basal surface of the alluvial fill corresponds to
265 a strong unconformity previously widely described and called strath. The second is found within the
266 foreland where the subsidence allows the vertical stacking of alluvial bodies, namely alluvial fans,

267 at the border of the foreland. The basal surface in such setting is a para-conformity characterized by
268 a pedogenetic interval that documents the time discontinuity (paleosoil). The mountain front
269 evolves as a wave of deformation, progressively incorporating the previously subsiding fans into
270 the front itself (Fig. 5). In such setting, new straths are inset into the uplifted fan deposits that act as
271 a bedrock for the new terraces, whereas forelandward of the intersection point, younger units
272 usually offlap the older ones. The intersection point is the point that separates the intra-montane
273 terraces from the alluvial fan, i.e. the point that separates strath from buried soils on single
274 sedimentary cycle (*sensu* Wilson et al., 2009, see Fig. 5). The movement of that point through time
275 describes the kinematics of the mountain front evolution. This movement depends on the interplay
276 between tilting rate of the mountain front and aggradation rate of the alluvial units. Increasing tilt
277 rate create a forelandward shift, whereas a decrease of the tilting produce the opposite, i.e. an onlap
278 of the younger units. The same onlap could be created also by an increasing aggradation of the
279 alluvial unit.
280 For Wilson et al., (2009) a fixed intersection point is due to a fold limb rotation mechanism with
281 fixed synclinal axial plane, while a moving intersection point characterizes a fold limb lengthening
282 mechanism where the synclinal axial plane migrates toward the foreland.
283

284 ***4.3 Field and laboratory methods***

285 Existing geologic maps (mostly digital), topographic maps (1–5 m contour intervals), field
286 exposures, 10-m digital elevation models (DEM), and air photos were used to identify fluvial
287 terraces and alluvial fan deposits. The stratigraphy, sedimentology, petrology, and weathering
288 characteristics (Fe and Mn oxides substitution on the gravels, degree and kind of cementation),
289 including soil and paleo-soil profile development (calcic horizon in particular) and at least Munsell
290 colors are the primary lithostratigraphic criteria used to describe and correlate terraces.
291 Separation of the strath surfaces from the modern channels was measured in the field from natural
292 and man-made outcrops by using a barometric altimeter accurate to 1-2 m for straths > 5 m above
293 the channel. The heights of straths less than 5 m above the channel and in some cases the thickness

294 of the alluvium on top, were measured with a Jacob staff and level (accurate to 0.5 m). In order to
295 determine the finite deformation recorded by a strath, the original geometry must be known and is
296 typically assumed to have the same geometry as the modern valley profile (e.g. Pazzaglia and
297 Brandon, 2001), implying a long-term steady-state. Modern valley-bottom strath profiles were
298 constructed from 1:5000 topographic maps and 10-m digital elevation models (DEM) by projecting
299 stream elevations to a straight profile that runs down the center of the valley (see Figs. 2 and 3).
300 Rates of fluvial incision have been determined at ~ 4–5 km upstream the mountain front along river
301 profiles using equations (1) and (2). Measured strath separations above the modern valley bottom
302 were then plotted above the valley profile to constrain strath profiles.
303
304 **4.4 Stratigraphy of the Middle Pleistocene to Holocene deposits and base level fall related**
305 **incision rates**
306 We here utilize a terrace stratigraphy, ranging from Qt0 to Qt9 that both corresponds to and
307 upgrades previous stratigraphy of Picotti and Pazzaglia (2008), Wegmann and Pazzaglia (2009),
308 and Wilson et al., (2009) that produced a unified inter-basin chronostratigraphy across the Northern
309 Apennines, based on a conceptual model of climate modulation of hillslope and fluvial geomorphic
310 processes through variable sediment discharge (Fig. 6). The functional benefit of cross-basinal
311 correlation available with this scheme outweights the disadvantage imposed by different numbering
312 of terraces in the basins studied. Furthermore, the proposed chronostratigraphy correlates the
313 Quaternary units adopted in the official cartography of Regione Emilia-Romagna, locally published
314 by Gasperi et al., (1999), Pizziolo et al., (submitted) and Carnicelli et al., (2003), (see Fig. 6).
315 Previous studies utilized AMS radiocarbon dating for the for Holocene and Upper Pleistocene
316 deposits (Eppes et al., 2008, Wegmann and Pazzaglia 2009) including mollusk shells and detrital
317 charcoal fragments extracted from bulk sediment samples of interstitial sand collected between
318 cobbles and from sandy lenses in otherwise coarse-grained axial channel facies terrace deposits,
319 sampling where possible directly above the strath. In particular Eppes et al., (2008) provided for the
320 Reno valley a well-dated chronosequence from soil exposures in alluvial terraces ranging in age

from hundreds of years to thousand of years. This soil chronosequence consistently exhibits morphologic characters related to age and climate, such as accumulation or dissolution of $CaCO_3$ (stages of Bk horizons), translocation and formation of clay minerals and iron oxides. Eppes et al. (2008) documented general discernible differences in profile horizonation as a function of deposit age, particularly for Holocene to uppermost Pleistocene soils (Qt6 ~ 12000 ka). We will use this distinctive descriptive methodology for correlating alluvial bodies and their topping soils and recognizing alluvial bodies on top of which soils develops.

Correlating terrestrial Quaternary sequences with the marine oxygen isotope record is now suitably well established (e.g. Bridgland and Westaway, 2008). In absence of numeric ages, particularly from terraces older then ^{14}C method, we use as a best approximation for terrace strath age, the chronology of the marine oxygen isotope record of Lisiecki and Raymo (2005) as a long-term framework for identifying likely times of strath cutting and channel aggradation or incision. In addition, we utilize terrace stratigraphy of nearby river valleys (Picotti and Pazzaglia, 2008, Wilson et al., 2009) and their downdip-equivalent subsurface marine, littoral an fluvial deposits beneath the southern Po Plain where cyclic lithofacies and pollen assemblages are recorded in well logs and dated by calibration to glacial-interglacial climate cycles as further controls on strath age (Amorosi et al., 1996, 2002, 2004; Di Dio et al., 1997; Gasperi et al., 1999; Picotti and Pazzaglia, 2008).

The strath ages we use in producing our chrono-stratigraphy directly correlate with glacial periods and consequently with the associated eustatic lowstands. To explain as tectonic signal the non-uniform and unsteady river incision, we need to exclude that eustatic fall could have driven similar responses upstream the river valleys (Pazzaglia and Gardner, 1993).

However, several lines of evidence lead us to reject the possible eustatic base-level fall as a factor in the observed spatial distribution and accelerations in river incision (Wegmann and Pazzaglia 2009). First, Pleistocene glacio-eustatic drawdowns did generate knickpoints on the Po River and some of its major tributaries, but none of these knickpoints had migrated to the mountain front or beyond on the Panaro, Tiepido, Enza channels before being drowned and arrested by the ensuing eustatic rise and transgression (Amorosi et al., 2004).

Second, we have shown clear evidence for the large alluvial fans that rivers draining to the Po Plain have constructed during glacial climates and eustatic lowstands (Di Dio, 1998; Amorosi et al., 2004). Third, the lower reaches of the Enza, Panaro, Guerro and Tiepido Rivers are incise on bedrock, indicating that they are at their base level of erosion documenting that deeply incised sediment backfilled paleovalleys do not exists in the lower reaches of either of these basins.

5 – Pleistocene stratigraphy and incision rates

5.1 Enza river and Ghiardo Plateau

5.1.1 Enza river section

In the Enza river, as in other rivers flowing to the Po Plain (e.g. Wilson et al., 2009) a recent, probably anthropogenically-driven incision took place at the mouth of the intramontane valley, with lowering of the valley floor 2–3 m below its floodplain downstream S. Polo d'Enza. A continuous outcrop, stretching ~ 2 km, exposes an outstanding section of Pleistocene growth strata, displaying the passage from shallow marine mudstones (Argille Azzurre Fm) to continental alluvial deposits (our unit Qt3), (Fig. 7). The geometry of this growth is the effect of the moving intersection point, due to limb lengthening and the continuous evolution of the deep thrust, as discussed in par. 4.2 and in Wilson et al., 2009. Such a good exposure provides the clearest description for deposits usually covered in their main characters far from the river. This references section allows physically correlate the subsurface deposits to their uplifted counterparts at the mountain front (see Fig. 5).

Starting from the 45° dipping Lower Pleistocene open shelf mudstones of the Argille Azzurre Fm (around 130 m), downstream the S. Polo d' Enza bridge, the shallowing-up succession grades, around a rhodolitic bed, to around 75 m of alternating sand and mudstones arranged in parasequences, the Torrente Stirone unit (Di Dio et al., 1997, Pizziolo et al., submitted). The marine succession ends with the Costa Mezzana unit, consisting of littoral sandstones topped by pebbly sandstones and a final conglomerate layer, interpreted as the progradation of a fan delta (a paleo Enza?) into the strand. The stratigraphic thickness of the Costa Mezzana unit is 29 m and the beds dip to the north, decreasing from 26° at the base to 20° at the top.

375 Floored by 80 to 100 cm of oxidized and mottled yellowish mudstones, a coastal plain unit of 33 m
376 of thickness, called Lower Emilian Synthem, shows dipping grading from 20° to 9° at the top. The
377 unit consists of three coarsening-upward cycles. The basal cycle starts with lagoonal mudstones,
378 dark gray and laminated, rich in fresh-water gastropods. The 8 m thick mudstones overlie the basal
379 pedogenetic interval, marked by carbonized wood and seeds (nuts) and are topped by a paleosoil, 2
380 m thick and 5YR 5/8 Munsell wet colour, again marked by the presence of *in situ* tree trunks (Fig.
381 7). The soil and trunks are buried by a scoured, 40 to 100 cm thick channelized body of sandy
382 gravel and pebbly sands, followed by 2 m of structureless matrix-supported mud-rich pebbly
383 sandstones. The ensuing paleosoil, developed on sandy and silty alluvial facies, has 10YR 5/6 wet
384 color. The lower mudstone interval is less developed in the overlying two cycles, that more or less
385 evolve with similar facies stacking. The topping paleosoil of this unit formed at the expenses of the
386 uppermost 3 m of a mud supported diamicton with poorly sorted, poorly rounded and strongly
387 weathered gravels. This paleosoil bears the most intense rubefaction in the Pleistocene section, with
388 Munsell color 2.5 YR 4/6 and has been already described by Cremaschi (1975) as the
389 pedostratigraphic unit of Collecchio, thought to be Günz-Mindel (middle Pleistocene). The
390 rubefaction and the weathering of pebbles in the parent material speak to the intensity and duration
391 of pedogenesis that we tentatively correlate to the interglacial stage MIS 17 (see chronostratigraphic
392 discussion in Picotti and Pazzaglia, 2008 and Wegman and Pazzaglia, 2009).
393 The Upper Emilian Synthem consists mainly of gravels and minor sands, arranged in three main
394 units in the Enza succession, each of them topped by a peculiar paleosoil. The first unit (Qt1) is 25
395 m thick and ends with a calcic soil (10YR 4/6, Munsell color), rich in sparse calcareous nodules,
396 suggesting a semi-arid climate during the formation of this unconformity. The second unit (Qt2) is
397 formed by ~ 25 m of alluvial fan gravels typically coated, and locally substituted, by Fe and Mn
398 oxides, while the dipping decrease from 4° to 2° at the top. The capping paleosoil shows a typical
399 brown orange color (7.5 YR 3/4 dry and 10YR 5/8 moist, Munsell) and 2 m of thickness. The last
400 unit visible in the section is Qt 3 a pre LGM alluvial fan, that consists of 30 m thick stratified gravel
401 , again capped by a brown orange soil, very similar in colour to the previous one. The latter soil is

402 covered by gravels of the Qt3b unit, whose top is not outcropping.

403

404 ***5.1.2. Enza mountain front and terraces***

405 Continental deposits from AEI to Qt1 and Qt3 are well preserved in the landscape, northward tilted
406 at the mountain front and anticlinally folded to form the Ghiardo Plateau (Figs. 2, 7 and 8).
407 The gravel bodies of the Lower Emiliano-romagnolo Synthem (AEI) deposits are well preserved
408 also west and east the Enza river, where its base reaches a maximum elevation of 320 m.a.s.l. at
409 around 5 km from the mountain front, with an incision of 155 m. The bottom of the AEI has a
410 variable dip, ranging from 20°at the river Enza and northwest of it, to the 50° at the Rio Monticelli
411 to the southeast of the river (Fig. 2). This dipping trend is clearly marked in the landscape, with
412 relief of foothills increasing from NW to SE.
413 The base of Qt1 reaches the elevation of 220 m south of Quattro Castella and its northward dipping
414 increases from 9° into the river to 33° in the Rio Monticelli in the east (Cremaschi and Papani,
415 1975, Figs 2 and 7). The increasing deformation intensity moving eastward explains the presence of
416 an elongated Qt1 terrace at the west side of the river, with strath elevations reaching 240 m.a.s.l.
417 This is the only strath terrace found south of the intersection point, thanks to the low dip of the
418 beds, whereas east of the river it has been more uplifted, and therefore eroded.
419 Qt2 deposits form the culmination of the Ghiardo Plateau, also west of the Enza near
420 Montechiarugolo. Surprisingly, the Qt2 unit does not outcrop at the mountain front, if we exclude a
421 small remnant at the eastern flank at the elevation of 250 m.a.s.l. (see Figs. 2 and 8).
422 Map unit Qt3 is thick becaue it includes at least two stacked units (Qt3a and Qt3b), and therefore
423 occupies a wide area, forming the lower flat surface that onlaps the uplifted Qt2 deposits at the
424 Ghiardo Plateau (see Fig 2). Qt3a lies on top of Qt1 deposits along the foothills both east and west
425 of the river Enza, while up-valley 5.5 km at the west side of the river, Qt3a is preserved as a strath
426 85 m high above the modern channel (elev: 250 m.a.s.l.). Qt3b is preserved only in the east side,
427 connecting the high valley margin to the Ghiardo Plateau by a long gently dipping surface (Figs. 2
428 and 8).

429 The absence of the Qt2 from the foothills surface is due to the fact that Qt3 unit onlapped the
430 previous intersection point. As discussed in chapter 4.2., the movements of the intersection point
431 should be interpreted playing with two factors (see Fig. 5): a decrease of the tectonic uplift and
432 tilting and/or a rapid vertical aggradation of the unit. The reconstructed tilting rate for the Enza river
433 section indicate an acceleration between the Costa Mezzana and AEI (early Middle Pleistocene),
434 whereas from Qt1 to Qt3 the rates progressively decelerate (see Fig. 5). Therefore, even if Qt3 is by
435 far the thicker unit, the changing from offlap to onlap of the units recorded since Qt2 is associated
436 to this deceleration of the tilting rate.
437 A wide Qt6 surface extends upstream and downstream valley in the east bank of the river and flanks
438 Qt3b downstream the mountain front along all the Ghiardo Plateau. A narrow surface of Qt6, ~ 1/5
439 in width respect to the correspondent in the other side of the river bank, is still preserved along the
440 west bank, where it stretches from km 4.5 to km 1.
441 The asymmetry of the Enza Valley at its mouth is remarked not only by the map distribution of the
442 alluvial terraces, but it is also visible on a transverse section (Fig. 8b). The section shows a
443 differential uplift of 0.13 mm/y that produces the tilting and the increasing bed attitude of the units
444 at the east of the valley. Therefore, we document the presence of a transverse structure across the
445 Enza river, possibly related to the NE trending "Passo della Cisa – Enza" Line of Papani et al.
446 (1987), as an important NW- verging thrust that cuts the Ligurian edifice (Fig. 2). The activity of
447 this structure, covered by the Quaternary and therefore blind, is compatible with the differential
448 uplift of the eastern side of the valley. This structure should interact with the deeper structure
449 responsible of the northward verging mountain front.
450 As previously pointed out, in the Enza river valley the strath terraces are locally preserved up to ~
451 5.5 km upstream for the Qt3a and Qt2, while the younger terraces suite as Qt6, Qt8 and Qt9 are
452 better represented and exposed along the river's cut banks and lower reaches of tributary streams.
453 The only dated sample among the suitable samples collected was taken from an excavation east of
454 San Polo d'Enza (black star in Fig. 2) at ~ 2.5 m of depth. The sampled gastropod shells belong to
455 the base of a fine-grained succession, interpreted as a pond, developed during an humid phase on

456 top of an alluvial terrace. The calibrated age of 9214±155 y BP allows us to correlate the underlying
457 terrace as Qt 6 (developed between 13 and 11 ky, see Fig. 6), by far the widest Upper Pleistocene
458 terrace.
459 Soils developed within Qt6–Qt5 terrace deposits show a progressive increase in the amount of
460 pedogenic carbonate with terrace age. Qt6 soils exhibit stage II carbonate morphology with
461 carbonate pendants on the bottoms of gravels and disseminated carbonate throughout the Btk
462 horizon (Eppes et al., 2008).
463
464 ***5.1.3. Enza longitudinal profiles and incision/uplift rates***
465
466 Vertical separation from the modern valley profile have been measured both for strath surfaces of
467 the wider younger and modern terraces (Qt6 and Qt8), and for the few remnants of older Qt1, Qt2
468 and Qt3a deposits that outcrop scattered and isolated at the tops of hills and low-relief surfaces, in
469 places located at the valley margins: their location with respect to the modern valley helps defining
470 the paleo-morphology of the Early to Middle Pleistocene valleys (Fig. 2 and 8).
471 We infer uplift and deformation rates by analyzing the older suite of continental deposits Qt1-Qt3b
472 that were deposited and deformed by the structures of the Quattro Castella mountain front and
473 syncline and Ghiardo anticline, recognizable in the Enza geology, validated by seismic, by well logs
474 and by modeling.
475 Rates of fluvial incision have been determined at km 5.5 and km 4.5 from the mountain front, the
476 most suitable place for the preservation of the suite, using equations (1) and (2), (profiles MM' and
477 PP' in Fig. 2). The results are summarized in tables 1, 2 and Fig. 8.
478 The incision rates for AEI through Qt1, along the western side vary little from 0.19 mm/yr to 0.16
479 mm/yr at km. 5.5. Rates for Qt3a decrease downstream (from 0.37 mm/yr at MM' to 0.33–0.2
480 mm/yr at PP') and vary also from east to west side valley, respectively from 0.33 mm/yr east at PP'
481 to 0.2 mm/yr west at PP'. This south to north and east to west uplift trend is even enhanced for the
482 younger Qt6: rates accelerate with respect to the previous time, from 1.23 mm/yr to 0.92 mm/yr

483 going downstream and from 0.92 mm/yr to 0.69 mm/yr at QQ' from east to west. The recent
484 increase of the differential uplift of the eastern side documents recent activity of the transverse
485 “Passo della Cisa – Enza” Line, as discussed in the previous chapter.
486 The incision rates calculated from Qt3 approximately double over the previous 570 ka with the
487 values of 0.33–0.37 mm/yr (Fig. 8; Table 1 and 2). Incision rates continue to accelerate to 1.23
488 mm/yr for Qt6 (Fig. 8). A similar twofold increase is observed between Reno valley Qt2 and Qt3
489 straths (Picotti and Pazzaglia, 2008).
490 Correlating the stratigraphic thickness of the deposits obtained by different sources such as the
491 seismic reflectors, the exposures into the river and the “SP3” borehole stratigraphy (Carnicelli et al.,
492 2003) located atop of the Ghiardo plateau (see Figs. 2 and 7), we infer an approximate, local uplift
493 rate for the Ghiardo anticline The thickness difference of AEI between syncline and top of the
494 anticline document an uplift rate of 0.28 mm/yr for the period 780 to 620 ky. The uplift over the
495 sea-level of the top of AEI, deposited as coastal plain facies close to the sea, strand documents a
496 decrease of the uplift rate in the last 620 ky to 0.18 mm/yr.
497

498 **5. 2 Castelvetro-Vignola area, Panaro and Guerro rivers**

499 ***5.2.1 Terraces and mountain front deposits***

500 In the Castelvetro – Vignola area a flight of nine terraces is present (see maps of Fig. 3) with the
501 underlying deposits consisting primarily of variably unconsolidated channel gravel with lesser
502 amounts of overbank sand and mud. The oldest terraces Qt0 and Qt1 are preserved only on the west
503 side of the Panaro valley as scattered sand and gravel remnants on isolated hilltops (Qt0) at
504 elevations typically above 240 m. Stepping downslope, one or more stratified deposits mantle the
505 prominent mid-valley bench (Qt2 and Qt3). These deposits all show signs of intense pedogenesis,
506 erosion, or post-depositional burial by younger colluvial and alluvial fan deposits. There are no
507 numeric ages from these deposits, but geomorphic, stratigraphic, pedogenic (Eppes et al., 2008),
508 and archaeological (Amorosi et al., 1996) data are used to constrain relative ages, using the same
509 correlation criteria as in the Enza region (see Fig 6). The Qt1 and Qt3 soils described for the Enza

510 river bed section are very distinct and permit correlation criteria and relative age assignments to
511 terrace deposits elsewhere in the northern Apennines.
512 Both Qt0 and Qt1 deposits outcrop at the northern flank of the Faellano creek valley, near Marano
513 (see Fig. 3). Qt0, the highest and oldest terrace remnants is correlated as the alluvial equivalent of
514 the AEI deposits, is here at least 18 m thick. The Qt0 deposits unconformably overlies Argille
515 Azzurre Fm mudstone and is composed of 11 m of weathered, unsorted, sandy matrix supported
516 gravels overlain by a 7m thick layer of silty-sandy yellow and brown deposit. The Qt1 deposit is
517 similar in the sense that it is 16 m thick, including 9 meters of weathered, unsorted, semi-
518 consolidated, gravels, overlain by a 3m thick sandy-silty interval. A 4–5 m thick red-brown soil
519 (Munsell 2.5 Y 6/6, Dry) containing abundant Fe-Mn pellets is developed in the Qt1 deposit.
520 Qt3 is mapped in the west side of the Panaro valley and in both the flanks of the Guerro valley
521 downstream of Castelvetro and contains at least two mappable treads that share the same or nearly
522 the same strath, Qt3a and Qt3b. Along the Panaro, Qt3a consists in a narrow surface that, gently
523 dipping toward to the Po plain, extends for up to 3km from the Campiglio wind gap to the west side
524 of Vignola (Fig. 3). At its highest elevation, near Campiglio, the Qt3a unit is 4 m thick and thickens
525 toward north, in Vignola, where the basal strath, unconformably cut over the Messinian bedrock
526 (Colombacci Fm) is covered by 8 m thick interval of gravels topped by a 2 m thick rubified soil.
527 The poorly sorted gravels are strongly weathered, matrix supported, and locally show Mn oxides
528 replacement of clasts (diameters from 2 to 20 cm). Soil colors vary from 7.5 YR 3/4 dry and 10YR
529 5/8 moist. The northward thickening indicates that Qt3a unit was deposited basinward of the
530 intersection point, in an alluvial fan setting (see Fig. 5). In the Guerro valley, the basal strath of
531 Qt3a has never been observed: in the plowed fields, a clay rich reddened soil (Munsell color is
532 10YR 5/8) shows sorted and weathered pebbles and a conspicuous presence of Fe-Mn pellets. In the
533 Panaro area, starting from Due Ponti, Qt3b deposits form a broad surface inset into the older Qt3a
534 deposits (see Fig. 3). This deposit was likely a broad alluvial fan lobe of the paleo Panaro River that
535 formerly flowed through the Campiglio wind gap. Toward the west, Qt3 deposits occur near the
536 mountain front at the Tiepido valley and toward Levizzano Rangone, where they form a wide and

537 highly elevated dipping surface. We assigned these deposits to the Qt3 in contrast to Gasperi et al.,
538 (1999), following the observations of the typical soil features described by Eppes et al., (2008),
539 such as distinct tan-orange color (5YR 5/6 – 7.5 YR) in Bt horizon, accumulation of Fe-Mn oxides
540 and development of Stage III carbonates accumulation in the calcic Bk horizon.
541 Four Holocene-Late Pleistocene terraces (Qt6, Qt7, Qt8, and Qt9) are preserved in the modern
542 valleys of the Panaro, Guerro and Tiepido channels. Qt6 is the widest and best-preserved pre-
543 Holocene terrace in the Panaro and Tiepido valleys: it is 4-5 meters thick, consisting entirely of well
544 sorted gravels, and capped by a 1.5 m thick rubified soil, (Munsell color 7.5 YR 3/4 moist) with
545 well-developed and distinct A, Bt, Bk, and C horizons. These characteristics correlate well with Qt6
546 terraces described elsewhere along the mountain front (Eppes et al., 2008) and locally
547 corresponding with the AES7b unit described by Gasperi et al. (1999), (see Fig. 6). Wegmann and
548 Pazzaglia (2009) suggest a latest Pleistocene to Holocene age of 13 ± 2 ka, correlative with the end
549 of OIS 2 (LGM). This interpretation agrees with Gasperi et al. (1999) that indicates a latest
550 Pleistocene age. Both Qt8 and Qt9 consist of thin (1-2 m), stratified, sandy gravel, capped locally
551 by a 0.5 m thick sandy-silty overbank deposit. Soils are weakly developed in these two terrace
552 deposits and locally exhibit a Stage I- calcic horizon. The landscape position and weakly-developed
553 soils are consistent with Holocene ages for these terraces.
554
555 ***5.2. 2. Terraces longitudinal profiles and incision/uplift rates***
556
557 We plot the strath longitudinal profiles only along the Panaro valley (km 4 – 10 upstream from the
558 mountain front), where terrace preservation allows for robust profile reconstructions (Figs. 3 and
559 10). Across the mountain front, in a short distance of no more than ~ 10 kilometers, all terrace
560 profiles converge to the intersection point, then diverge beneath the Po Plain as staked alluvial fan
561 deposits (Di Dio, 1998; Gasperi et al., 1999) (Figs 3 and 10). Rates of fluvial incision have been
562 determined along km 4 – 10 reach of Panaro valley, using equations (1) and (2). The incision rates
563 accelerate from 0.23 mm/yr for Qt0-Qt1 to 20 mm/yr of Qt8 (anthropogenic) through 0.34 -1.23

564 mm/yr of Qt3a and Qt6 respectively (Fig. 10 ; Table 3).

565

566 Figure 9 shows a suite of three geological sections traced across the Castelvetro-Vignola foothills
567 (see Fig. 3). Section AA' intercepts the topographic high covered by Qt3a alluvium, eastward of the
568 Campiglio wind gap, where the Villa Camilla (VC) fault-related fold culminates and turns from a
569 north into a northwest vergence (Figs 3; 9a; 9b). The intersection of sections AA' and BB' (Fig. 9a
570 and b) shows that the VC anticline uplifts and deforms Middle Pleistocene deposits (Qt3a) leaving a
571 thin SW-NE elongated high topographic surface, that gently dips toward the Po plain (Figs 3 and
572 9a). The Qt3a strath underlaying this surface is here carved into the mudstone of the Argille
573 Azzurre Fm and into the sandstone of the Colombacci Fm, while few meters northwest and ~ 12 m
574 downhill, the Qt3b alluvium lies on top of again Qt3a and AEI deposits. The inset of figure 9a
575 evidences the Campiglio wind gap is uplifted 45 meters above the terrace immediately lower
576 toward the Panaro valley, which has been recognized as Qt6 in our chronostratigraphy (AES7b in
577 Gasperi et al., 1999).
578 Cross section CC' (fig. 9c) shows the pronounced Castelvetro anticline, nicely underlined by the
579 topography and likely not associated to a fault at the surface. The Villa Camilla anticline is here
580 close to its periclinal tip, therefore is poorly pronounced.
581 Moving northwest along BB' section, the topography evidences an anticline with axis around the
582 Guerro valley, associated to a fault at surface, verging to the northwest. At the culmination, the
583 marine Sabbie Gialle (SGf) deposits and the AEI (Lower Emiliano-romagnolo Synthem) are
584 present. Along the flanks of the Guerro valley, the base of these deposits are uplifted several meters,
585 ~ 120 for SGf and ~ 80 for AEI, respect to the correspondent sedimentary bodies laterally buried
586 beneath the surface of Po plain, either toward the Panaro and the Tiepido valleys.
587 To measure the uplift rate we used different base levels: sea-level for the Sabbie Gialle and 2 meters
588 a.s.l. for the coastal plain AEI, whereas we used the present-day Guerro valley floor as a base level
589 for the reconstruction of vertical separation of the uplifted strath Qt3b terraces. Being Qt3b the
590 youngest deposit downstream the small Campiglio valley (see Fig. 3), the deactivation of this

591 branch of the paleo Panaro alluvial fan has to been occurred after Qt3a deposition time and with a
592 mean uplift rate of 0.35±0.08 mm/yr necessary to create in ~ 127 ky (MIS 6 -MIS 2) the existing 45
593 m of topographic vertical separation between Qt3b and Qt6 strath surfaces (see inset in Fig. 9a).
594 Notably, in the Panaro valley, the Qt3a strath separation (79 m) and Qt6 strath separation (16 m) are
595 surveyed near the hinge of villa Camilla anticline passing through Campiglio. Measured uplift rate
596 for this culmination is 0.29 ± 0.05 mm/yr averaged in the last 230 ka. Both comparable rates of
597 uplift and the wind gap can be explained as a result of the Villa Camilla anticline growth.
598 Around the Castelvetro area, fold trends with both SW-NE and NW-SE trends are visible in
599 geological section BB' and CC' (Fig. 9) and in map view (Fig. 3), documenting a dome-and-swell
600 interference pattern. The maximum culmination for both topography and the anticline is associated
601 to the northeast trending anticline, with maximum uplift rates of 0.35 mm/yr. the associated
602 northwest verging fault is unconstrained as dip, but it creates an important stratigraphic separation
603 of around 0.15 mm/yr. The pairs of anticlines are uplifted by a longer wavelength fold, as
604 documented also by the strong incision of the synclinal axis (see Figs 3 and 9).
605

606 **6 Kinematics of a growing structure: trishear modeling of the Ghiardo anticline**

607 ***6.1 Trishear modeling***

608 Deformation of the unconformity at the base of AEI has been modeled assuming a Trishear
609 geometry (Erslev, 1991; Hardy and Ford, 1997), using the publicly available software FaultFold,
610 version 4.5.4 (Allmendinger, 1998; Zehnder & Allmendinger, 2000). A trishear geometry assumes
611 the propagation of a triangular symmetric area of deformation at the tip of a fault plane and predicts
612 deformation of growth strata in the hangingwall anticline and footwall syncline. The model allows
613 for easy manipulation of ramp angle, tip location (depth), P/S ratio, displacement, and trishear
614 angle. We are able to run it in an inverse mode, retrodeforming the fold, that searches for the best
615 combination of these parameters (Table 4). Forward modeling is then applied to determine the total
616 slip on the blind thrust (Fig. 11).
617

6.2 A cross section across mountain front and Ghiardo anticline

We interpret the subsurface geology in a cross section running across the mountain front and the Ghiardo anticline. The section is anchored using wells and seismic lines (Fig. 7). A high-resolution reflection line (courtesy of Edison S.p.a.) strikes SW-NE parallel to the Enza river across the mountain front and part of the Ghiardo plateau (see SS' blue trace in Fig. 2). Seismic interpretation shown in fig. 7 integrates field survey data coming from the outcropping succession of the river and the log data available from the San Polo d'Enza 1, Traversetolo 3 and Vignale 1 wells.

At the mountain front, it is clear the divergence of Pleistocene reflectors that onlaps the Ligurian nappe and Epiligurian units. This documents the tilting of the limb of the growing mountain front. The underlying high-amplitude reflectors (basically Pliocene) at the center of the synclinal are deformed by a backthrust, going toward the Ghiardo anticline. This reflector package is parallel along the faulted flank of the anticline, documenting it deposited prior to the fold growth (Fig.7). Therefore, at the top of the Ghiardo anticline, only Pleistocene deposits are thinning and onlapping the structural high.

The cross section of Fig. 11 shows that the coeval growth of the mountain front and the Ghiardo anticline during Pleistocene can be associated to a unique structure, detached at the base of the foredeep deposits, at around 4 km below the Ghiardo anticline, following the indications of the model. The flat under the Ghiardo anticline has been drawn at 6°, again following the indications of the model that agrees with the general dip of the foredeep deposits. The mountain front flexure is interpreted as a hangingwall ramp anticline, folding the whole stack of the foredeep deposits and the Ligurian and Epiligurian units. The whole structure depicted is folded by the longer wavelength fold related to the deeper structure, with final effect of enhancing the forelimb of the ramp anticline to form the actual mountain front. At a map view, the mountain front and the Ghiardo anticlines have different orientations (Figs 2 and 8a). The culmination of the ramp anticline, maximum at Quattro Castella, abruptly decreases to the west of S. Polo d'Enza, when crossing the Cisa – Enza Line, that is therefore considered as a lateral ramp accounting for a notable part of the shortening. It should be recalled that the active differential uplift across the latter Line (Fig. 8A and b) documents

a component of active shortening to the west.

7 - Discussion and conclusions

7.1 The Northern Apennines mountain front: surficial versus deep structures

Two wavelengths characterize the topography and structures at the mountain front of the Northern Apennines. The first is the main flexure of the Northern Apennines that builds the whole mountain front and has already discussed in the area of Bologna as a long wavelength fold (>150 km along strike) formed by a deep structure (Picotti and Pazzaglia, 2008) (see Fig. 12). It is remarkable that east of Bologna, this flexure is very straight and not affected by the recesses that indeed are visible at the mountain front west of Bologna (see Fig. 1). These perturbations are due to the presence of shorter wavelength structures, such as the Castelvetro hills and the Ghiardo plateau that culminates for 15 to 25 km along strike. Similar wavelength characterizes other structures observed in the west, at Salsomaggiore (see Picotti et al., 2007 and Wilson et al., 2009), a structure growing at the mountain front, or at S. Colombano al Lambro (e.g. Pellegrini et al., 2003), an isolated hill in the Po plain.

The long wavelength structure of the mountain front is due to a lower to mid-crustal thrust tipped at around 15 to 20 km that overprints the previous thin skinned fold and thrust belt, separating a subsiding Po Plain from the uplifting chain (see Picotti and Pazzaglia, 2008) and deactivating it east of Bologna. The shorter wavelength structures west of Bologna are associated to new structures or, more often, to the reactivation of previous thrusts. The location of the surficial structures with respect to the deep flexure is important to explain their geology. For instance, the Castelvetro hill are located south of the main flexure hinge, whereas the Ghiardo hill north of it, the latter being formed by younger deposits, since it is found at the margins of the subsiding Po plain (see Fig. 12). The same is true for Salsomaggiore, south of the flexure hinge and cored by Miocene deposits, whereas the S.Colombano al Lambro hill, very far from the mountain front is formed by uplifted Pleistocene units (Fig. 12 sect. AA'). This fact documents the superposition of the mountain front flexure over shorter wavelength structures.

672

673 ***7.2 Incision and uplift/subsidence rates: unsteady versus steady thrusting***

674 The history of the incision and uplift rates is rather complex and illustrates the evolution of the two
675 interacting deep and surficial thrusts (Fig. 5). The tilting rate of the mountain front was measured
676 both for the Enza section (Fig. 5) and the Quattro Castella cross section (Fig. 11, see inset in Fig. 5).
677 The rate is unsteady and much faster for the Quattro Castella section, documenting the different
678 behavior of the hangingwall ramp, already described as separated by the Cisa – Enza Line.
679 Interestingly, the trend of both section is equal between 900 and 600 ky, whereas after 600 ky it
680 increases east of the Cisa – Enza lateral ramp (Quattro Castella) and decreases west of it. We
681 interpret this time of parallelism to the onset of the long wavelength structure, namely the deep
682 thrust, interacting with the surficial fold and enhancing the tilt of its forelimb. The different
683 behavior after 600 ky is interpreted as a decrease of surficial thrusting west of the lateral ramp,
684 whereas east of it the thrusting is still more active, but mainly associated to a vergence to the
685 Northwest. In fact, the uplift rate of the Ghiardo anticline decreases from 0.28 to 0.18 mm/yr at
686 around 600 ky, suggesting decreasing of shortening activity with northeast vergence. After 230 ky
687 and until now, the differential uplift of the Cisa – Enza lateral ramp (0.13 mm/yr) is particularly
688 active and account for west-verging shortening. Finally, notwithstanding the decrease of tilting rate
689 west of the Cisa – Enza line at the Enza river section, the incision rates of the river (Fig. 8)
690 increases from 0.34 to 1.23 mm/yr from 230 to 12 ky. This trend is the same observed at the Reno
691 river near Bologna (Picotti and Pazzaglia, 2008) that is associated to the focusing of deformation
692 along the deep thrust.

693 At Castelvetro, we observe the same trends and similar values, with a decrease of the uplift rates in
694 the northeast-verging anticlines from 0.09 mm/yr between 600 and 150 ky to 0.05 mm/yr since 150
695 ky for the northeast Castelvetro anticline. At the Panaro river, again an increase of the incision rates
696 is recorded (Fig. 10). The west-verging thrusts are active especially after the late Middle
697 Pleistocene and apparently they did not change their rates.

698 Therefore, whereas the surficial structures is decreasing their activity, or they are keeping constant

699 only the west-verging ones, increasing incision rates are interpreted as indicative of increasing
700 deformation along the deep thrust.
701
702 ***7.3 Active structures and seismicity***
703 The mountain front is the expression of the main processes that act at the southwestern margin of
704 the Adria plate. Several indicators of stress and strain document important variations east and west
705 of the Bologna area. The paleostress reconstructions available in literature document for the area
706 west of Bologna a superposition of two almost perpendicular stress fields, trending northwest and
707 northeast. These trends are superposed not only in space, giving place to dome-and-swell structures,
708 such as Castelvetro, and complex reactivations of lateral ramps, such as the Enza and
709 Salsomaggiore, but also in time, as documented by the microstructural record (see chapt. 2). The
710 reconstructed maximum stress tensor switched from northeast to northwest several times in the past
711 (Serravallian to Pleistocene), creating a spatial and temporal pattern, lacking of a clear trend (see
712 also Fellin et al., 2005 for a similar discussion to the west of the Apennines). East of Bologna, the
713 paleostress reconstructions display a clearer trend of prevailing northeast tensor, and also the
714 deformations are more regular, both the Miocene and Pliocene thrusts and the Pleistocene mountain
715 front. The indications from the seismicity suggest that the active tectonics is inheriting this
716 geodynamic frame, and the area of Bologna is separating two seismotectonic regions (Fig. 12), as
717 suggested also by Boccaletti et al., (2004). Northwest of Bologna, the continuous switching of
718 stress tensors documents they are very close as modulus: under such a tectonic regime, σ_2 can easily
719 switch to σ_1, but also to σ_3, explaining the two alternating perpendicular tensors (σ_1 to σ_2 switch),
720 but also the strike slip earthquakes (σ_2 to σ_3 switch) that are recorded only in this region (see Fig.
721 4). Some focal mechanisms are related to northwest thrusting both west and east of Bologna, but,
722 overall, the main mechanisms are compatible with a northeast maximum axis of shortening.
723 We now interpret the depicted stress and strain history in the geodynamic frame of the Northern
724 Apennines (Fig. 12). The convergence at the Apennines is associated to the far field of the Africa-
725 Europe collision, providing the northwest oriented stress field that interact with the northeast-

726 oriented one. This direction of convergence is documented by the velocity field reconstructed from
727 GPS data by D'Agostino et al. (2008, see their Fig 4c). The same data document that the oblique
728 subduction of the Adria plate creates a velocity field oriented northeast (D'Agostino et al., 2008,
729 see their Fig 4a) that increases away from the rotation center of the orogen, fixed to the
730 northwestern tip of the Northern Apennines (see Fig. 12). The vicinity to the rotation center of the
731 orogen could explain the changing stress state of the belt and the two seimotectonic regions. In the
732 west, the main tensors shows similar modulus of both the northwest (Af-Eu convergence) and
733 northeast axes (the Adria subduction), whereas going eastward of Bologna the rotation of the
734 Apennine orogen contributes more and more to the deformation. The increasing strain at the
735 mountain front moving south-eastward is documented also by the activity of the deep thrust
736 forming the mountain front that is traced by the incision at the mouth of the rivers flowing to the Po
737 plain. Available data allow a good synthesis along around 250 km of the front. The common trend
738 all along the mountain front of the northern Apennines is the progressive increase of the incision
739 rates from the beginning of the Middle Pleistocene to the end of the Late Pleistocene, interpreted by
740 Picotti and Pazzaglia (2008) as the effect of focusing of the deformation along the new structure.
741 However, in the western sectors, around Salsomaggiore (Wilson et al., 2009) the rates increase
742 slightly from 0.1-0.2 to 0.2-0.3 mm/yr, whereas at Enza and Castelvetro they increase from 0.2 to
743 1.2 mm/yr. At Bologna, Picotti and Pazzaglia (2008) documented an increase from 0.05 to 2.1
744 mm/yr, whereas more to the east, in the Romagna Apennines, Wegmann and Pazzaglia (2009)
745 measured an incision rate increasing from 0.2 to 2.2 mm/yr. Therefore, we interpret this increase of
746 incision rate as increasing activity of the deep thrust moving away from the rotation point (Fig. 12).
747 Also at depth, the two regions show different features, with compressional deformation in the upper
748 crust evident only in the western sector (Fig. 12). The general feature of active deformation in the
749 Northern Apennines belt is given by the presence of a deep thrust propagating from the lower crust
750 and tipped at around 15 to 20 km. This structure is responsible of the mountain front location and of
751 the main compressional seismicity, whose hypocenters occur between 30 and 18 km at depth
752 (sections of Fig. 4). The shallowest compressional (and strike-slip) earthquakes are recorded in the

western area (see section AA', Fig. 4). The other general feature is the presence of extensional deformation, documented within the belt as diffused presence of extensional fault up to the foothills (see Picotti et al., 2009). Extensional earthquakes are distributed at depth only in the upper crust between 8 and 20 km, and they characterize both the western and eastern sectors. One can conclude that the seismicity confirm the deep thrusting as the most active and seismogenic structure of the Northern Apennines mountain front. Depth distribution of available focal mechanisms document as well two strain regimes spatially overlapping, extensional at surface and compressional at depth (see f.i. section BB', Fig. 4). The absence of surficial compressional earthquakes in the western sector suggest that the compressional activity recorded at surface behave aseismically and/or is presently moving too low, therefore the recurrence time is longer than our observation window. Aseismic creep in the upper crust could be highly possible in the western sector under study, given the presence of the Ligurian lid that act as an impervious boundary, allowing fluid accumulations at their interface (Picotti et al., 2007; Capozzi and Picotti, 2002). The role of fluid overpressure in the upper crust to control the local rheology has been recently highlighted for some recent earthquake at the mountain front (Calderoni et al., 2009).

Acknowledgments

The authors are grateful with Edison spa for kindly providing the permission of using the seismic profile. ^{14}C analysis have been provided by CEDAD, CEnter for Dating and Diagnostics

AMS Radiocarbon Dating, Facility Department of Innovation Engineering,

University of Salento, Lecce. Funds RFO, University of Bologna are kindly acknowledged.

Table captions

Table1. *Strath elevations and rates of river incision are from terraces in the vicinity of S.Polo d'Enza, ~ 5.5 km up valley from the mountain front (see profile MM' in Figs 2)*

[a]*Local correlation with the Regione Emilia-Romagna nomenclature: see also Panaro valley*

781 *deposits subdivision in Fig.6*

782 [b] *Di Dio (1998)*

783 [c] *MIS = Marine Isotope Stage*

784 [d] *Subsintema di Agazzano*

785 [g] *Anthropogenic incision since the early 1950's, see Wilson et al., (2009)*

786

787 ***Table 2.*** *Strath elevations and rates of river incision are from terraces at S.Polo d'Enza bridge, ~*
788 *4.5 km up valley from the mountain front (see profile PP' in Figs 2 and 8). Elevation of the valley*
789 *profile in to the river is correct for anthropogenic recent incision from the DEM measured 148*
790 *m.a.s.l. to 151 m.a.s.l.*

791 [a]*Local correlation with the Regione Emilia-Romagna nomenclature.*

792 [b] *Di Dio (1998)*

793 [c] *MIS = Marine Isotope Stage*

794 [d] *West side river Qt3a terrace*

795 [g] *Anthropogenic incision since the early 1950's, see Wilson et al., (2009)*

796

797 ***Table 3.*** *Strath elevations and rates of river incision are from terraces in the vicinity Vignola in a*
798 *reach comprise between 4 8 km up valley from the mountain front (see kilometric profile in Figs 3*
799 *and 10)*

800 [a]*LoLocal correlation with the Regione Emilia-Romagna nomenclature: see also deposits*
801 *subdivision in Fig.6*

802 [b] *Di Dio (1998) and Gasperi et al., (1999)*

803 [d] *Subsintema di Torre Stagni*

804 [c] *Subsintema di Liano*

805 [g] *Anthropogenic incision since the early 1950's, see Wilson et al., (2009)*

806

807 ***Table 4.*** *Range of variation for the modeled parameters in the backward processing and best fit*
808 *values used in the trishear forward modeling of the geometry of bottom AEI.*
809
810 **Figure captions**
811
812 ***Figure 1****. Location of the studied area (blue boxes) at the foothills of the Northern Apennines, at*
813 *the boundary between the extensional and the compressional realms.*
814
815 ***Figure 2****.* ***a)*** *Geologic map modified from R.E.R. Pizziolo et al., (submitted). Quaternary fluvial*
816 *terraces chronostratigraphy in accordance with the inter-basin correlation of Picotti and*
817 *Pazzaglia, (2008) and Wegmann and Pazzaglia (2009). Geologic structure traces are adjusted on*
818 *the base of well's stratigraphy and seismic lines. Black star near San Polo d'Enza is location of*
819 *sampling for ^{14}C age. Dark red dashed traces are for topographic profiles and river incision rates*
820 *location shown in figure 8a and 8b. Kilometric profile of river valley bottom is measured with 0 at*
821 *the mountain front (MF).* ***b)*** *Geologic section AA' across the Ghiardo Plateau, modified from*
822 *Carnicelli et al., (2003), and vertical exaggerated.*
823
824 ***Figure 3****. Geologic map, modified from Gasperi, 1999, Dark red traces define profiles of the*
825 *geologic sections of Fig 9. Kilometric profiles of river valley bottom are measured with 0 at the*
826 *mountain front (MF). Quaternary fluvial terraces chronostratigraphy follows the inter-basins*
827 *correlation from Picotti and Pazzaglia 2008 and Wegmann and Pazzaglia 2009.*
828
829 ***Figure 4.*** *Upper map: the CSI1.1 Catalog (20 years of instrumental seismicity, Chiarabba et al.,*
830 *2005; Castello et al., 2006) is plotted with symbols dimension proportional to magnitude (from*
831 *lowest value of 2.0) and with colors for different hypocentral depth: yellow for h lower than 20 km*
832 *and red for h greater than 20 km. Red squares represent historical seismicity with M>6.0, showing*
833 *mostly activity in the basins within the chain (Gruppo di Lavoro CPTI, 2004). Moment tensors*

available for more than the last 30 years, for events with magnitude Mw between 4.1 to 5.4, including CMTs (Ekstrom et al., 2005; HYPERLINK "http://www.globalcmt.org" www.globalcmt.org), RCMTs (HYPERLINK "http://www.bo.ingv.it/RCMT" www.bo.ingv.it/RCMT; Pondrelli et al., 2002, 2004, 2006, 2007) and QRCMT (Reggio-Parma 2008, December 23, earthquakes; http://mednet.rm.ingv.it/quick_rcmt.php). Red focal mechanisms are for thrust events, green focal mechanisms are for strike-slip events and blue focal mechanisms are for extensional events (following the Zoback .... criteria). On the map are also reported boxes and traces of the lower sections. Lower sections: in the four sections are reported the data with the same symbols used in the map, but the CSI1.1 seismicity is represented with small dots if magnitude is lower than 3.0 while thicker dots are for events with magnitude greater than 3.0. Swath topographic profiles for a 50 km wide box from SRTM 90 m DEM, shaded gray area is for maximum and minimum topography.

***Figure 5**. **a)** Sketch illustrating the concept of intersection point and fold limb lengthening at the mountain front of the Northern Apennines. **b)** Graph of tilting rates of the mountain front calculated on the base of the growth strata measured both in the Enza river and in the Rio Monticelli.*

***Figure 6.** Apennines Chronostratigraphic correlation diagram for fluvial and near-shore marine deposits of the Northern Apennines mapped onto the oxygen isotope curve of Lisiecki and Raymo (2005) and placed into a common nomenclature for the Ghiardo and Castelvetro-Vignola areas basins. Parenthetical designations for the Enza and Panaro Rivers column are for terrace-equivalent alluvial deposits beneath the Po Plain; AEI = Emiliano-Romagnolo Inferiore Synthem; AES = Emiliano- Romagnolo Superiore Synthem (Di Dio, 1998); IMO = Imola Sand Fm (Sabbie Gialle) (Martelli et al., 2008). Aquifer Complex Number (Complesso Acquifero) corresponding to Po subsurface deposits of the Emilia–Romagna Region (Di Dio, 1998). See also Wegmann and Pazzaglia (2009) for 'Sabbie Gialle'' ages.*

Figure 7. *A seismic profile along the Enza river (see blue trace SS' in Fig 3) crossing the Ghiardo anticline: dip data have been surveyed on field along the exposed succession of Pleistocene deposits outcropping along the river, while thickness of subsurface deposits has been calibrated on the base of the near S. Polo d'Enza 1 and Traversetolo 3 wells. On top, a representative sketch of the Enza river succession.*

Figure 8. a) *Northwest view of the topographic profiles GG' and HH' (Fig.2) comparing the east and west Enza river mountain front topography: in orange the deformed surfaces of Qt3a and Qt3b terraces dipping toward the Po Pain in the east river bank.* ***b)*** *PP' topographic profile. Strath elevations have been used to infer incision rates in the inset graph. Difference in elevation of the Qt3a deposit show a differential uplift between the two sides of the valley.*

Figure 9. *Geological sections across the Castelvetro – Vignola foothills. See dark red AA', BB' and CC' traces in Fig. 3 for location. Correlated borehole of section CC' is SP8 in Gasperi et al., (1999).*

Figure 10. *Correlation of the Panaro river strath surfaces across the mountain front and into the Po subsurface. The solid black line is the modern Panaro longitudinal profile. Solid circles along the profiles indicate locations of measured bedrock strath elevations projected to the modern longitudinal profile. Numbers on inset graphs are fluvial incision rates in mm/yr. Subsurface data are from oil and water well logs (labeled) compiled by Di Dio (1998) and Gasperi et al. (1999). MIS1/4 Oxygen Isotope Stage, used for climatic tuning of subsurface deposits to the Tyrrhenian and pre-Tyrrhenian sea level highstands.*

Figure 11. *A cross section across the mountain front and the Ghiardo anticline, showing the possible kinematic association of the two structures and the deep-seated thrust that provides an additional and larger wavelength folding. a) Best fit geometry from the trishear modeling provides*

insights into the depth and dip of the décollement (see Tab. 4).

Figure 12. *The composition of the regional stress field in the Northern Apennines in the Pleistocene and Holocene. The Af-Eu contribution is considered constant, whereas the northeast oriented tensor should increase, moving away from the rotation point. The section AA' is running in the Emilia sector and shows the activity of the thin skinned thrusts, reactivating the Neogene structures, as well as the deep-seated structure that flexures the mountain front. East of Bologna (BB'), the deep structure account for increased shortening, as documented by the incision rates of the rivers cutting the mountain front, whereas the thin-skinned thrust belt is inactive.*

References

Allmendinger, R. W., (1998). Inverse and forward numerical modeling of trishear fault-propagation folds. Tectonics, v. 17, no. 4, p. 640-656.

Amato, A. (1998). The 1997 Umbria–Marche, Italy, earthquake sequence: a first look at the main shocks and aftershocks, Geophys. Res. Lett., 25 (15), 2861–2864.

Amorosi, A., Farina, M., Severi, P., Preti, D., Caporale, L., Di Dio, G., (1996). Genetically related alluvial deposits across active fault zones: an example of alluvial fanterrace correlation from the upper Quaternary of the southern Po Basin, Italy. Sedimentary Geology 102 (3–4), 275–295.

Amorosi, A., L. Caporale, U. Cibin, M. L. Colalongo, G. Pasini, F. Ricci Lucchi, P. Severi, and S. C. Vaiani (1998). The Pleistocene littoral deposits (Imola Sands) of the northern Apennines piedmont, G. Geol., 60, 83 – 118.

Amorosi, A. (2001). Cyclic patterns of facies and pollen associations from Late Quaternary deposits in the subsurface of Bologna. GeoActa, 1, 1–11.

915

916 Amorosi, A., M. C. Centineo, E. Dinelli, F. Lucchini, and F. Tateo (2002). Geochemical and
917 mineralogical variations as indicators of provenance changes in Late Quaternary deposits of SE Po
918 Plain, Sed. Geol., 151, 273–292.

919

920 Amorosi, A., M. Colalongo, et al. (2004). Palaeogeographic and palaeoclimatic evolution of the Po
921 Plain from 150-ky core records. Global and Planetary Change, 40, 55–78.

922

923 Bernini M., and Papani G., (1987). Alcune considerazioni sulla struttura del margine appenninico
924 emiliano fra il T. Stirone ed il T. Enza (e sue relazioni con il Sistema del Taro), Atti Meeting
925 "Brittle deformation analysis in neotectonics", Firenze, 17 aprile 1986, L'Ateneo Parmense.

926

927 Boccaletti, M., Bonini, M., Corti, G., Gasperini, P., Martelli, L., Piccardi, L.,Tanini, C., Vannucci,
928 G., (2004). Seismotectonic Map of the Emilia-Romagna Region, 1:250000. Regione Emilia-
929 Romagna CNR. SELCA, Firenze.

930

931 Bridgland, D.R., (2000). River terrace systems in north-west Europe: an archive of environmental
932 change, uplift and early human occupation, Quaternary Science Reviews 19 (13), 1293–1303.

933

934 Bridgland, D.R., Westaway, R., (2008). Preservation patterns of Late Cenozoic fluvial deposits and
935 their implications: results from IGCP 449. Quaternary International 189, 5–38.

936

937 Bull, W.L., Knuepfer, P.L.K., (1987). Adjustments by the Charwell River, New Zealand, to uplift
938 and climatic changes. Geomorphology 1 (1), 15–32.

939

940 Bull, W.B., (1991). Geomorphic Response to Climatic Change. Oxford University Press,New York,
941 326 pp.

942

943 Burbank, D.W., Leland, J., Fielding, E., Anderson, R.S., Brozovic, N., Reid, M.R., Duncan, C.,
944 (1996). Bedrock incision, rock uplift and threshold hillslopes in the northwestern Himalayas.
945 Nature 379, 505–510.

946

947 Calderoni, C., Di Giovambattista R., Burrato P., and Ventura, G., (2009). A seismic sequence from
948 Northern Apennines (Italy) provides new insight on the roleof fluids in the active tectonics of
949 accretionary wedges. Earth and Planetary Science Letters, 281, 99-109.

950

951 Carnicelli, S., Caporale, L., Marchi, N., Iasio, C., Ferrari, G. A., Guermandi, M., Tarocco, P., 2003.
952 Paleosoils of the margin, a case of study in the reggio-emilia province; notes for field excursion.
953 Pre-congress field trip, 4th Cartography European Congress, Bologna, Italy.
954 http://www.regione.emilia-romagna.it/wcm/geologia/canali/convegni e seminari/congresso
955 europeo/congresso_04/Pre_Congress_Field_Trip.pdf

956

957 Capozzi R. and Picotti V., (2002). Fluid migration and origin of a mud volcano in the Northern
958 Apennines (Italy): the role of deeply rooted normal faults. Terra Nova 14 (5), 363-370.

959

960 Castello B., Selvaggi G., Chiarabba C. and Amato A., (2006). CSI Catalogo della sismicità italiana
961 1981-2002, versione 1.1. INGV-CNT, Roma. http://www.ingv.it/CSI/

962

963 Chiarabba, C., Jovane, L., Di Stefano, R., (2005). A new view of Italian seismicity using 20 years
964 of instrumental recordings. Tectonophysics 395 (3–4), 251–268.

965

966 Cremaschi, M., and G. Papani (1975). Contributo preliminare alla neotettonica del margine padano
967 dell'appennino: le forme terrazzate comprese tra cavriago a quattro castella (Reggio E.), Acta
968 Naturalia, Ateneo Parmense, 11, 335–371.

D'Agostino, N., Avallone, A., Chelone D., D'Anastasio E., Mantenuto S. and Selvaggi , G., (2008). Active tectonics of the Adriatic region from GPS and earthquake slip vectors. J. Geophys. Res., 113, B12413, doi:10.1029/2008JB005860.

De Luca G., Cattaneo M., Monachesi G. and Amato A., (2009). Seismicity of Central and Northern Apennines integrating the Italian national and regional networks, Tectonophys., in press.

De Martini, P.M., Pino, N.A., Valensise, G., Mazza, S., (2003). Geodetic and seismologic evidence for slip variability along a blind normal fault in the Umbria-Marche 1997–1998 earthquakes (central Italy). Geophysical Journal International 155, 819–829.

Di Dio, G., S. Lasagna, D. Preti, and M. Sagne (1997). Stratigrafia dei depositi quaternary della Provincia di Parma, Boll. Soc. Paleontol. Ital., 36, 179 – 187.

Di Dio, G. (Ed.), (1998). Riserve idriche sotterranee della Regione Emilia–Romagna. RER and Eni-AGIP, S.E.L.C.A., Firenze, p. 120.

Dziewonski, A. M., Chou, T.-A., and Woodhouse, J. H., (1981). Determination of earthquake source parameters from waveform data for studies of global and regional seismicity, J. Geophys. Res., 86, 2825-2852.

Dziewonski, A. M., Ekström, G., and Maternovskaya, N. N., (2001). Centroid-moment tensor solutions for April-June 2000, Phys. Earth Planet. Inter., 123, 1-14.

Eppes, M. C., R. Bierma, et al. (2008). A soil chronosequence study of the Reno valley, Italy: Insights into the relative role of climate versus anthropogenic forcing on hillslope processes during

the mid-Holocene, Geoderma 147 (3-4), 97-107.

Ercolani E., A. Rossi, M. Vecchi, I. Leschiutta, F. Bernardini, S. Del Mese, R. Camassi, S. Pondrelli, A. Tertulliani, (2009). Rilievo macrosismico del terremoto emiliano del 23 dicembre 2008, Quaderni di geofisica, Centro Editoriale INGV, http://portale.ingv.it/produzione-scientifica/quaderni-di-geofisica.

Erslev, E. A. (1991). Trishear fault-propagation folding, Geology, 19, 617–620.

Fellin, M. G., V. Picotti, and M. Zattin (2005). Neogene to Quaternary rifting and inversion in Corsica; retreat and collision in the Western Mediterranean, Tectonics, 24, TC1011, doi:10.1029/2003TC001613.

Frepoli A. and Amato A. (1997). Contemporaneous extension and compression in the Northern Apennines from earthquake fault-plane solutions. Geophys. J. Int., vol. 129 (2), 368-388, ISSN: 0956-540X

Gasperi, G., Bettelli, G., Panini, F., Pizziolo, M., (1999). Note illustrative alla carta geologica d' italia a scala 1:50000 foglio n 219 Sassuolo. Servizio Geologico d'Italia.

Ghiselli, F. and Martelli L. (1997). Evoluzione dei campi di *stress* lungo il margine appenninico-padano dal Pleistocene medio all'Attuale: analisi strutturale dei depositi pleistocenici affioranti tra Castell'Arquato (Piacenza) e Rimini. Il Quaternario (Italian Journal of Quaternary Sciences), 10, 439 – 444.

Hardy, S., and M. Ford (1997). Numerical modelling of trishear fault-propagation folding and associated growth strata, Tectonics, 16, 841– 854.

1023

1024 Hartshorn, K., Hovius, N., Dade, W.B., Slingerland, R.L., 2002. Climate-driven bedrock incision in
1025 an active mountain belt. Science 397, 2036–2038.

1026

1027 Lambeck, K., Antonioli, F., Purcell, A., Silenzi, S., (2004). Sea level change along the Italian coast
1028 for the past 10000 yr. Quaternary Science Reviews 23 (14–15), 1567–1598.

1029

1030 Lave´, J., Avouac, J.P., (2001). Fluvial incision and tectonic uplift across the Himalayas of central
1031 Nepal. Journal of Geophysical Research 106 (B11), 26,561–26,591.

1032

1033 Lisiecki, L.E., Raymo, M.E., (2005). A Pliocene–Pleistocene stack of 57 globally distributed
1034 benthic d18O records. Paleoceanography 20, PA1003, doi:10.1029/2004PA001071.

1035

1036 Morelli G.L. and Costa, E. (1997). Ricostruzione dei campi di sforzi plio-quaternari nel
1037 Pedeappennino Piacentino. Il Quaternario (Italian Journal of Quaternary Sciences), 10, 563 – 570.

1038

1039 Pazzaglia, F. J., and M. T. Brandon (2001). A fluvial record of rock uplift and shortening across the
1040 Cascadia forearc high, American Journal of Science, 301, 385 – 431.

1041

1042 Pazzaglia, F.J., Gardner, T.W., (1993). Fluvial terraces of the lower Susquehanna River.
1043 Geomorphology 8, 83–113.

1044

1045 Pellegrini, L., Boni, P., and Carton, A. (2003). Hydrographic evolution in relation to neotectonics
1046 aidedby data processing and assessment: some examples from the Northern Apennines (Italy).
1047 Quat. Intern., 101-102, 211-217.

1048

1049 Piana Agostinetti, N., F. P. Lucente, G. Selvaggi, and M. Di Bona (2002). Crustal structure and

1050 Moho geometry beneath the Northern Apennines (Italy), Geophys. Res. Lett., 29(20), 1999,
1051 doi:10.1029/2002GL015109.
1052
1053 Piccinini, D., Chiarabba, C., Augliera, P., (2006). Compression along the northern Apennines.
1054 Evidence from the Mw 5.3 Monghidoro earthquake. Terra Nova 18 (2), 89–94.
1055
1056 Picotti, V., R. Capozzi, G. Bertozzi, F. Mosca, A. Sitta, and M. Tornaghi, (2007). The Miocene
1057 petroleum system of the Northern Apennines in the central Po Plain (Italy), in Thrust Belts and
1058 Foreland Basins, From Fold Kinematics to Hydrocarbon System, edited by O. Lacombe et al., pp.
1059 117 – 131, Springer Verlag, Berlin.
1060
1061 Picotti, V., Pazzaglia, F. J., (2008). A new active tectonic model for the construction of the
1062 Northern Apennines mountain front near Bologna (Italy), Journal of Geophysical Research. V. 113
1063 (B8), p. 1-24.
1064
1065 Picotti, V., Ponza, A., Pazzaglia, F. J., (2009). Topographic expression of active faults in the
1066 foothills of the Northern Apennines. Tectonophysics 474 285–294: 285–294.
1067
1068 Pizziolo, M., Segadelli, S., Vaiani S. C., submitted. Note illustrative alla carta geologica d' italia a
1069 scala 1:50000 foglio n 200 Reggio nell'Emilia. Servizio Geologico d'Italia.
1070
1071 Pondrelli, S., A. Morelli, G. Ekström, S. Mazza, E. Boschi, and A. M. Dziewonski, (2002).
1072 European-Mediterranean regional centroid-moment tensors: 1997-2000, Phys. Earth Planet. Int.,
1073 130, 71-101.
1074
1075 Pondrelli S., A. Morelli, and G. Ekström, (2004). European-Mediterranean Regional Centroid
1076 Moment Tensor catalog: solutions for years 2001 and 2002, Phys. Earth Planet. Int., 145, 1-4, 127-

147.

Pondrelli, S., S. Salimbeni, G. Ekström, A. Morelli, P. Gasperini and G. Vannucci, (2006). The Italian CMT dataset from 1977 to the present, Phys. Earth Planet. Int., doi:10.1016/j.pepi.2006.07.008, 159/3-4, pp. 286-303.

Pondrelli S., A. Morelli, G. Ekström, and E. Boschi, (2007). European-Mediterranean Regional Centroid Moment Tensor catalog: Solutions for years 2003 and 2004, Phys. Earth Planet. Int., 164, 1-2, 90-112.

Schumm, S.A., (1969). River metamorphosis. Proceedings of the American Society of Civil Engineers, Journal of the Hydraulics Division 95, 255–273.

Schumm, S.A., Mosley, M.P., Weaver, W.E., (1987). Experimental Fluvial Geomorphology.

Selvaggi, G. et al., (1996). The October 15, 1996, Reggio Emilia seismic sequence: active compression tectonics in the Po Plain Italy, Geophys. J. Int., 144, 1–13.

Serpelloni, E., Anzidei, M., Baldi, P., Casula, G., Galvini, A. (2005). Crustal velocity and strain-rate fields in Italy and surrounding regions: new results from the analysis of 22 permanent and non-permanent GPS networks. Geophysical Journal International 161,
861–880.

Vann, I. R., R. H. Graham, and A. B. Howard (1986), The structure of mountain fronts, J. Struct. Geol., 8, 215–227.

Wegmann, K. W., Pazzaglia, F. J., (2009). Late Quaternary fluvial terraces of the Romagna and

1104 Marche Apennines, Italy: Climatic, lithologic, and tectonic controls on terrace genesis in an active
1105 orogen. Quaternary Science Reviews 28, 1-2, 137-165. doi 10.1016/j.quascirev.2008.10.006
1106
1107 Wilson L.F., Pazzaglia F. J., Anastasio D. J., (2009). A fluvial record of active fault-propagation
1108 folding, Salsomaggiore anticline, northern Apennines, Italy. J. Geophys. Res. 114 (B8), doi
1109 10.1029/2008JB005984.
1110
1111 Zattin, M., Picotti, V., Zuffa, G.,(2002). Fission-track reconstruction of the front of the northern
1112 Apennine thrust wedge and overlying Ligurian unit. American Journal of Sciences 302, 346–379.
1113
1114 Zehnder, A. T., and Allmendinger, R. W., (2000). Velocity field for the trishear model: Journal of
1115 Structural Geology, v. 22, p. 1009-1014 FaultFold 4.5.4 by Richard W. Allmendinger
1116 http://www.geo.cornell.edu/RWA/trishear/default.html
1117
1118 Gruppo di lavoro CPTI (2004), Catalogo Parametrico dei Terremoti Italiani, INGV, Bologna,
1119 HYPERLINK "http://emidius.mi.ingv.it/CPTI04/" http://emidius.mi.ingv.it/CPTI04/.
1120

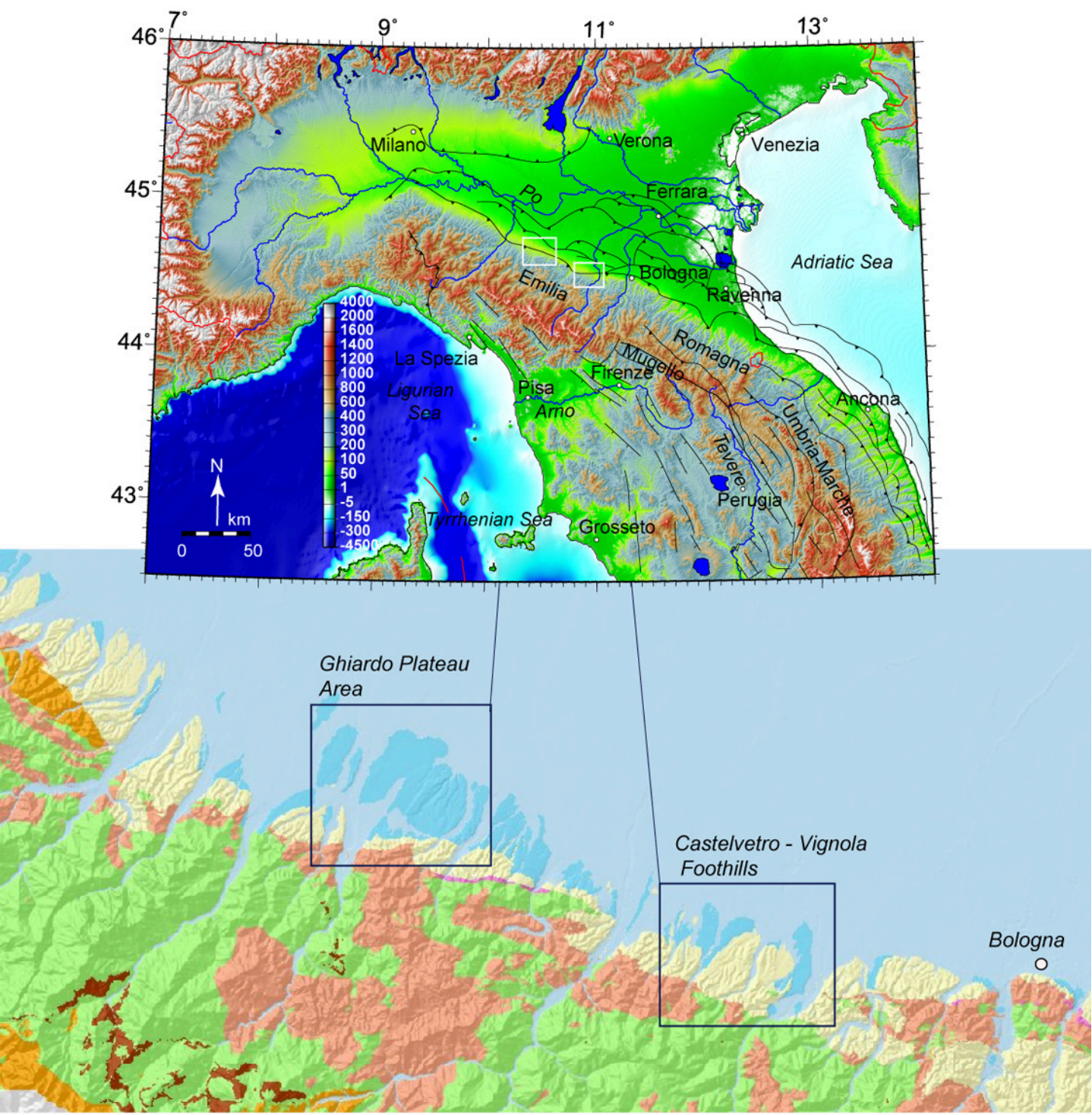

Figure 1, Ponza et al.

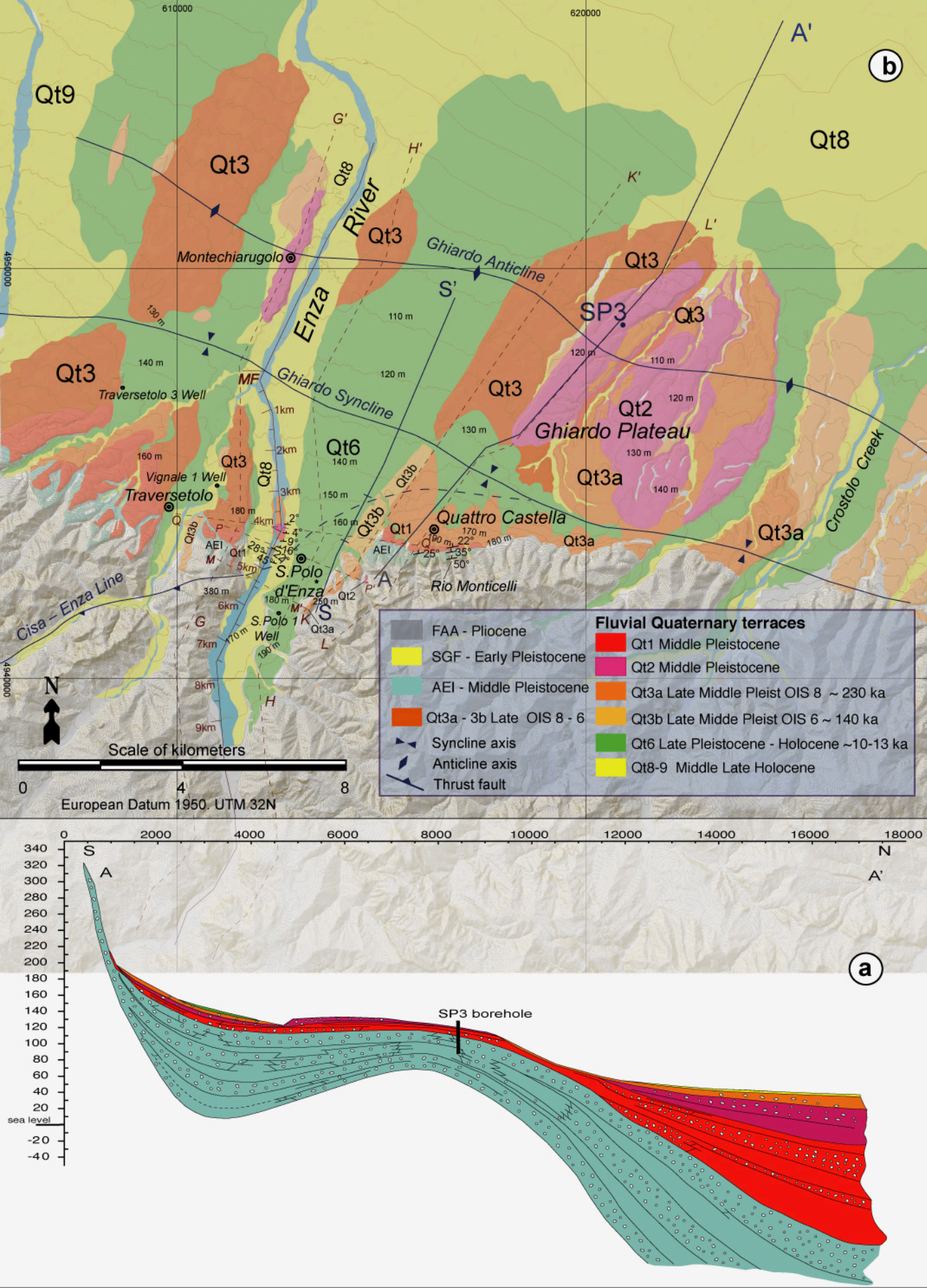

Figure 2. Ponza et al.

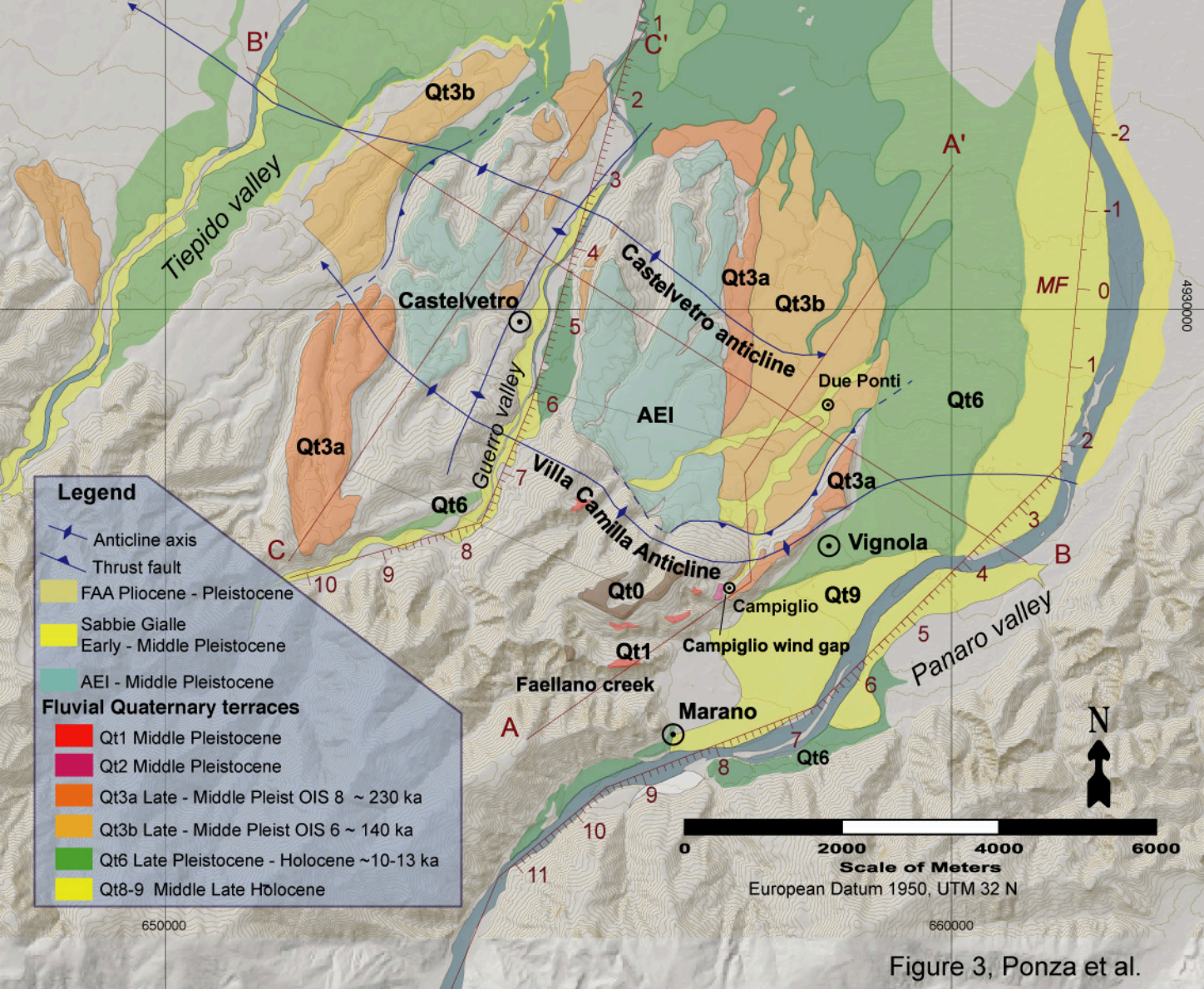

Figure 3, Ponza et al.

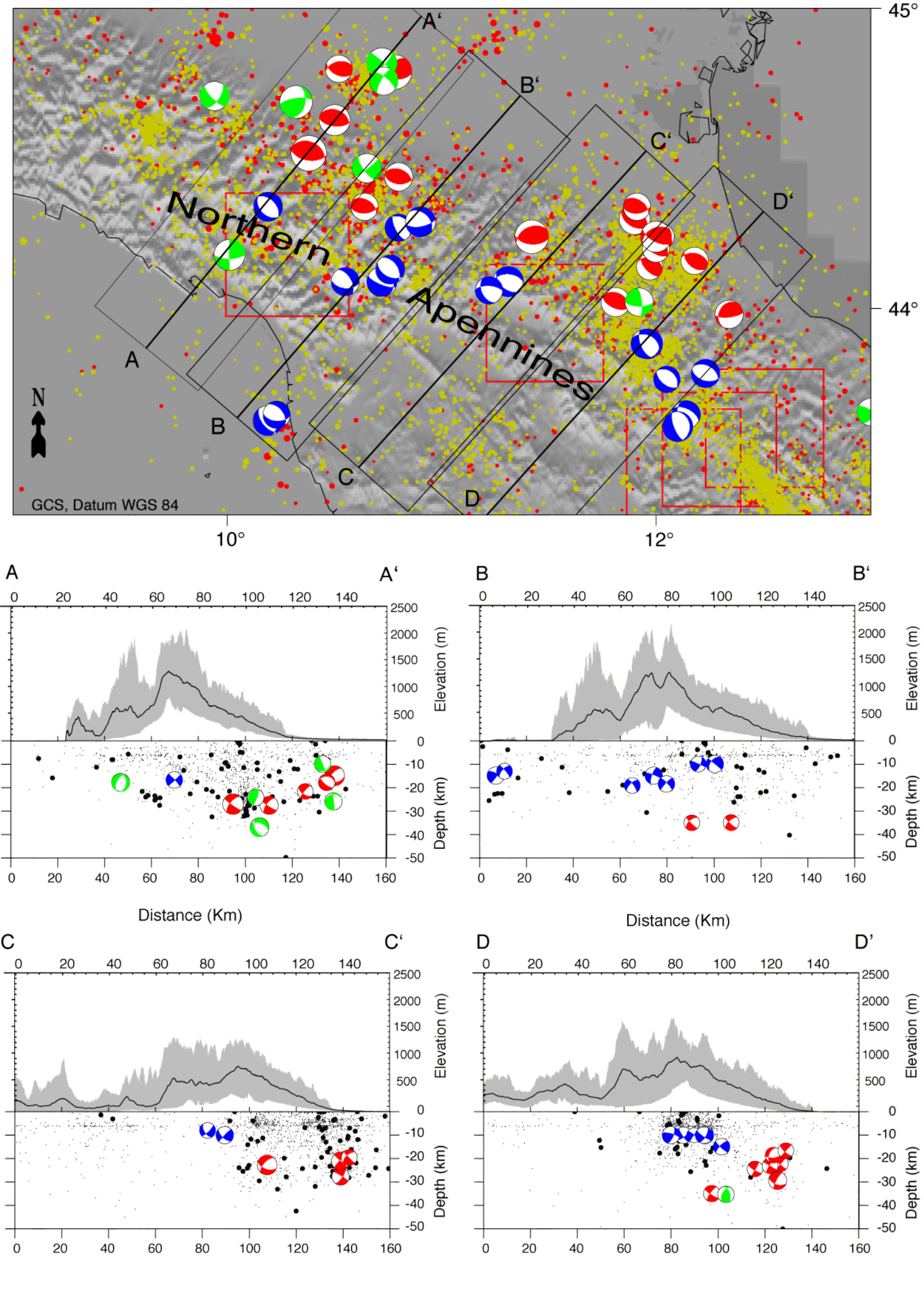

Figure 4, Ponza et al.

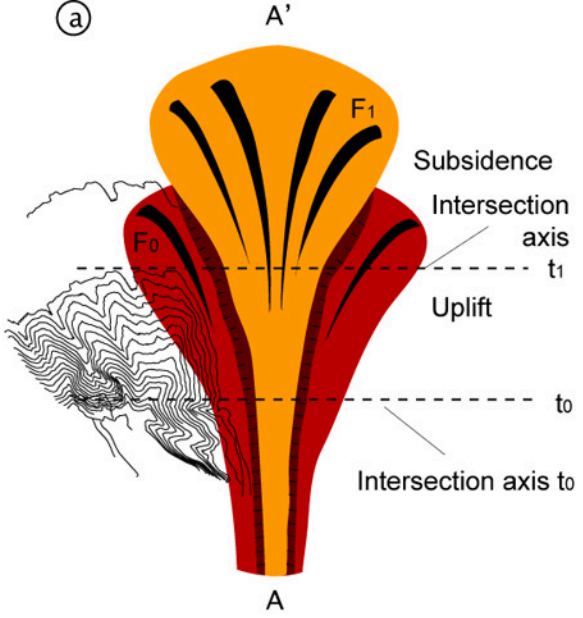

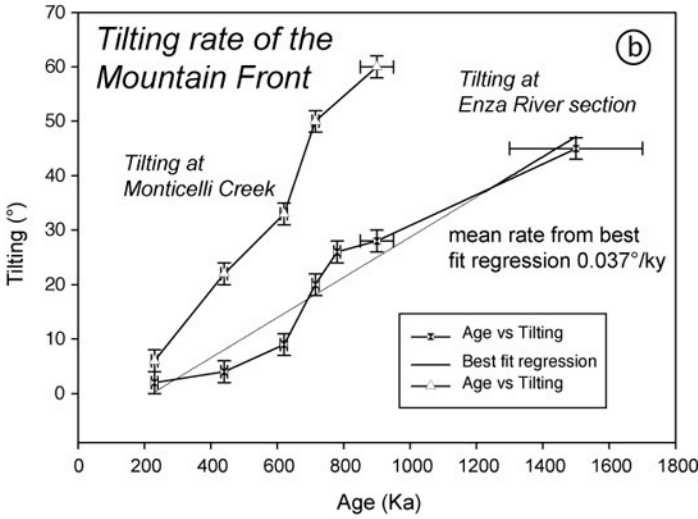

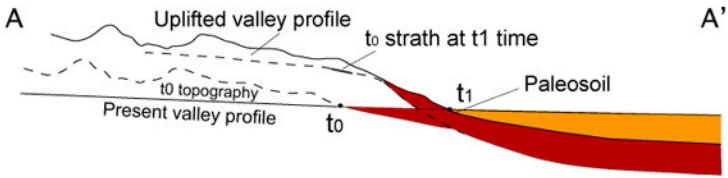

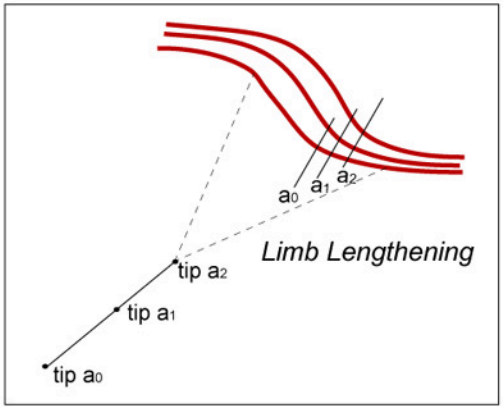

Figure 5, Ponza et al.

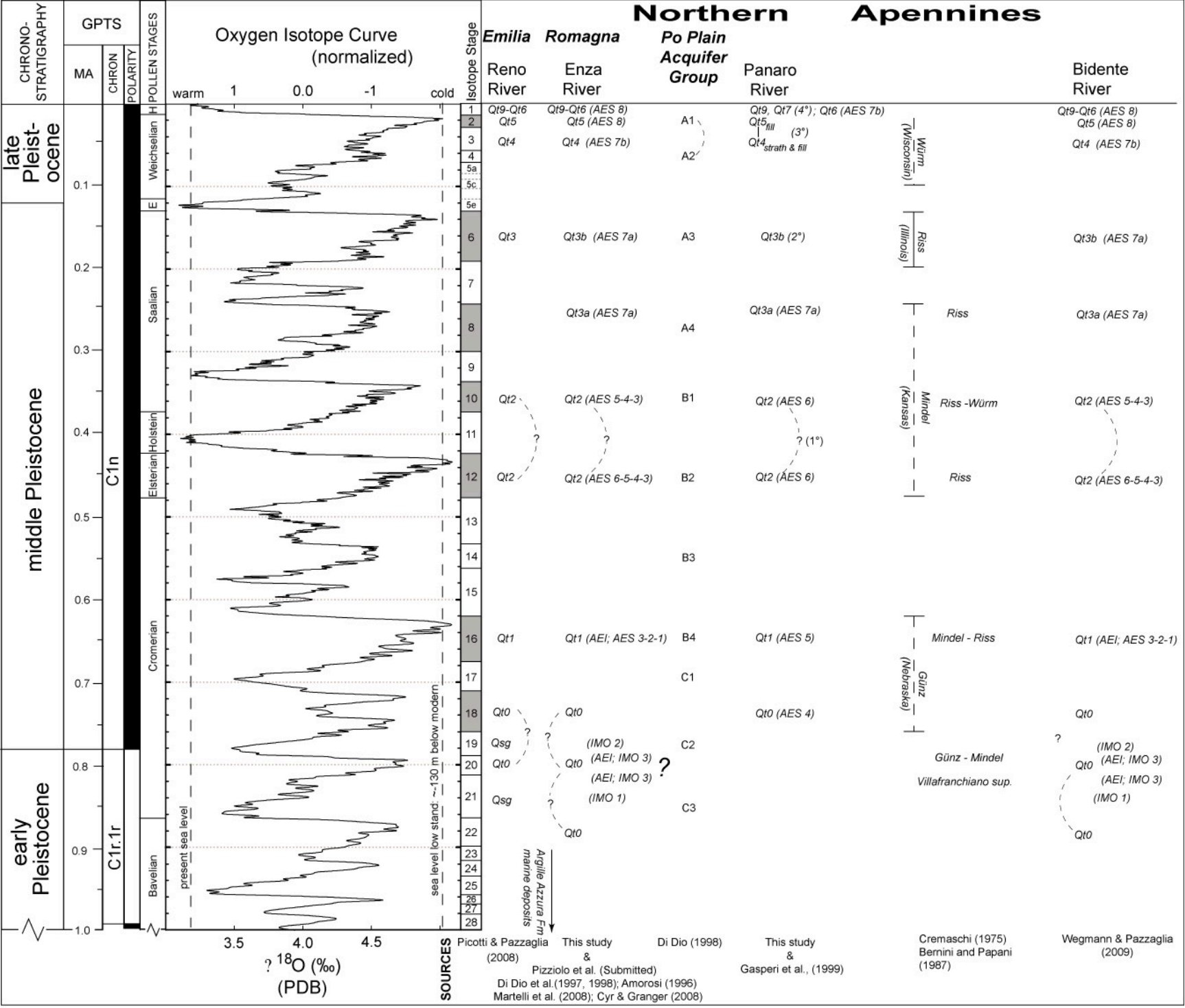

Figure 6, Ponza et al.

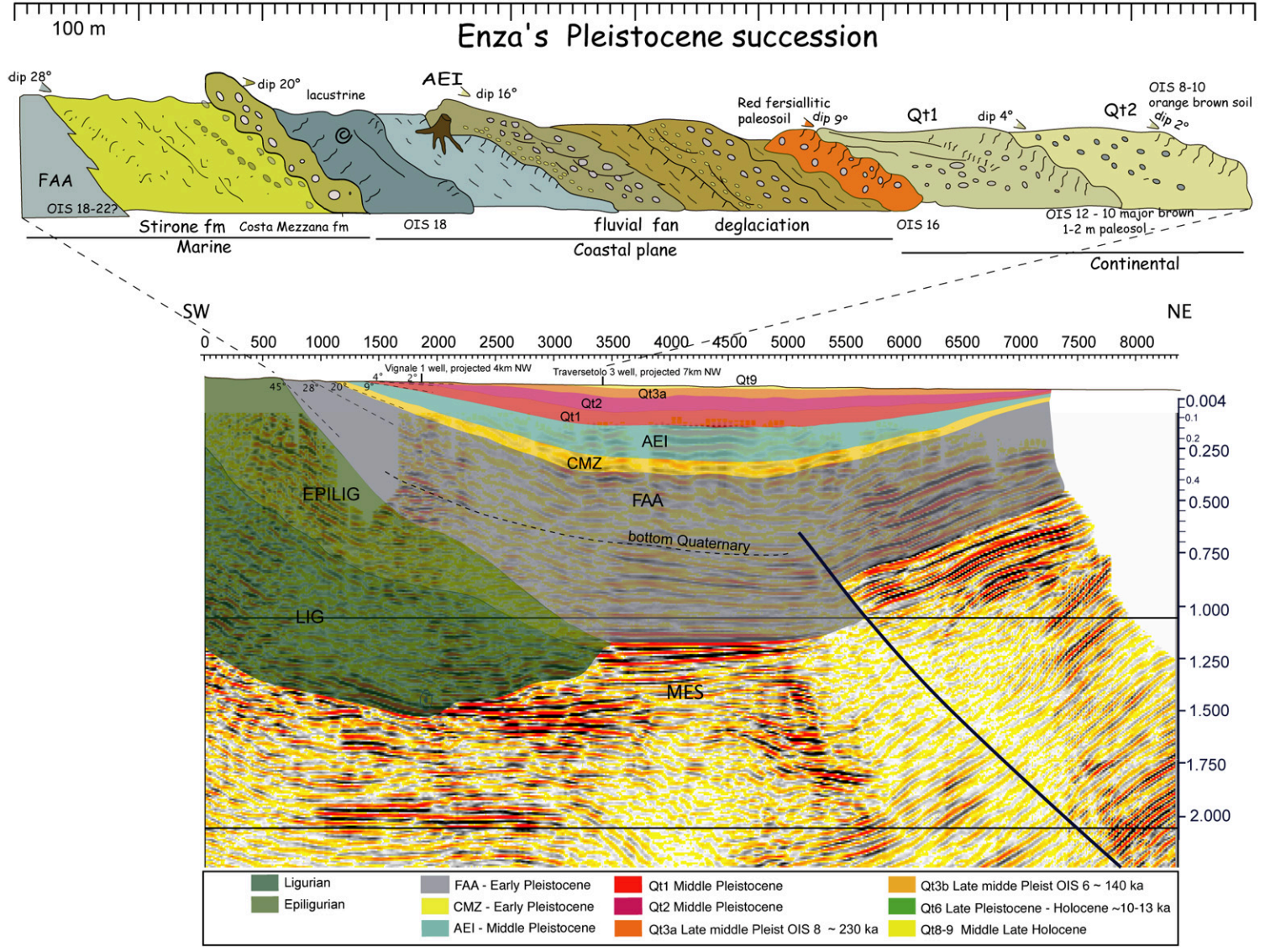

Figure 7, Ponza et al.

Table1, Ponza et al.

Terrace	Regione a Map	Aquifer Po b plain	c MIS	Strath height above channel (m)	Age (ka)	Incision Rate (mm/yr)	Source
Qt8	AES8a	A1	1	3±1	0.05±0.01	$_{60}$ g	
Qt6	AES 8	A2	2	16±3	13±2	1.23±0.05	^{14}C
Qt3a	AES7a	A3	6	85±10	230±10	0.37±0.05	Di Dio, (1998) Pizziolo et al., (submitted)
Qt1	AES 3 d	B4	16	95±10	600±25	0.16±0.02	Di Dio, (1998) Pizziolo et al., (submitted)
AEI	AEI	C3	18-22	155±10	700-900	0.19±0.02	Di Dio, (1998) Pizziolo et al., (submitted)

Table 2, Ponza et al.

Terrace	Regione a Map	Aquifer Po b plain	c MIS	Strath height above channel (m)	Age (ka)	Incision Rate (mm/yr)	Source
Qt9	AES8a	A1	1	2±0.5	0.05±0.01	40±0.17 [g]	
Qt6	AES 8	A2	2	12±3	13±2	0.92±0.27	^{14}C
Qt3a	AES7a	A3	8	77±10	230±10	0.33±0.05	Di Dio (1998)
Qt3b	AES7a	A3	6	57±10	140±10	0.40±0.08	Di Dio (1998)
Qt2	AES6	B1-B2-B3	10-12	89±10	440±10	0.20±0.05	Di Dio, (1998) Pizziolo et al., (submitted)
Qt3a [d]	AES7a	B4	16	47±10	230±10	0.20±0.04	Di Dio, (1998) Pizziolo et al., (submitted)

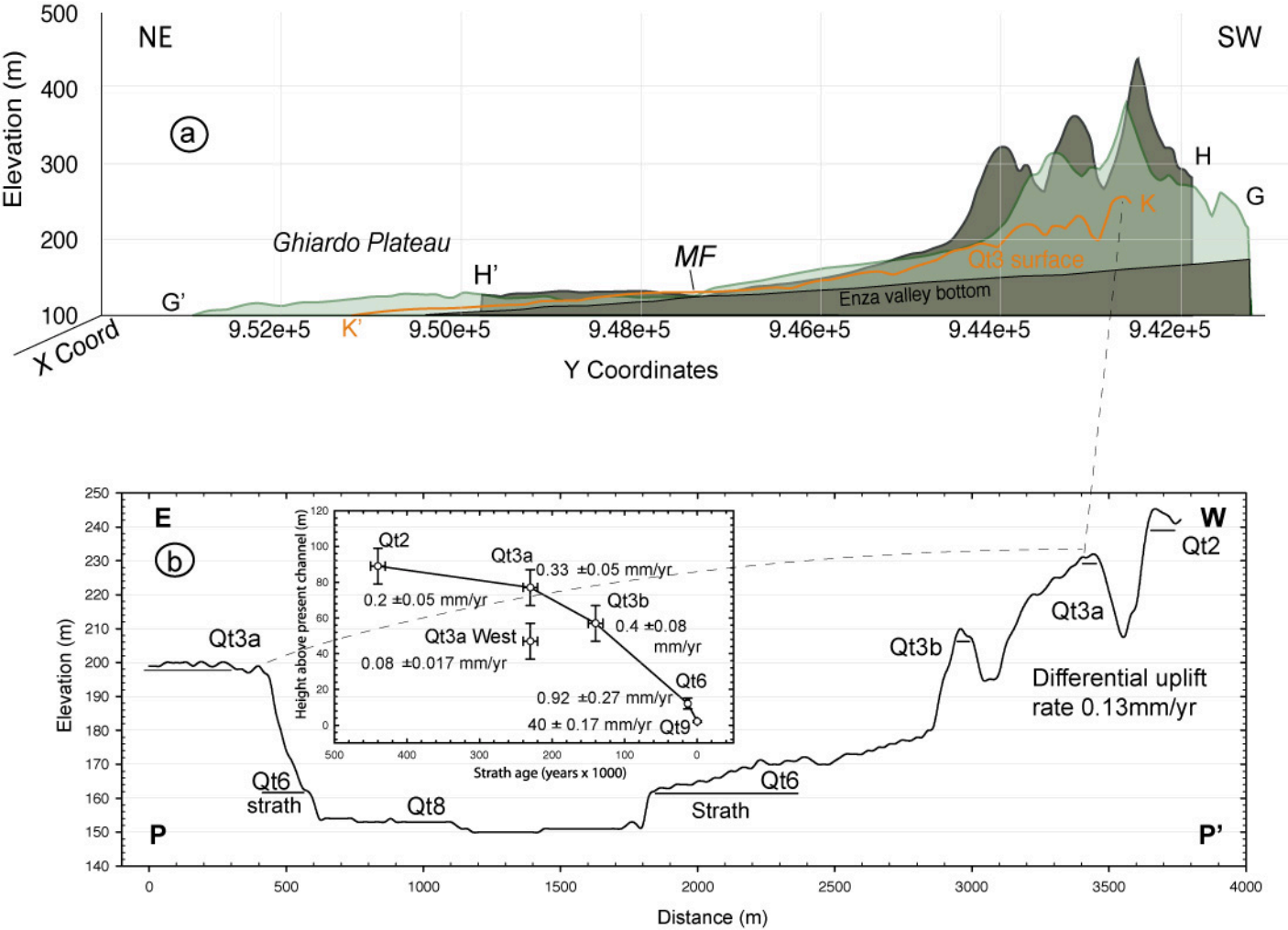

Figure 8, Ponza et al.

Table 3, Ponza et al.

Terrace	Regione a Map	Aquifer Po b plain	c MIS	Strath height above channel (m)	Age (ka)	Incision Rate (mm/yr)	Source
Q9	AES8a	A1	1	1±1	0.05	g 20±	^{14}C
Q6	AES7b	A2	2	16±3	13±2	1.23±0.05	Gasperi et al., (1999)
Qt3a	AES6	A3	6	79±10	230±10	0.34±0.05	Di Dio (1998), Gasperi et al., (1999)
Qt1	AES 5[d]	B4	16	123±10	600±25	0.20±0.03	Gasperi et al., (1999)
Qt0	AEI, AES c 4	B4	18-22	180±10	700-900	0.23±0.03	Gasperi et al., (1999)

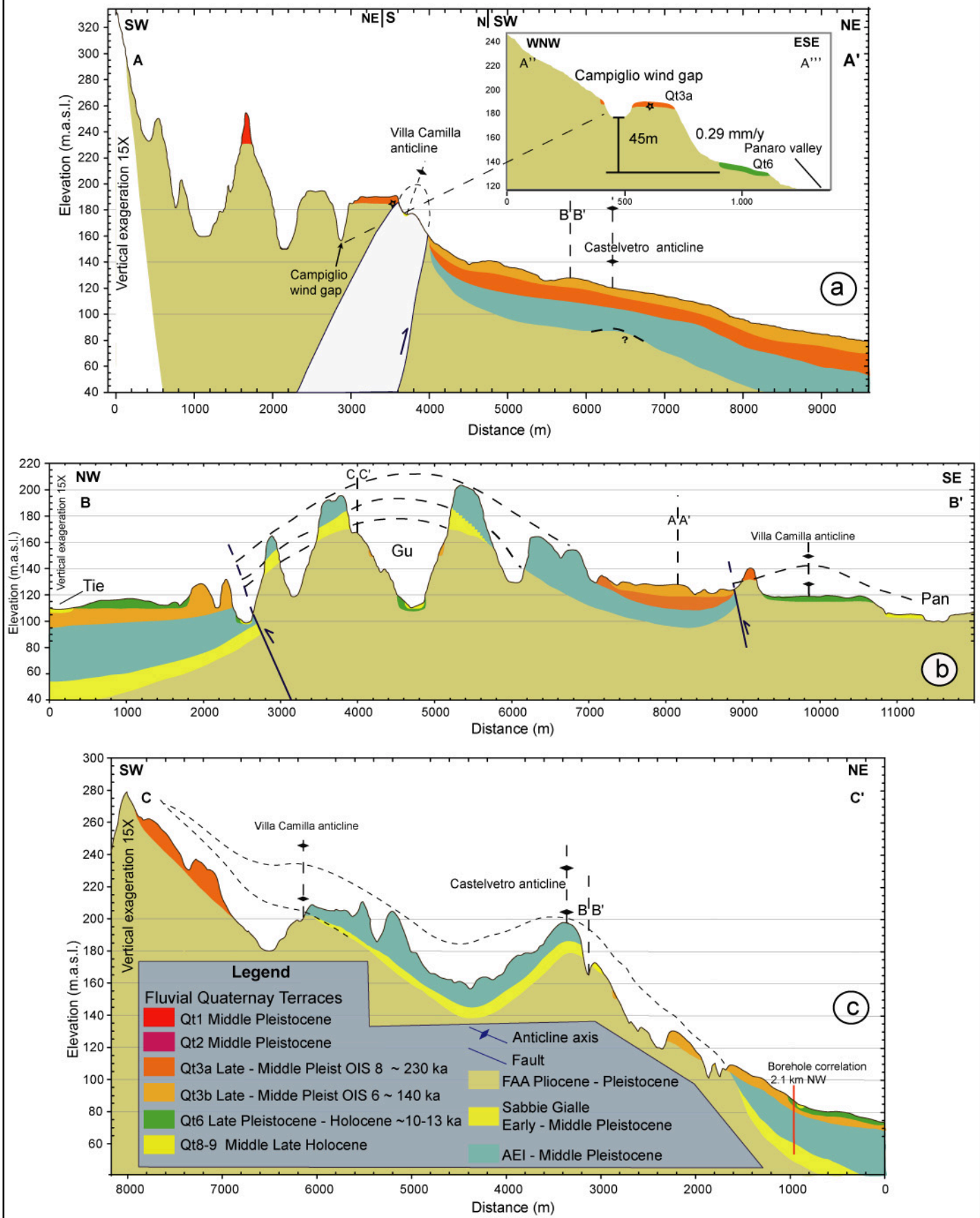
SW
NE
A
A'
Elevation (m.a.s.l.)
Vertical exageration 15X
Villa Camilla anticline
Campiglio wind gap
Castelvetro anticline
B B'
a
Distance (m)
N SW
NE
WNW
ESE
A''
A'''
Campiglio wind gap
Qt3a
45m
0.29 mm/y
Panaro valley
Qt6
NW
SE
B
B'
C C'
A A'
Gu
Tie
Pan
b
C
C'
Borehole correlation
2.1 km NW
c
Legend
Fluvial Quaternay Terraces
Qt1 Middle Pleistocene
Qt2 Middle Pleistocene
Qt3a Late - Middle Pleist OIS 8 ~ 230 ka
Qt3b Late - Midde Pleist OIS 6 ~ 140 ka
Qt6 Late Pleistocene - Holocene ~10-13 ka
Qt8-9 Middle Late Holocene
Anticline axis
Fault
FAA Pliocene - Pleistocene
Sabbie Gialle
Early - Middle Pleistocene
AEI - Middle Pleistocene

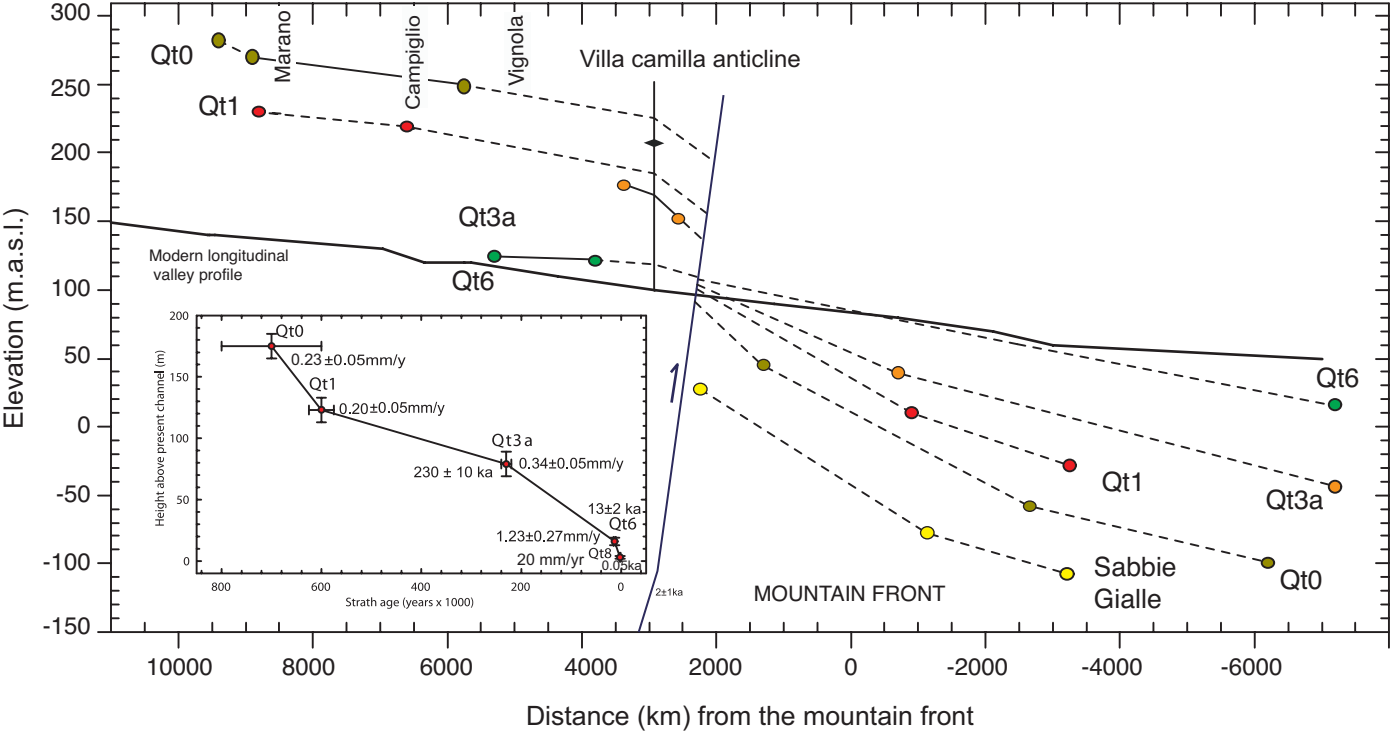

Figure 10, Ponza et al.

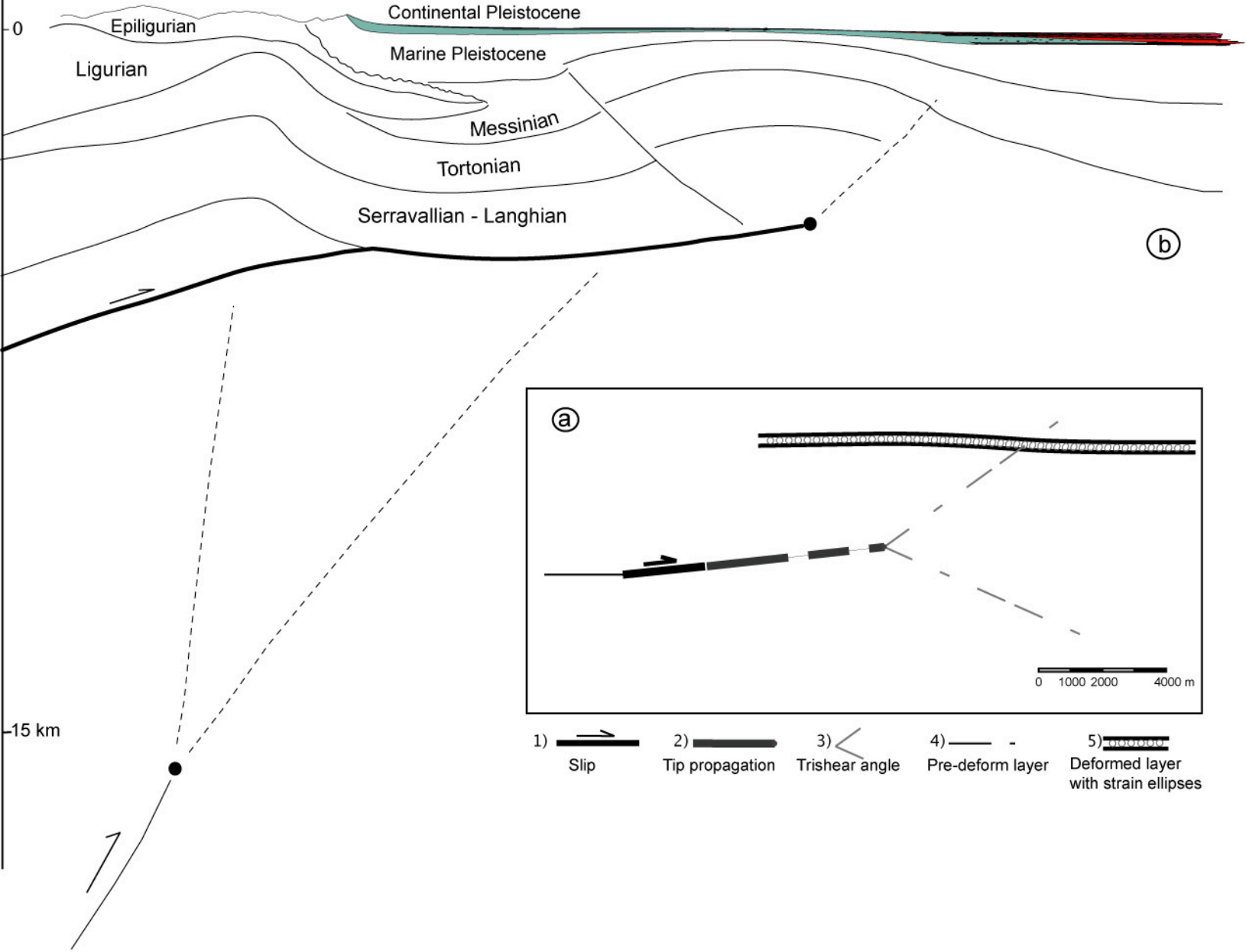

Figure 11, Ponza et al.

Table 4, Ponza et al.

Fault parameters	Min	Max		Best fit
Ramp angle (°)	5	30		6
Tip depth (m)	2500	8000		3240
P/S ratio	0.5	5		3.2
Slip (m)	-5000	5000		2580
Trishear angle (°)	10	75		60

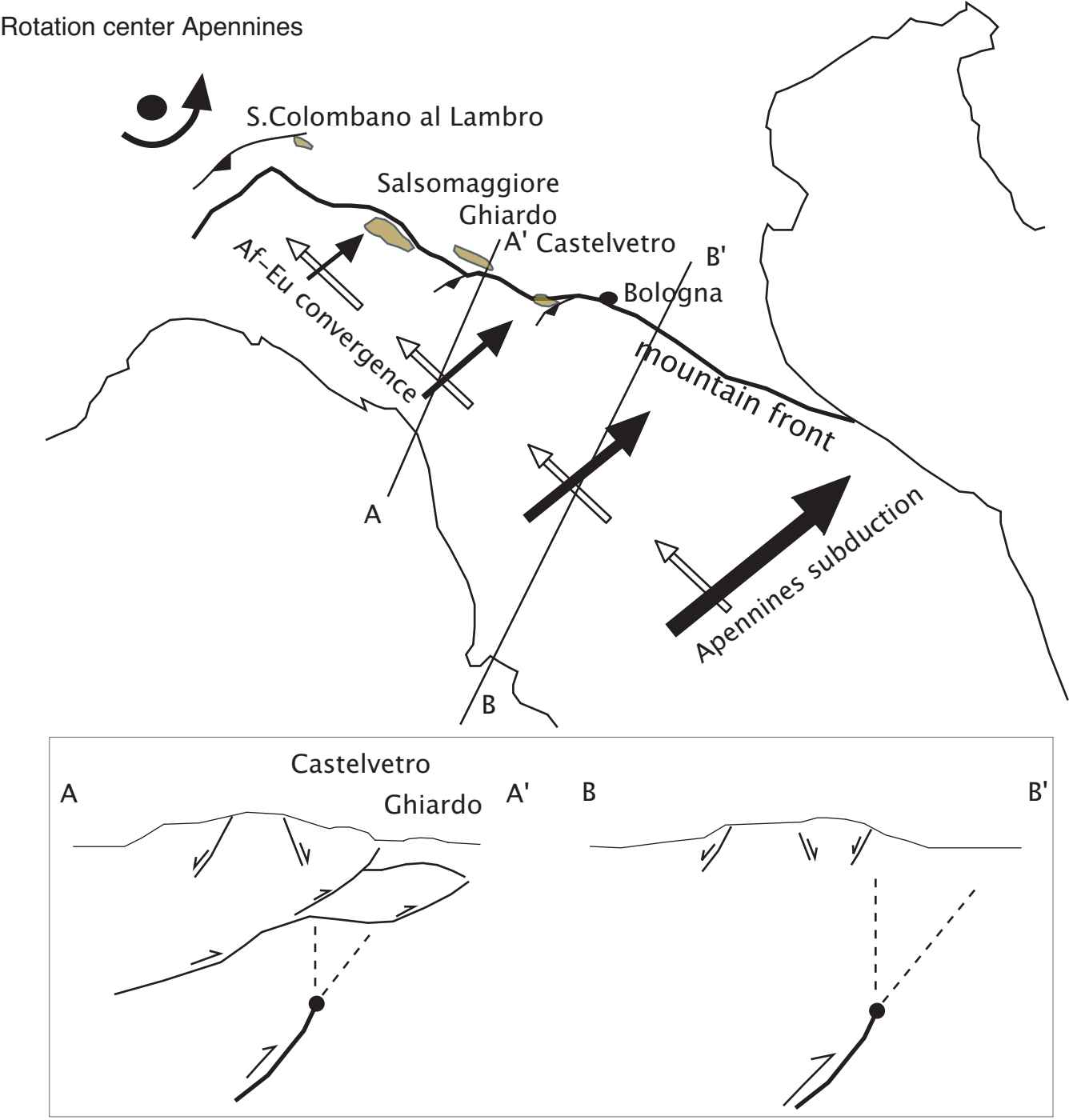

Figure 12, Ponza et al.

Discussion and Conclusions

This research constrain a series of geomorphic and geodynamic implications on the evolution of the Northern Apennines mountain front. The new data provided can contribute to define a new seismotectonic framework of the area.

Both the use of river terraces deposits to measure tectonic uplift rates through rates of vertical river incision, and the use of their correlative deformed alluvial fan deposits to measure tilting rates have been effective. The combined use of these methodologies has enabled the detection of tectonic signals with different wavelength and rates, distinguishing between surficial and deep location, and between local and regional extension of the investigated structures.

The results of vertical incision rates for the Panaro and Enza valleys are significant on a regional scale too. In fact, these data have been added to the previous dataset (Picotti and Pazzaglia, 2008; Wegmann and Pazzaglia, 2009; Wilson et al., 2009) produced using the same methodology and same terrace stratigraphy. The consistency of data distributed 250 km along the mountain front outlines a clear trend for the incision rates, useful for comparison with regional seismic and geodetic datasets.

Despite the possible overlap of tectonic signals coming both from the deep and the surficial structures, the quantitative landscape analysis have been able to isolate and record the low rate tectonic signal of the short wavelength structures, also providing the growth history of these anticlines. Particularly, this study has illustrated a possible lower boundary for the steepness index modeling technique in identifying channel responses to actively deforming landscapes.

The analysis of the instrumental seismicity shows that the different deformations styles are separated not only laterally, as reported in previous studies (e.g. Frepoli and Amato, 1997), but also vertically. This leads to the idea that the extensional deformation pervades the shallower part of the wedge of Northern Apennines, while at a depth (on average around 25 km) thrust earthquakes are nucleating along one or more deep blind thrusts. Extensional earthquakes are in fact distributed at depth only in the upper crust between 8 and 20 km, and they characterize both the western and eastern sectors of the Northern Apennines. The absence of surficial compressional earthquakes in the western sector suggests that the compressional activity recorded at surface behaves aseismically and/or is presently moving too low, therefore the recurrence time is

longer than our observation window. The seismicity seems to confirm the deep thrusting as the most active and seismogenic structure of the Northern Apennines mountain front.

The history of the incision and uplift rates is rather complex and illustrates the evolution of the two interacting deep and surficial thrusts. As suggested by the structural data obtained from the trishear modeling and from the behavior of incision rates, the investigated shallow compressional structures do not appear to be connected to the deep blind thrust but, rather, are local reactivations of shallow-dipping late Neogene thrusts, or new northwest-vergent structures. In fact the surficial structures give evidence to be growing more slowly than the long-term, general rate of emergence of the Apennines from the Po Plain. Rates of uplift for both the Castelvetro hills and the Ghiardo plateau average from 0.1 to 0.3 mm/yr, showing a general trend to decrease since 600 ky. These rates also represent the possible lower boundary of the tectonic recorded by stream channels and that we are able to extract from the steepness index analysis. The incision rates of the major rivers such as the Panaro and the Enza increase from 0.34 to 1.23 mm/yr from 230 to 12 ky. This trend is the same observed at the Reno river near Bologna (Picotti and Pazzaglia, 2008) and has been interpreted as the effect of focusing of deformation along the deep thrust. Therefore, while the surficial structures are generally decreasing their activity, increasing incision rates are indicative of increasing deformation along the deep thrust. The normal faults located closer to the foothills represent stretching of the carapace that is folding at the mountain front: the results consistently indicate that the faults have a moderate activity with slip rates ranging from 0.1 to 0.3 mm/yr, an order of magnitude lower of the uplift rate of the long wavelength fold in which they are imbedded.

The convergence at the Apennines is associated with the far field of the Africa-Europe collision, providing the NW oriented stress field that interacts with the NE-oriented one. Available GPS data (D'Agostino et al. 2008) reconstruct the velocity field for the Af-Eu convergence, documenting as well that the oblique subduction of the Adria plate creates a velocity field oriented NE. This field increases away from the rotation center of the orogen, fixed to the northwestern tip of the Northern Apennines. The vicinity to the rotation center of the orogen could explain the changing stress state of the belt and the two seismotectonic regions. In the west, the main tensors show similar modulus of both the northwest (Af-Eu convergence) and northeast (Adria subduction) axes, whereas going eastward of Bologna the rotation of the Apennine orogen contributes more and more to the deformation. The increasing strain at the mountain front moving south-eastward is documented also by the activity of the deep thrust forming the mountain front, traced by the incision at the

mouth of the rivers flowing to the Po plain.

References

Bernini, M., and G. Papani (1987), Alcune considerazioni sulla struttura del margine appenninico emiliano fra lo Stirone e lÕEnza (e sue relazioni con il sistema del f. Taro), Acta Naturalia, Ateneo Parmense, 23.

Boccaletti, M., M. Coli, C. Eva, G. Ferrari, G. Giglia, A. Lazzarotto, A. Merlanti, F. Nicolich, R. Papani, and G. Postpischl (1985), Considerations on the seismotectonics of the Northern Apennines, Tectonophysics, 117, 7-38.

Boccaletti, M., Bonini, M., Corti, G., Gasperini, P., Martelli, L., Piccardi, L.,Tanini, C., Vannucci, G. (2004). Seismotectonic Map of the Emilia-Romagna Region, 1:250000. Regione Emilia-Romagna CNR. SELCA, Firenze.

Bridgland, D.R., 2000. River terrace systems in north-west Europe: an archive of environmental change, uplift and early human occupation. Quaternary Science Reviews 19 (13), 1293-1303.

Bridgland, D.R., Westaway, R., (2008). Preservation patterns of Late Cenozoic fluvial deposits and their implications: results from IGCP 449. Quaternary International 189, 5-38.

Bull, W.L., Knuepfer, P.L.K., 1987. Adjustments by the Charwell River, New Zealand, to uplift and climatic changes. Geomorphology 1 (1), 1532. Bull, W.B., (1991). Geomorphic Response to Climatic Change. Oxford University Press,New York, 326 pp.

Burbank, D.W., Leland, J., Fielding, E., Anderson, R.S., Brozovic, N., Reid, M.R., Duncan, C., (1996). Bedrock incision, rock uplift and threshold hillslopes in the northwestern Himalayas. Nature 379, 505-510.

Burbank, D.W., Anderson, R.S., 2001. Tectonic Geomorphology. Blackwell Science Malden, MA, 274 pp.

DÕAgostino, N., Avallone, A., Chelone D., DÕAnastasio E., Mantenuto S. and Selvaggi , G., (2008). Active tectonics of the Adriatic region from GPS and earthquake slip vectors. J. Geophys. Res., 113, B12413, doi:10.1029/2008JB005860.

Elter, P., G. Giglia, M. Tongiorgi, and L. Trevisan (1975). Tensional and compressional areas in the recent (Tortonian to present) evolution of the Northern Apennines, Boll. Geofis. Teor. Appl., 17, 3 - 18.

Eppes, M. C., R. Bierma, et al. (2008). A soil chronosequence study of the Reno valley, Italy: Insights into the relative role of climate versus anthropogenic forcing on hillslope processes during the mid-Holocene. Geoderma, 147 (3-4), 97-107.

Frepoli A. and Amato A. (1997). Contemporaneous extension and compression in the Northern Apennines from earthquake fault-plane solutions. Geophys. J. Int., vol. 129 (2), 368- 388

Gasperi, G., Bettelli, G., Panini, F., Pizziolo, M. (1999). Note illustrative alla carta geologica dÕ italia a scala 1:50000 foglio n 219 sassuolo. Servizio Geologico dÕItalia.

Hancock, G. S., and R. S. Anderson (2002), Numerical modeling of fluvial strath-terrace formation in response to oscillating climate, Geol. Soc. Am. Bull., 114, 1131-1142.

Lavecchia, G., P. Boncio, and N. Creati (2003a). A lithospheric-scale seismogenic thrust in central Italy, J. Geodyn., 36, 79 - 94.12,143 - 12,157.

Lavé?, J., Avouac, J.P., 2000. Active folding of fluvial terraces across the Siwaliks Hills, Himalayas of central Nepal. Journal of Geophysical Research 105 (B3), 5735-5770.

Laveé, J., Avouac, J.P., 2001. Fluvial incision and tectonic uplift across the Himalayas of central Nepal. Journal of Geophysical Research 106 (B11), 26,561-26,591.

Lavecchia, G., P. Boncio, N. Creati, and F. Brozzetti (2004). Stile strutturale, stato termo-meccanico e significato sismogenetico del thrust Adriatico; dati e spunti da una revisione del profilo CROP 03 integrata con lÕanalisi di dati sismologici, Boll. Soc. Geol. Ital., 123, 111 - 125.

Mackin, J.H., 1948. Concept of the graded river. Geological Society of America Bulletin 59, 463-512.

Merritts, D., Vincent, K., Wohl, E., 1994. Long river profiles, tectonism, and eustasy: a guide to interpreting fluvial terraces. Journal of Geophysical Research 99 (B7), 14031-14050.

Meyer, G.A., Wells, S.G., Jull, A.J.T., 1995. Fire and alluvial chronology in Yellowstone National Park: climate and intrinsic controls on Holocene geomorphic processes. Geological Society of America Bulletin 107, 1211-1230.

Pazzaglia, F.J., Gardner, T.W., Merritts, D.J. (Eds.), 1998. Bedrock Fluvial Incision and Longitudinal Profile Development over Geologic Time Scales Determined by Fluvial Terraces. Geophysical Monograph Series, vol. 107. Bedrock Channels: American Geophysical Union, pp. 207-235.

Pazzaglia, F.J., Brandon, M.T., 2001. A fluvial record of rock uplift and shortening across the Cascadia forearc high. American Journal of Science 301, 385-431.

Personius, S.F., 1995. Late Quaternary stream incision and uplift in the forearc of the Cascadia subduction zone, western Oregon. Journal of Geophysical Research 100, 20193-20210.

Picotti, V., R. Capozzi, G. Bertozzi, F. Mosca, A. Sitta, and M. Tornaghi, (2007). The Miocene petroleum system of the Northern Apennines in the central Po Plain (Italy), in Thrust Belts and Foreland Basins,

From Fold Kinematics to Hydrocarbon System, edited by O. Lacombe et al., pp. 117 - 131, Springer Verlag, Berlin.

Picotti, V., Pazzaglia, F. J. (2008). A new active tectonic model for the construction of the Northern Apennines mountain front near Bologna (Italy). Journal of Geophysical Research. V. 113 (B8), p. 1-24.

Rockwell, T. K., E. A. Keller, M. N. Clark, and D. L. Johnson (1984), Chronology and rates of faulting of Ventura River terraces, California, Geol. Soc. Am. Bull., 95, 1466 -1474

Royden, L. (1993). Evolution of retreating subduction boundaries formed during continental collision, Tectonics, 12, 629 - 638.

Schumm, S. A. (1969), River metamorphosis, J. Hydraul. Div. Am. Soc. Civ. Eng., 95, 255-273.

Schumm, S.A., Mosley, M.P., Weaver, W.E., 1987. Experimental Fluvial Geomorphology. Wiley Interscience, New York, 413 pp.

Scrocca, D. (2006), Thrust front segmentation induced by differential slab retreat in the Apennines (Italy), Terra Nova, 18, 154 - 161.

Scrocca, D., E. Carminati, C. Doglioni, and D. Marcantoni (2007). Slab retreat and active shortening along the Central-Northern Apennines, in Thrust Belts and Foreland Basins, From Fold Kinematics to Hydrocarbon System, edited by O. Lacombe and F. Roure, pp. 471 - 487, Springer Verlag, Berlin.

Wegmann, K.W., Pazzaglia, F.J., 2002. Holocene strath terraces, climate change, and active tectonics; the Clearwater River basin, Olympic Peninsula, Washington State. Geological Society of America Bulletin 114 (6), 731-744.

Wegmann, K. W., Pazzaglia, F. J. (2009). Late Quaternary fluvial terraces of the Romagna and Marche Apennines, Italy: Climatic, lithologic, and tectonic controls on terrace genesis in an active orogen. Quaternary Science Reviews 28, 1-2, 137-165. doi 10.1016/j.quascirev.2008.10.006

Wilson L.F., Pazzaglia F. J., Anastasio D. J. (2009). A fluvial record of active fault-propagation folding, Salsomaggiore anticline, northern Apennines, Italy. J. Geophys. Res. 114 (B8), doi 10.1029/2008JB005984.

Whipple, K. X., Tucker, G. E., 1999. Dynamics of the stream-power river incision model: Implications for height limits of mountain ranges, landscape response timescales, and research needs. Journal of Geophysical Research 104, 17661 - 17674.

Willgoose, G., Bras, R.L., and Rodriguez-Iturbe, I., 1991. A coupled channel network growth and hillslope evolution model: I. Theory: Water Resources Research, v. 27, no. 7, 16711684, 689 doi: 10.1029/91WR00935.